Universitetet i Stavanger

FACULTY OF SCIENCE AND TECHNOLOGY

MASTER'S THESIS

Study programme/specialisation: Petroleum Engineering – Well Engineering	Spring semester, 2018 **Open** / Restricted access
Author: Juan Carlos Martinez Vidaur	…… (signature of author)
Faculty Supervisor: Dan Sui	
Title of master's thesis: Experimental Study of Automated Characterization of Non-Newtonian Fluids	
Credits (ECTS): 30	
Keywords: • Automation • Drilling fluid properties evaluation • Flow loop • Experimental • Drilling hydraulics	Number of pages: …… + supplemental material/other: …… Stavanger, June 2018

Master's Thesis

Experimental Study of Automated Characterization of Non-Newtonian Fluids

Submitted by

Juan Carlos Martinez Vidaur

Faculty of Science and Technology
University of Stavanger

This thesis is submitted in partial fulfillment of the requirements for the degree of
Master of Science in Petroleum Engineering

June 2018

Acknowledgements

This thesis is the culmination of my Masters Studies at the University of Stavanger, two years well-worth the effort and sacrifice in the pursuit of knowledge. I am grateful to the University of Stavanger and to the people of Norway for the opportunity given, you set an example of how universal access to education can make this world a better place.

I would like to express my gratitude to my supervisor Dan Sui for her guidance and assistance throughout the development of this research work. Also, I want to thank M-I SWACO Norge for providing the fluid additives used in this study.

Lastly, I wish to thank my family and especially my dear wife Almaz for their unconditional support and encouragement to pursue my goals, this achievement is dedicated to you and I will be eternally thankful for being there on every step of this endeavor.

Abstract

The automation of the drilling fluid properties measurement is a research area that has been pursued in the last few years by the oil industry. Adequate control and monitoring of the density and rheology of the drilling mud have been fundamental responsibilities of the Mud Engineer and the Derrickman; this reliance in human intervention introduces a range of error and uncertainty in the measurements. A system that could provide automated measurements in real-time of the most critical fluid properties, namely density and viscosity, would significantly improve the control over the fluid that goes into the well, thus reducing drilling problems associated to improper management of the bottom hole pressure.

A setup that emulates a measurement system that could be installed in the standpipe of a drilling rig was built at the University of Stavanger in 2016. The basic concept is to measure the differential pressure in two sections of pipe: one horizontal and one vertical; based on this pressure data, a mathematical model is then used to estimate the density of the fluid and subsequently the viscosity. Last year, a first study to validate the measurements and the mathematical model used in the algorithm was conducted with Newtonian and Non-Newtonian Fluids. The results obtained showed significant discrepancies, particularly in the density measurements arguably related to the foam appearance in the flowloop setup.

This thesis explores further the applicability of the automated measurement of drilling fluid properties using the instrumented standpipe concept; a wider set of fluid formulations has been studied extending the analysis to heavier densities. The study has been constrained to solids-free fluid formulations due to the limitations of the current flowloop setup. It is recommended to continue this research in the future by modifying the system at UiS to accommodate the safe handling and disposal of weighted muds and potentially even oil-based drilling fluids using a non-smooth pipe.

Table of Contents

List of Figures

List of Tables

List of Appendix Tables

List of Abbreviations and Symbols

API	American Petroleum Institute
cP	Centipoise
ECD	Equivalent Circulating Density
ERD	Extended Reach Drilling
ESD	Equivalent Static Density
HPHT	High Pressure, High Temperature
lpm	Liters per Minute
LSRV	Low Shear Rate Viscosity
mbar	Millibar
ppb	Pounds per Barrel
ROP	Rate of Penetration
RPM	Revolutions per Minute
NaCl	Sodium Chloride
SG	Specific Gravity
UiS	University of Stavanger
XCD	Xanthan Gum Polymer

ε	Absolute pipe roughness
μ_a	Apparent viscosity
ν	Average fluid velocity
$D_{eff\text{-}HB}$	Effective pipe inner diameter for Herschel-Bulkley fluids
$D_{eff\text{-}PL}$	Effective pipe inner diameter for Power Law fluids

μ_e	Effective viscosity
ρ	Fluid density
μ	Fluid viscosity
n_a	Generalized flow index
g	Gravitational constant
DP1	Horizontal differential pressure
dP_{hor}	Horizontal differential pressure
dx	Length of differential volume element
lpm	Liters per minute
D	Pipe diameter
A	Pipe cross-sectional inner area
μ_p	Plastic viscosity
K	Power Law consistency index
n	Power Law index
P	Pressure exerted on differential volume element
ΔP	Pressure Loss
Q	Pump rate
r	Radius of differential volume element
ε/D	Relative pipe roughness
Re	Reynolds number
Re_{HB}	Reynolds number for Herschel-Bulkley fluids
Re_{PL}	Reynolds number for Power Law fluids
γ	Shear rate
γ_w	Shear rate in the pipe wall

τ	Shear stress
τ_w	Shear stress in the pipe wall
dr	Thickness of differential volume element
DP2	Vertical differential pressure
dP_{ver}	Vertical differential pressure
Δh	Vertical distance
θ	Viscometer dial reading
θ_1	Viscometer dial reading at lower shear rate
θ_2	Viscometer dial reading at higher shear rate
θ_{600}	Viscometer dial reading at 600 RPM
θ_{300}	Viscometer dial reading at 300 RPM
θ_{200}	Viscometer dial reading at 200 RPM
θ_{100}	Viscometer dial reading at 100 RPM
θ_6	Viscometer dial reading at 6 RPM
θ_3	Viscometer dial reading at 3 RPM
k	Viscometer overall instrument constant
ω	Viscometer rotational speed
ω_1	Viscometer rotational speed at lower shear rate
ω_2	Viscometer rotational speed at higher shear rate
f	Viscometer torsion spring factor
τ_o	Yield point

Chapter 1

Introduction

1.1 The Importance of Fluid Properties Monitoring and Control

The drilling fluid fulfills a set of different functions during the well construction process, two of the most important ones are: to provide the energy required to control the formation pressures, and to carry out drilling cuttings out of the well. These two crucial functions of the drilling mud are the result of two fundamental fluid properties, density and viscosity. The most widely used techniques to measure these properties are the mud balance and the rheometer, respectively, but they both are subject to the assessment done by the person who operates the equipment, this role has typically been delegated to the Mud Engineer and the Derrickman in the drilling rig.

The accuracy of the measurements has improved over time with the introduction for instance of pressurized mud balances and digital rheometers, but still, data is just available whenever the operator runs a check, which at best occurs every 15min for density and a few times per day for rheology. Although, it is prudent here to clarify that a routine viscosity check is done along with the density measurement using a Marsh Funnel, but the results of this quick analysis are merely for reference purposes and provide little insight of the full rheological profile of the fluid in the well. Furthermore, when these tests are run, a small sample of fluid is collected from the active mud pits and assumed to be representative of the considerably larger volume of fluid that is pumped into the well.

Thus, in practice, we have limited information of the fluid properties in the borehole. As wells become ever more challenging, there is an increased demand for a system that monitors and controls the fluid properties in a more systematic way, and that provides real-time data of the fluid that goes into the well. This is where automation comes into play, and where the instrumented standpipe concept used in this experimental study finds its applicability. The reasoning is simple, a more thorough monitoring and control of the drilling fluid properties reduces the risk of drilling problems associated to inadequate wellbore pressures, which ultimately translates into safer and less expensive drilling operations.

1.2 The Contribution of this Experimental Study

The aim of this project is to continue with the development of an automated measurement system of drilling fluid properties that could potentially be the basis for a real-time monitoring arrangement that provides the drilling crew with a tighter control of what is actually being pumped downhole. The basis of this study is the instrumented standpipe concept and the flowloop built at the University of Stavanger in 2016; a more detailed explanation of the system is given in Chapter 3 of this thesis, as well as a description of the algorithm used in the data processing.

The findings of the previous study conducted in 2017 are used as the building blocks to continue exploring the accuracy and validity of both the pressure data acquisition system and the mathematical model that calculates viscosity and density values. The study performed last year was focused first on calibrating the pressure data acquisition system with Newtonian fluids (water) and then extending the *calibrated* model to Non-Newtonian fluids. The results presented in the aforementioned experimental work showed significant discrepancies that were explored and addressed in more detail in the current study.

The approach that was selected for the present work was to extend further the investigation of Non-Newtonian fluids. The starting point was the calibration parameters generated last year; once the flowloop was tested and verified with water measurements, several different fluid formulations were investigated. The issues previously encountered in the determination of accurate density measurements were addressed by modifying the fluid formulations to include a defoamer additive that minimizes the flow composition fluctuations in the system. Additionally, the testing matrix was extended to include heavier fluid densities than water; in this respect, sodium chloride brine was identified as the only viable option due to the limitations related to fluid disposal in the laboratory. The restrictions of the current experimental setup do not allow either to test fluids with any weighting materials content.

Chapter 4 of this document presents a detailed analysis of the experimental results. The data acquisition system and the mathematical model show an acceptable accuracy of the viscosity and density calculations of Non-Newtonian solids-free fluids in laminar and transitional flow regimes. The automated measurement system of drilling fluid properties based on the instrumented standpipe concept is a promising application, and further work will have to be performed to resolve the applicability in turbulent flow, and furthermore, to investigate the applicability in weighted fluids with a high solids concentration. The limitations of the current flowloop setup have to be addressed first prior to continue extending the scope of this application. The last Chapter of this thesis outlines what the author considers necessary to further continue developing this research.

Chapter 2

Drilling Fluids Fundamental Concepts

This chapter is an introduction to the basic drilling fluids concepts that are the foundation of this experimental study. Drilling Fluids Engineering is on its own right an essential subdiscipline in Well Engineering, and the information contained in this chapter is by no means exhaustive of the continuous research and developments conducted by the specialized service companies. Although, it is on the judgement of the author that all those involved in the well construction process should have a minimum working knowledge of the basic concepts herein presented.

2.1 Drilling Fluids Functions

Drilling Fluids are designed and formulated to perform a number of functions that allow to drill and complete a well, although, not all of them are as essential as removing drill cutting from the borehole and controlling the formation pressures. Unconventional drilling methods, such as Underbalanced Drilling, have introduced new considerations into the subject, but they are still the exception rather than the rule, thereafter the following list has typically been accepted as the most common drilling fluids functions:

- Control formation pressures
- Remove drill cutting from the well
- Preserve wellbore stability
- Cool and lubricate the drill string and bit
- Seal permeable formations
- Minimize formation damage
- Transmit hydraulic energy to downhole tools
- Convey information to surface
- Minimize environmental impact

The following subsections elaborate further on the two main functions that are on the interest of this study, the remaining elements are not in the scope of this thesis and will not be further pursued.

2.1.1 Controlling Formation Pressures

As drilling progresses, the overlying rock layers are removed in order to reach the target reservoir; when this occurs, the subsurface stresses are disturbed and the force that used to be exerted by the rock column is partially replaced by the hydrostatic pressure exerted by the drilling fluid column. In conventional drilling, keeping the well *under control* means to maintain a hydrostatic column that is at least equal or exceeds the formation pore pressure to prevent formation fluids from flowing into the wellbore and ultimately causing a *blowout*.

The hydrostatic pressure of the fluid column is controlled by adjusting the density of the fluid in the wellbore. The upper boundary of the fluid density is determined by the formation fracture pressure; if the equivalent mud weight exceeds this limit, the formation can break down, fluid losses could occur and the hydrostatic pressure in the well could be reduced to the point that an influx of formation fluids would occur. Consequently, maintaining an adequate fluid density in the wellbore is critical to safely carry out any drilling operation.

2.1.2 Remove Drill Cuttings from the Well

When the drill bit penetrates the formation, drill cuttings are generated. The circulating system in a drilling rig is designed to pump down a fluid that carries the drill cuttings up to the annulus and out of the well, the cuttings are then removed by the solids control equipment on surface and the fluid is circulated back into the system. From the drilling fluid properties perspective, the two critical properties that enable to remove cuttings from the well are viscosity and density; although, it is important to note that cuttings removal, in other words hole cleaning, is a function of several different factors beyond fluid properties, including well inclination, hole size, ROP, RPM, pumping rate, cuttings size and shape, cuttings density, etc.

Later in this chapter further details are given on the fundamentals of fluid density and viscosity, for now, it is sufficient to address that density improves cutting removal by increasing the buoyancy forces acting on the drill cuttings, whereas viscosity gives the fluid the ability to suspend solid particles in both static and dynamic conditions. It is worth mentioning that a trade-off exists between the fluid properties needed to clean the hole and the Equivalent Circulating Density (ECD); as the fluid becomes thicker, the frictional pressure losses in the annulus increase, thus increasing the ECD; similarly, if the fluid density increases so does the ECD. Thereafter, the Drilling Engineer, in close coordination with the Drilling Fluids Engineer, has to determine the balance point between mud properties and operational parameters that ensures an adequate hole cleaning, and that minimizes the potential for drilling related problems.

2.2 Drilling Fluid Properties

As previously noted, for the purposes of this experimental study, we shall solely elaborate further on the two critical fluid properties that are relevant to understand the findings of this investigation, namely density and viscosity, other fluid properties used to characterize the drilling fluid are beyond the scope of this document.

2.2.1 Density

Density, most commonly referred to as mud weight, is the most significant fluid property, yet the easiest to quantify. It is defined as mass per unit volume, and it is usually expressed as kilograms per cubic meter [kg/m^3], pounds per gallon [lb/gal], or in specific gravity [SG]. The fluid density ultimately determines the hydrostatic pressure exerted by the fluid column, hence the importance of accurately controlling the mud weight to be as close as possible to the target value defined in the well planning stage.

Fluid density is commonly increased by adding weighting agents such as barite or hematite, and typically decreased by means of dilution using the base fluid of the mud system, namely base oil or water. In the present study, the density of the different formulations was achieved by adjusting the salt content of the sodium chloride brine, this is the preferred method for reservoir drill-in fluids and completions brines, since the conventional weighting agents significantly increase formation damage.

One important consideration that is often disregarded is the effect of temperature and pressure in the fluid density. All fluids expand as temperature increases, and compress as pressure increases; these competing effects tend to offset each other but there is always one dominating characteristic. When the net result is a decrease in the Equivalent Static Density (ESD) at downhole conditions, it is said that the well is *temperature dominated*; conversely, if the net result is an increase in the ESD, it is said that the well is *pressure dominated*. The degree of the effect is directly dependent of the type of base fluid used in the mud formulation; being oil-based fluids the most affected due to their higher compressibility. In critical applications such as HPHT or ERD wells, it is of utmost importance to thoroughly evaluate the effect of pressure and temperature in the fluid density to prevent any potential drilling problems.

The selection of the adequate fluid density is the result of a comprehensive examination of the formation and well characteristics including formation pore pressure, collapse pressure, horizontal stresses, formation fracture pressure, etc. For our intend, it suffices to say that an insufficient fluid density can lead to well control and wellbore stability issues, whereas an excessive mud weight may result in lost circulation and stuck pipe incidents; consequently, it is vital to understand the basic mechanisms affecting the drilling fluid density in the well.

2.2.2 Viscosity

Viscosity can be described as the resistance of a fluid to flow. We frequently encounter the term *thickness* describing how viscous a fluid is, where a *thick* fluid refers to a high-viscosity mud, and contrarywise, a *thin* fluid indicates a low-viscosity formulation. When reviewing a drilling fluids report, you may find several terms denoting viscosity, so it is necessary to always clarify what the value represents; some of the common headings are:

- Marsh Funnel Viscosity
- Plastic Viscosity (PV)
- Apparent Viscosity
- Low Shear Rate Viscosity (LSRV)
- Effective Viscosity

The *funnel viscosity* is measured using the Marsh Funnel, further details of the testing procedure are given in the next subsection. Funnel viscosity is used as a relative indicator of fluid condition. It does not provide sufficient information to determine the rheological properties or flow characteristics of a fluid; it is only used to detect relative changes in the fluid properties [1].

The other terms for viscosity can be described in terms of the ratio of the shear stress (τ) to the shear rate (γ). By definition:

$$\text{Viscosity } (\mu) = \frac{\text{Shear stress } (\tau)}{\text{Shear rate } (\gamma)} \tag{2.1}$$

This relationship between shear rate and shear stress for a fluid defines how that fluid flows. Figure 2.1 is a simplified depiction of two fluid layers (A and B) moving past each other when a force has been applied. When a fluid is flowing, a force exists in the fluid that opposes the flow; this force is known as the shear stress, and it can be thought of as a frictional force that arises when one layer of fluid slides by another. Since it is easier for shear to occur between layers of fluid than between the outermost layer of fluid and the wall pipe, the fluid in contact with the wall does not flow. The rate at which one layer is moving past the next layer is the shear rate, thus the shear rate is a velocity gradient [1].

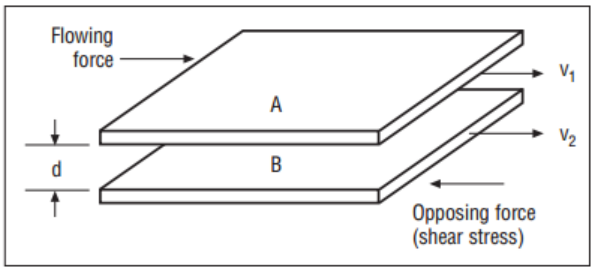

Figure 2.1. Shear rate and shear stress [1]

The formula for the shear rate is [1]:

$$\gamma\ (\sec^{-1}) = \frac{V_2 - V_1}{d} \tag{2.2}$$

Where:

γ	Shear rate [s^{-1}]
V_2	Velocity at Layer B [m/s]
V_1	Velocity at Layer A [m/s]
d	Distance between A and B [m]

The testing method to determine rheology will be discussed later in this chapter, but for illustrative purposes it is convenient to introduce at this point the relations that are commonly used in the oilfield to calculate shear rate and shear stress from the viscometer data obtained with the methodology to be presented.

The shear rate can be found by multiplying the viscometer rotational speed (ω) by a factor given by the specifications of the rheometer, particularly by the geometry of the rotor-bob-torsion spring combination; the most common configuration of these elements is referred to as *R1-B1-F1*. The endorsed values by the API Recommended Practice 13B-2 *Recommended Practice for Field Testing Oil-Based Drilling Fluids* are given below [2].

$$\gamma\ (\sec^{-1}) = 1.7023 \times \omega \tag{2.3}$$

Likewise, to calculate shear stress we use the following expression, where shear stress is reported in standard oilfield units as the pounds of force per hundred square feet ($lb/100ft^2$) required to maintain the shear rate, and where θ represents the mud viscometer dial reading:

$$\tau\ \left(lb/100ft^2\right) = 1.065 \times \theta \tag{2.4}$$

A word of caution to the reader, the values presented above are the same when testing water-based drilling fluids, they can be consulted in the API Recommended Practice 13B-1 *Recommended Practice for Field Testing Water-based Drilling Fluids* [3]. You are also encouraged to explore further the details of the rheometer configurations and specifications in the following reference for the Fann® Model 35 Viscometer [4].

The concepts of shear rate and shear stress apply to all fluid flow. Within a circulating system, shear rate is dependent on the average velocity of the fluid in the geometry in which it is flowing. Thus, shear rates are higher in small geometries (e.g. inside the drillstring), and lower in larger geometries (e.g. casing and riser annuli). Higher shear rates usually cause a greater resistive force of shear stress. Therefore, shear stresses in the drillstring - where higher shear rates exist - exceed those in the annulus - where lower shear rates exist. The sum of pressure losses throughout the circulating system, in other words the pump pressure, is often associated with shear stress while the pump rate is associated with shear rate [1].

The viscosity of a Non-Newtonian fluid changes with shear. The *Effective Viscosity (μ_e)* of a fluid is a fluid's viscosity under specific conditions; these conditions include shear rate, pressure and temperature [1].

The effective viscosity is sometimes referred to as the *Apparent Viscosity (μ_a)*. The apparent viscosity is reported as either the mud viscometer reading at 300 RPM (θ_{300}) or one-half of the meter reading at 600 RPM (θ_{600}). It should be noted that both of these apparent viscosity values are consistent with the following viscosity formula [1]:

$$\mu_a \text{ (cP)} = \frac{300 \text{ x } \theta}{\omega} \tag{2.5}$$

Plastic Viscosity (μ_p) can be described as that part of resistance to flow caused by mechanical friction. Mostly, it is affected by the solids concentration in the fluid, the size and shape of those solids, and the viscosity of the fluid phase. The plastic viscosity is also calculated from the viscometer data using the relation presented below, which is given by the API Recommended Practice 13B-2 *Recommended Practice for Field Testing Oil-Based Drilling Fluids* [2].

$$\mu_p \text{ (cP)} = \theta_{600} - \theta_{300} \tag{2.6}$$

Drilled solids adversely affect rheological properties of the fluid and are undesirable. They are continually being added to the fluid while drilling, causing an increase in solids concentration. If the solids are not removed promptly, they continue to break up into smaller pieces as they are circulated and recirculated through the system.

Viscosity problems will occur if drilled solids are not controlled; there are three main ways to cope with them, namely, solids control equipment, settling, and dilution or displacement. Changes in plastic viscosity can result in significant changes in pump pressure while drilling; this is extremely critical in wells where ECD management is of utmost importance. It is imperative to minimize plastic viscosity in these situations, because a low PV can result in greater energy at the bit, greater flow in the annulus for hole cleaning, as well as less wear and tear on the equipment [1].

2.3 Conventional Testing of Drilling Fluids

The American Petroleum Institute (API) is widely recognized as the entity that develops the standards and recommended practices in many aspects of the petroleum industry value chain. The API has compiled the recommended standard testing procedures to evaluate drilling fluid properties in the API Recommended Practices 13B-1/13B-2 *Recommended Practice for Field Testing Water/Oil-Based Drilling Fluids* [3] [2], respectively. The following section summarizes the testing procedures relevant for this experimental study, namely, determining density and viscosity, you can consult the references provided for any other tests.

2.3.1 Determination of Drilling Fluid Density (Mud Weight)

The mud balance is the instrument generally used for drilling fluid density determinations, see Figure 2.2. It should be of sufficient accuracy to measure within 0.1 lb/gal. The mud balance is designed such that the drilling fluid holding cup, at one end of the beam, is balanced by a fixed counterweight at the other end, with a sliding-weight rider free to move along a graduated scale. A level-bubble is mounted on the beam to allow for accurate balancing. The instrument should be calibrated frequently with fresh water, e.g. bi-weekly or weekly [2]. It is vital that the user understands that any density measurement generated with a mud balance shall be referenced to the temperature at which the reading was taken; the reason behind this is that any future density comparisons have to take into consideration the thermal effects affecting the mud weight, as previously described in section 2.2.1 of this document.

Figure 2.2. Metal mud balance complete with carrying case [5]

In recent years, an improved method for density determination has gained popularity particularly in field applications where ECD control is of critical importance, that of the pressurized mud balance, see Figure 2.3. The pressurized mud balance provides a more accurate method for determining the density of a drilling fluid containing entrained air or gas than does the conventional mud balance. The pressurized mud balance is similar in operation to the conventional mud balance, the difference being that the drilling fluid sample is placed in a fixed-volume sample cup under pressure. The purpose of placing the sample under pressure is to minimize the effect of entrained air or gas upon drilling fluid density measurements. By pressurizing the sample cup, any entrained air or gas is decreased to a negligible volume, thus providing a drilling fluid density measurement more closely in agreement with that obtained under downhole conditions [2].

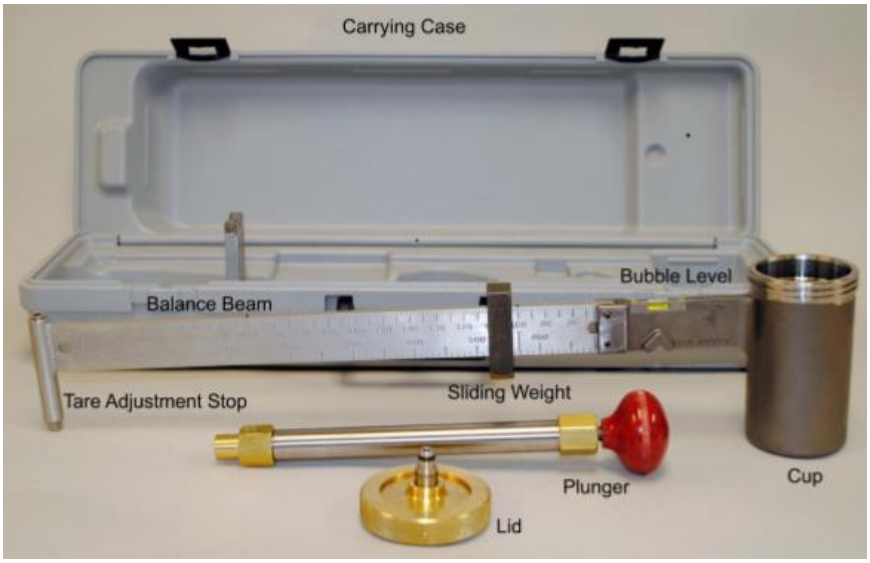

Figure 2.3. TRU-WATE™ fluid density balance [6]

The pressurized mud balance has been selected as the standard method for density measurements in the course of this investigation. It is recommended that any future work to be done using the flowloop system is correlated with laboratory density measurements using solely the pressurized mud balance. Needless to say, both density values shall be accompanied by the corresponding reference temperature at which the test is performed; for the present work, all testing was conducted at room temperature, but still this has to be clearly noted.

A detailed testing procedure to operate the pressurized mud balance has been excerpted from the API Recommended Practice 13B-2 *Recommended Practice for Field Testing Oil-Based Drilling Fluid*, and it is presented in Appendix A of this thesis.

2.3.2 Determination of Viscosity Using the Marsh Funnel

The Marsh funnel provides a rapid indication of relative changes in the mud viscosity. It is a simple test routinely run by the Derrickman while drilling or circulating, usually every 15 minutes or whenever the density check is done (although this varies depending on the Drilling Contractor's and Operator's requirements). The Marsh funnel is named after Hallan N. Marsh who published in 1931 the design and use of this viscometer.

Funnel viscosity is the ratio of the speed of the fluid as it passes through the outlet tube (shear rate) to the force (weight of the fluid) causing the fluid to flow (shear stress) [7]. It is expressed as the time in seconds required for a volume of fluid equal to 1 quart (one quarter of gallon ~ 946ml) to flow through the outlet tube of the Marsh funnel. As reference and calibration value, one quart of fresh water should be collected in 26 seconds (±0.5) at a temperature of 70 °F (±5).

The Marsh funnel, see Figure 2.4, is a conical-shaped funnel of 6 in. (152.4 mm) diameter at the top and 12 in. (304.8 mm) long. At the bottom, a smooth-bore tube 2 in. (50.8 mm) long having an inside diameter of 3⁄16 in. is attached in such a way that there is no constriction at the joint. A wire screen having 1⁄16-in. openings, covering one-half of the funnel, is fixed at a level of 3⁄4 in. (19 mm) below the top of the funnel to remove large particles that might plug the tube [1].

Figure 2.4. Marsh funnel and measuring cup [7]

Funnel viscosity is used as a relative indicator of fluid condition. It does not provide sufficient information to determine the rheological properties or flow characteristics of a fluid [1]. It is only used to detect relative, and often sudden changes in the drilling fluid viscosity so that corrective action can be adequately taken by the Mud Engineer.

2.3.3 Determination of Viscosity Using a Direct-Reading Viscometer

Direct-reading viscometers are rotational types of instruments powered by an electric motor or a hand crank [8], they are also known as Couette viscometers, and have been the most widely used method to determine the rheological profile of a drilling fluid since their introduction to the market.

In this viscometer, drilling fluid is contained in the annular space between two concentric cylinders, the mechanism is illustrated in Figure 2.5. The outer cylinder or rotor sleeve is driven at a constant rotational velocity (RPM). The rotation of the rotor sleeve causes a viscous drag exerted by the fluid, this drag produces a torque on the bob or inner cylinder. A torsion spring restrains the movement of the bob, and a dial attached to the bob indicates its deflection [8].

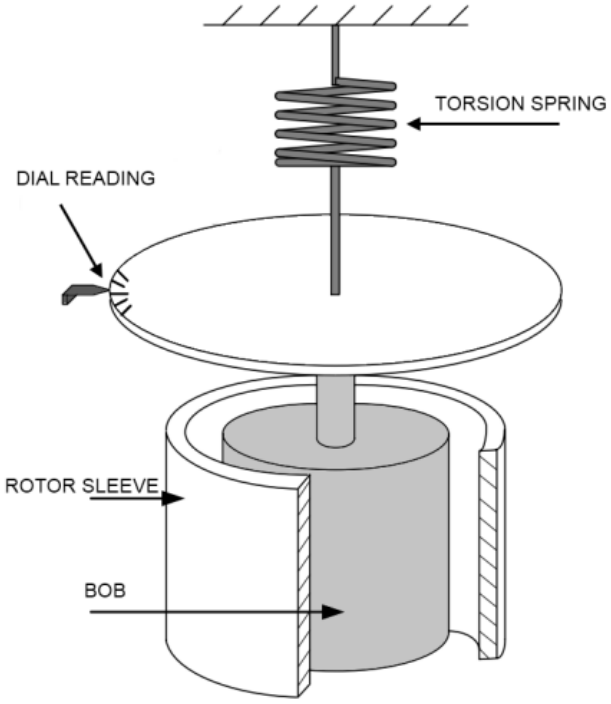

Figure 2.5. Concentric cylinder viscometer [8]

Several models of direct-reading viscometers are available in the market, they differ on the available rotational speeds, driving mechanism, etc. The most common type is the 115 volt version, see Figure 2.6, which is powered by a two-speed motor to obtain readings at 600, 300, 200, 100, 6 and 3 RPM. This model operates with the standard rotor-bob-torsion spring combination, referred to as R1-B1-F1, this geometry of the arrangement allows to obtain Plastic Viscosity and Yield Point values directly from the θ_{600} and θ_{300} readings. Other rotor-bob-torsion combinations may be used to evaluate different shear rates, but they are almost never used in field applications.

Figure 2.6. Fann® model 35SA viscometer [4]

Once more, it is important to emphasize that the rheological data obtained with the rotational viscometer has to be referenced to the temperature at which the test was conducted. The standard temperature to perform this test proposed by the API Recommended Practice 13B-2 *Recommended Practice for Field Testing Oil-Based Drilling Fluid* is 120 °F (±2 °F); although it is not uncommon for Mud Engineers to carry out the test at two additional temperatures, 40 °F and 150 °F, this is particularly instructed in deepwater wells and HPHT developments.

The present experimental study was performed using a conventional direct-reading viscometer like the one shown above, nevertheless, it is beneficial to bring to the attention of the reader that some other viscometers are available for special applications, for example the Fann® Model 70 which works under the same principle as the conventional rotational type but with an operating limit of 20,000 psi and 500 °F, and which is predominantly used to test mud formulations designed for HPHT wells.

A detailed testing procedure to operate the direct-reading viscometer has been excerpted from the API Recommended Practice 13B-2 *Recommended Practice for Field Testing Oil-Based Drilling Fluid*, and it is presented in Appendix B of this thesis.

2.4 Fundamentals of Fluid Mechanics

Rheology is the study of flow and deformation of matter under the effect of applied forces. The measurement of rheological properties of a drilling fluid has been described on the previous subsection of this document; these rheological properties are directly connected to the flow characteristics and hydraulic behavior in the well. Measurement of rheological properties also makes possible mathematical descriptions of circulating fluid flow important for the following hydraulics related determinations:

- calculating frictional pressure losses in pipes and annuli,
- determining ECD of the drilling fluid under downhole conditions,
- determining flow regimes,
- estimating hole cleaning efficiency,
- estimating swab/surge pressures, and
- optimizing the drilling fluid circulating system to improve drilling efficiency [9].

The notions of shear rate, shear stress and viscosity presented in subsection 2.2.2, are fundamental to understand the flow characteristics of the drilling fluid in the well. An understanding of rheology is essential if wellsite engineering of the drilling fluid is to cost effectively complement the objective of drilling the well. Rheology and hydraulics of drilling fluids are not exact sciences, but are based upon mathematical models that closely describe the rheology and hydraulics of the fluid and do not conform exactly to any of the models. Consequently, different methods are used to calculate rheology and hydraulic parameters [10], the specifics of those methods are presented in the following analysis.

2.4.1 Classification of Fluids

Based on their flow behavior, fluids can be classified into two different types: Newtonian and Non-Newtonian. The simplest type of fluid is called *Newtonian*. The base fluids of most drilling muds (freshwater, brines, diesel oil, mineral oils, etc.) are Newtonian. In these fluids, the shear stress (τ) is directly proportional to the shear rate (γ), as shown in Figure 2.7. The curve is a straight line commencing at the origin of the graph on rectangular coordinates. Viscosity (μ) of a Newtonian fluid is the slope of this shear stress vs shear rate line. The yield stress (stress required to initiate flow) of a Newtonian fluid will always be zero [1].

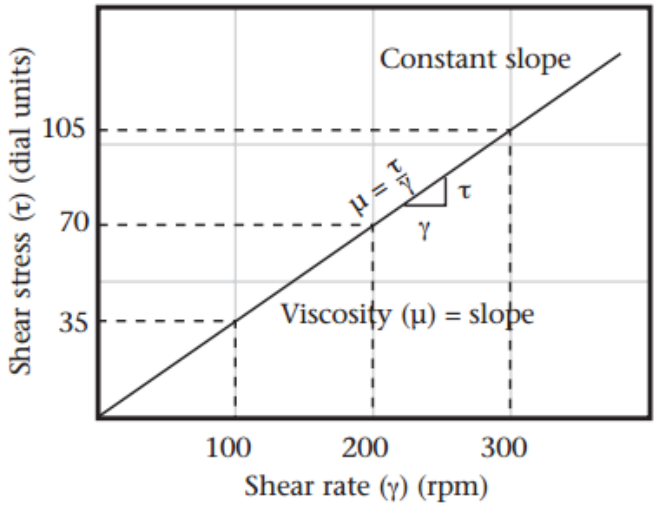

Figure 2.7. Schematic representation of a Newtonian fluid [1]

Newtonian fluids will not suspend cuttings and weighting material under static conditions. When Newtonian fluids are used for drilling, the hole should be circulated or swept clean periodically and before trips [1], as is often the case in subsea wells when drilling riserless the conductor and surface casing sections. For a Newtonian fluid, only one shear stress measurement is necessary to characterize the fluid, since it is directly proportional to the shear rate.

Non-Newtonian fluids exhibit a shear stress (τ) vs shear rate (γ) relationship as shown in Figure 2.8. Most drilling fluids fall into this category. The ratio of shear stress to shear rate is different at each shear rate. This means that a Non-Newtonian fluid does not have a single or constant viscosity that describes its flow behavior at all shear rates [1].

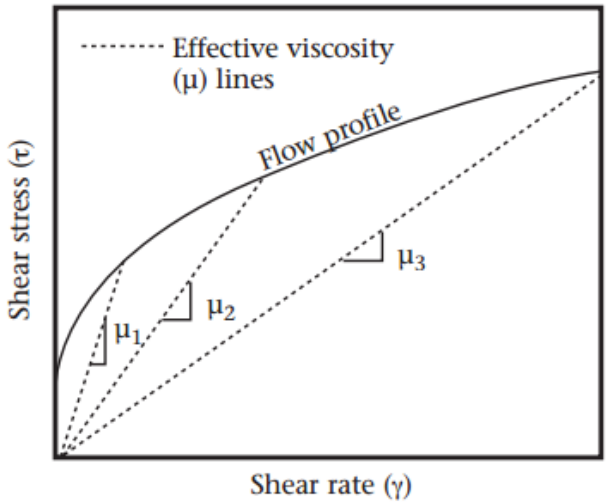

Figure 2.8. Effect of shear rate on effective viscosity of a Non-Newtonian fluid [1]

To describe the viscosity of a Non-Newtonian fluid at a particular shear rate, an *effective viscosity* is used. Effective viscosity is defined as the ratio (slope) of shear stress to shear rate at a particular shear rate, and is illustrated as the slope of a line drawn from the shear stress curve (at the shear rate of interest) back to the origin, see Figure 2.8 [1].

Most Non-Newtonian fluids exhibit *shear-thinning* behavior so that the effective viscosity decreases with increasing shear rate. As shown in Figure 2.9, when the effective viscosity is plotted alongside the shear stress vs shear rate curve, it is easy to see the shear-thinning nature that most drilling fluids exhibit [1].

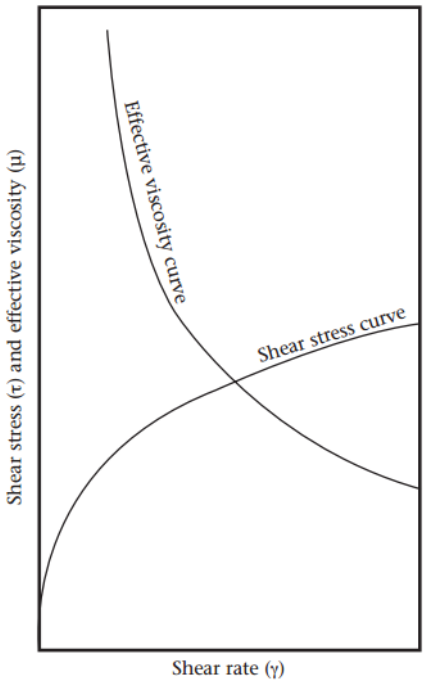

Figure 2.9. Shear-thinning effect in Non-Newtonian fluids [1]

Shear-thinning characteristics have very important implications in drilling fluids as it provides what we desire most:

- At high velocities (high shear rates) in the drillstring and through the bit, the mud shear-thins to low viscosities. This reduces the circulating pressure and pressure losses.
- At lower velocities (low shear rates) in the annulus, the mud has a higher viscosity that aids in hole cleaning.
- At ultra-low velocity the mud has its highest viscosity and when not circulating will develop gel strengths that aid in suspending weight material and cuttings [1].

2.4.2 Rheological Models

A rheological model is a description of the relationship between the shear stress and shear rate. Newton's law of viscosity is the rheological model describing the flow behavior of Newtonian fluids. It is also called the *Newtonian model*. However, since most drilling fluids are Non-Newtonian fluids, this model does not describe their flow behavior [1]. In fact, there is no generalized expression to describe all Non-Newtonian fluids, several rheological models have been developed instead, but none of them describes exactly the behavior of Non-Newtonian fluids, consequently the models to be presented next, are all mere close approximations.

We focus the following discussion on the models that are most widely used to characterize drilling fluids behavior, namely, the *Bingham Plastic*, *Power Law* and *Modified Power Law* models. Contrarywise to what was established for Newtonian fluids in the previous subsection, the models to be described henceforth require a minimum of two measurements of shear stress vs shear rate; from this information, the shear stress at any other shear rate can be determined.

The *Bingham Plastic model* has been used most often to describe the flow characteristics of drilling fluids. It is one of the older rheological models currently in use. This model describes a fluid in which a finite force is required to initiate flow (τ_o - yield point) and which then exhibits a constant viscosity with increasing shear rate (μ_p - plastic viscosity). The equation of this model is [1]:

$$\tau = \tau_o + \mu_p \cdot \gamma \tag{2.7}$$

Where:

τ	Shear stress [lb/100ft^2]
τ_o	Yield point or shear stress at zero shear rate [lb/100ft^2]
μ_p	Plastic viscosity or rate of increase of shear stress with increasing shear rate [cP]
γ	Shear rate [s^{-1}]

It is worth to note that the rotational viscometer described in subsection 2.3.3, along with the selection of the standard rotor-bob-torsion spring combination (R1-B1-F1), were initially devised to provide direct measurements of the yield point and plastic viscosity values used in the Bingham Plastic rheological model based on the θ_{600} and θ_{300} readings. Thus, it is prudent to introduce herein the expression to calculate yield point from the viscometer data, given by:

$$\tau_o \left(\text{lb}/100\text{ft}^2\right) = (2 \times \theta_{300}) - \theta_{600} \tag{2.8}$$

or

$$\tau_o \left(\text{lb}/100\text{ft}^2\right) = \theta_{300} - \mu_p \tag{2.9}$$

Most drilling fluids are not true Bingham Plastic fluids. For most muds, the true yield stress is actually less than the Bingham yield point. Figure 2.10 illustrates an actual drilling fluid flow profile with the ideal Bingham Plastic model. It shows not only the comparison of the *true yield point* to the Bingham yield point, but also shows the deviation in viscosity at low and high shear rate as compared to the Bingham Plastic viscosity [1].

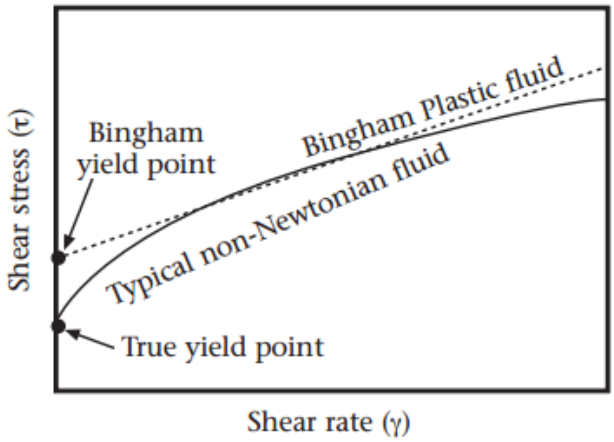

Figure 2.10. Bingham model and typical Non-Newtonian fluid [1]

The *Power Law model* attempts to solve the shortcomings of the Bingham Plastic model at low shear rates. The Power Law model is more complicated than the Bingham Plastic model in that it does not assume a linear relationship between shear stress and shear rate, as shown in Figure 2.11. However, like Newtonian fluids, the shear stress vs shear rate curve for Power Law fluids departs from the origin of the graph on rectangular coordinates [1].

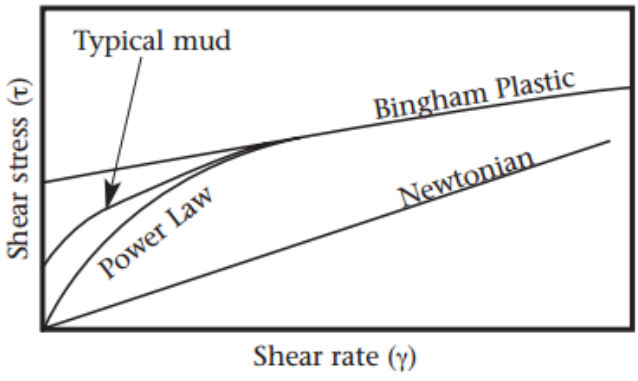

Figure 2.11. Power Law model comparison [1]

In the Power Law model, the shear stress increases as a function of the shear rate raised to some power *n*, the expression that defines this model is given by:

$$\tau = K \cdot \gamma^n \tag{2.10}$$

Where:

τ	Shear stress [$lb/100ft^2$]
K	Consistency index [$lb \cdot sec^{-n}/100ft^2$]
γ	Shear rate [s^{-1}]
n	Power Law index [dimensionless]

If we plot a Power Law fluid shear stress vs shear rate relationship on a log-log scale, we obtain a straight line as shown on Figure 2.12. In this schematic, it is easier to illustrate both indices, where the slope of the curve is *n*, and *K* is the intercept on the vertical axis.

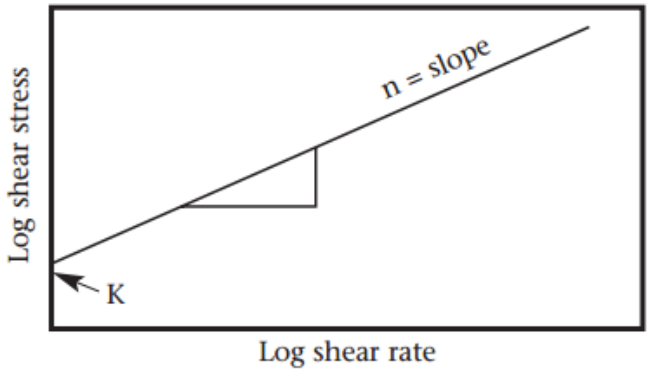

Figure 2.12. Log plot of Power Law model [1]

The consistency index *K* is the viscosity at a shear rate of one reciprocal second (sec^{-1}), so it can be said that *K* is related to the viscosity of the fluid at low shear rates. The hole-cleaning and suspension effectiveness of a fluid can be improved by increasing the *K* value. The consistency index *K* is usually reported in $lb \cdot sec^{-n}/100ft^2$, but may be reported in other units [1].

The Power Law index *n* indicates a fluid's degree of Non-Newtonian behavior over a given shear rate range. The lower the *n* value the more shear-thinning a fluid is over that shear rate range and the more curved the shear stress vs shear rate relationship is, as shown in Figure 2.13 [1].

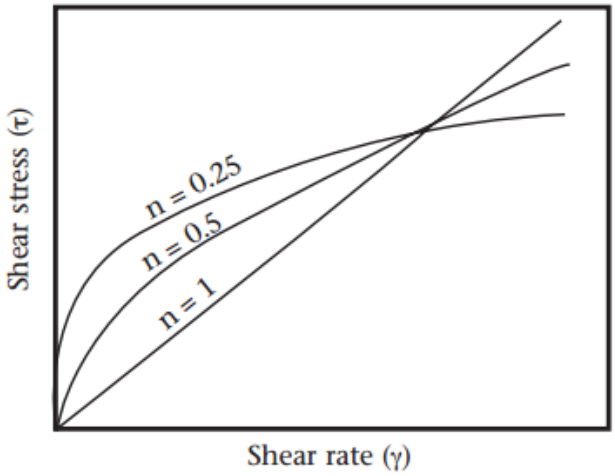

Figure 2.13. Effect of Power Law index *n* on shape of flow profile [1]

Depending on the value of *n*, three different types of flow profiles and fluid behavior exist:

- n < 1 The fluid is shear-thinning
- n = 1 The fluid is Newtonian
- n > 1 The fluid is dilatant or shear-thickening (drilling fluids are not in this category)

A comparison of a typical drilling fluid to a shear-thinning, Newtonian and dilatant fluid is shown in Figure 2.14 [1].

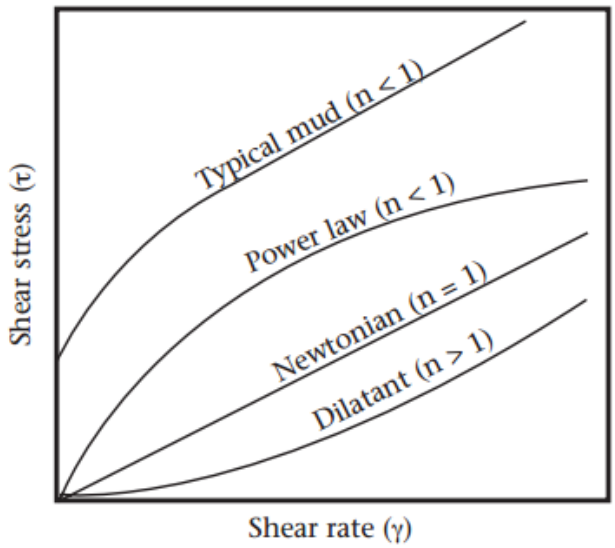

Figure 2.14. Effect of Power Law index *n* on fluid behavior [1]

The Power Law indices *K* and *n* can be obtained from the rotational viscometer readings using the following expressions:

$$n = \frac{\log\left(\frac{\theta_2}{\theta_1}\right)}{\log\left(\frac{\omega_2}{\omega_1}\right)} \tag{2.11}$$

$$K = \frac{\theta_1}{\omega_1{}^n} \tag{2.12}$$

Where:

K	Consistency index [$lb \cdot sec^{-n}/100ft^2$]
n	Power Law index [dimensionless]
θ_1	Viscometer dial reading at lower shear rate [°Fann]
θ_2	Viscometer dial reading at higher shear rate [°Fann]
ω_1	Viscometer rotational speed at lower shear rate [rpm]
ω_2	Viscometer rotational speed at higher shear rate [rpm]

The Power Law model, however, does not fully describe drilling fluids because it does not have a yield stress and underestimates LSRV, as shown previously in Figure 2.11. The *modified Power Law* or *Herschel-Bulkley model* can be used to account for the stress required to initiate fluid movement, that is yield stress [1].

Figure 2.15 demonstrates the differences between the models discussed thus far, namely *modified Power Law*, the *Power Law* and *Bingham Plastic models.* From this diagram, it is clear that the modified Power Law model is the one that more closely resembles the behavior of a typical drilling fluid, therefore the most widely used to characterize a fluid in hydraulics optimization analyses.

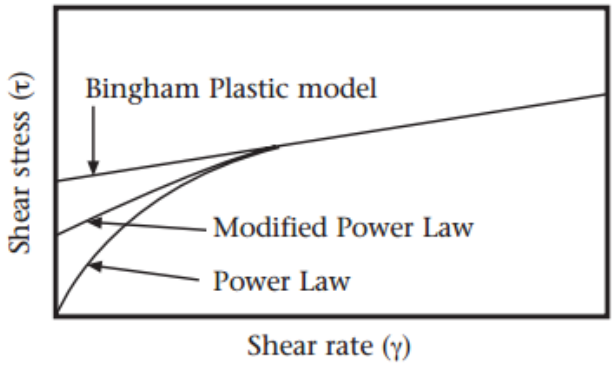

Figure 2.15. Rheological models comparison [1]

In Figure 2.15, the modified Power Law is between the Bingham Plastic model, which is highest, and the Power Law, which is lowest. The modified Power Law is a slightly more complicated model than either the Bingham Plastic or the Power Law model. However, it can approximate more closely the true rheological behavior of most drilling fluids. Mathematically the Herschel-Bulkley model is given by [1]:

$$\tau = \tau_o + K \cdot \gamma^n \tag{2.13}$$

Where:

τ	Shear stress [$lb/100ft^2$]
τ_o	Yield stress (in practice, it has been accepted to be the value for the θ_3 reading)
K	Consistency index [$lb \cdot sec^{-n}/100ft^2$]
γ	Shear rate [s^{-1}]
n	Power Law index [dimensionless]

A word of caution to the reader, some other rheological models have been developed over the years, such as the Heinz-Casson (1959) and Robertson-Stiff (1976), but we have deliberately selected the most widely used in the industry as the terms of reference for the comparison with the experimental results of this investigation.

We have now enough tools to understand the fundamentals of flow behavior prediction and its relation to hydraulics calculations, I have purposely decided to elaborate further on those concepts in next chapter, as they will be central ideas to understand the basic functioning of the flowloop system, and why they are the basis of automated measurement of drilling fluid properties using the instrumented standpipe concept.

Chapter 3

Automated Characterization of Drilling Fluids

This chapter is intended to explain in detail the principles behind the automated characterization of drilling fluids using the instrumented standpipe concept. The first section is dedicated to an overall description of the flowloop setup build at the University of Stavanger. Then, the reader will be presented with a review of the basic hydraulics concepts upon which the flowloop functioning is based. Lastly, I shall provide you with a thorough discussion of the mathematical models and algorithms used to calculate fluid properties based on the data acquired with the flowloop setup.

3.1 The Instrumented Standpipe Concept

The reasoning behind the instrumented standpipe concept it to use accurate pressure sensors installed in the surface connections of the circulating system in a drilling rig, in order to measure differential pressures in real-time that would then be used to calculate density and viscosity of the fluid being pumped into the hole. This would allow the Driller to monitor closely the fluid properties like any other drilling parameter. In drilling rigs where a density meter is installed in the flowline, for example where a coriolis meter is available, a continuous automated comparison of the fluid properties in and out of the well could then be feasible.

The automatic measurement of drilling fluid properties based on the instrumented standpipe concept does not intend to eliminate the periodic mud checks conducted by both the Derrickman and the Mud Engineer; it should be conceived as a tool to allow real-time monitoring of what is being pumped downhole. Nonetheless, in non-critical applications that do not demand such a tight control over the ECD, we could rely on the system to provide fluid properties monitoring and reduce the need for manual checks.

Figure 3.1 illustrates a simplified schematic of the instrumented standpipe concept. There are four pressure sensors installed, two in the horizontal section, and two in the vertical section. The pressure sensors could be installed at any point between the discharge of the mud pumps and the rotary hose. Although, one caveat in this experimental study is the assumption that in this segment of the surface connections, there are at least two sections, one vertical and one horizontal, with the same pipe diameter, the same length, and the same pipe roughness.

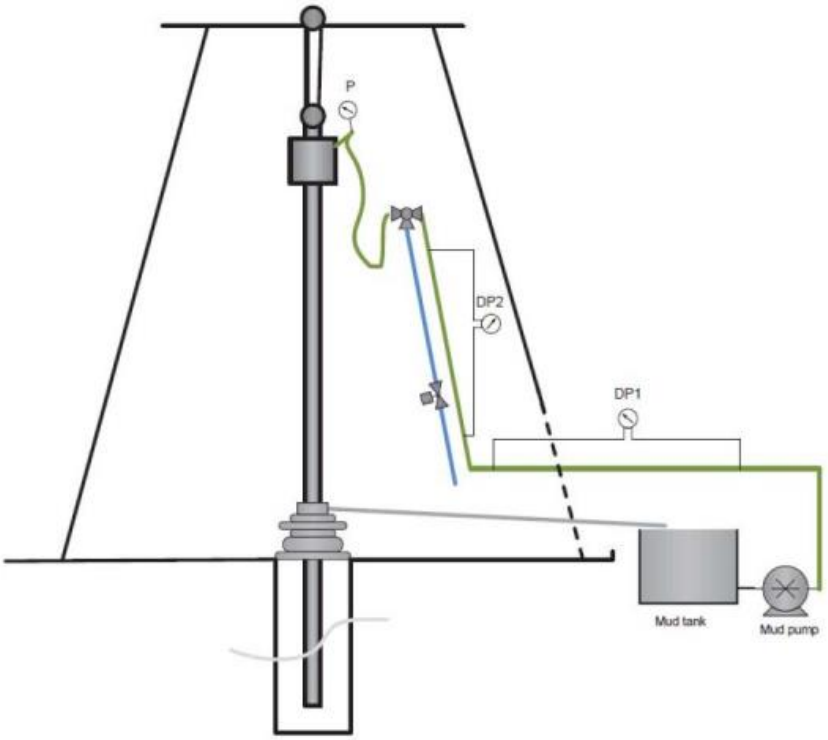

Figure 3.1. Simplified schematic of the instrumented standpipe concept [11]

In the schematic, the horizontal differential pressure between pressure sensors 1 and 2 is given by *DP1*, from now on referred to as dP_{hor}; whereas the vertical differential pressure between pressure sensors 3 and 4 is given by *DP2*, correspondingly denoted as dP_{ver}. The working principle of the instrumented standpipe concept is to measure first the dP_{hor}, and since there is no gravitational effect on the horizontal section of the pipe, all pressure losses in this segment are presumed to be caused by friction. Now, the differential pressure in the vertical section, dP_{ver}, is the result of both frictional and gravitational pressure losses; but as stated before, the assumption is that the pipe size, length, and roughness are the same in both sections, thus the frictional pressure losses are equal in both pipe segments. Consequently, we can net both values dP_{ver} - dP_{hor}, to obtain the gravitational pressure losses, which result is then used to back-calculate the fluid density. Once the first fluid property is determined, we utilize the algorithm described later in this chapter to finally obtain the fluid viscosity.

3.2 Experimental Flowloop Setup

An experimental setup was built at the University of Stavanger in 2016 to replicate in scale the instrumented standpipe concept. The flowloop was developed as part of a Bachelor's thesis [12] project, and ever since it has been used to further investigate the applicability of the concept. The description to be presented next is based on the original document.

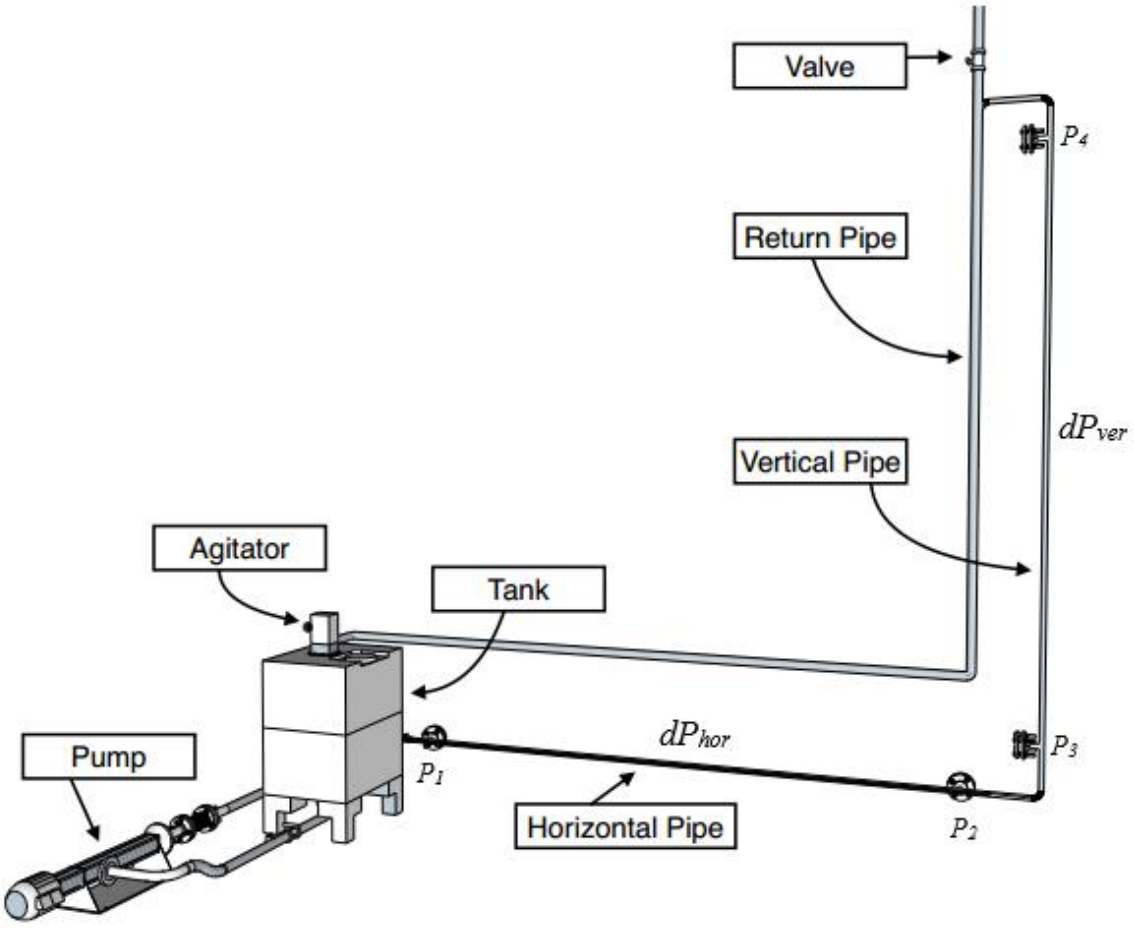

Figure 3.2. Schematic of the experimental flowloop setup at UiS [12]

The setup is a flowloop system that consists of a suction/return tank, a pump, one discharge line of 24mm inner diameter, one return pipe of 50mm inner diameter, and two differential pressure sensors distributed as shown in Figure 3.2. Other components not shown in the schematic above include: aluminum support structure, a flowmeter on the pump discharge, one additional pressure sensor to monitor pump pressure, temperature and fluid level sensors inside the tank, and all the electrical installation to power up the system and to transmit data to/from the computer.

Transparent acrylic pipes connected with PVC fittings are used in the setup; the pipes are fixed to the aluminum structure with clamps. The return pipe was purposely selected to be of a larger diameter (50mm) in order to reduce the pressure losses in the system [12]; this has been identified as an area of improvement in the design, since the difference in diameter causes a large degree of turbulence and bubbles in the vertical section of the return line when first filling the flowloop with fluid, this is particularly difficult to deal with the more viscous the fluid is.

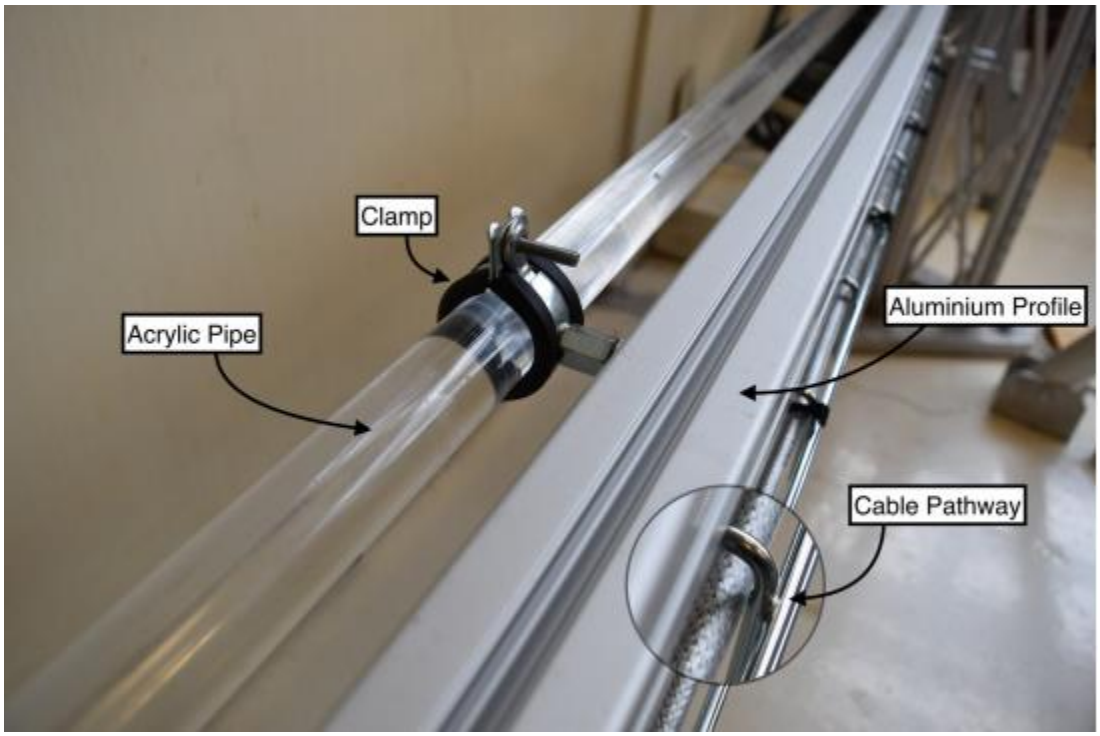

Figure 3.3. Section of discharge pipe (24mm) attached to the aluminum support structure [12]

A 200 liters rectangular tank with conical bottom stores the fluid in the system. The tank is equipped with an agitator (although it was never used during the experimental runs), a temperature sensor and a fluid level sensor, both of which are connected to the data acquisition system. The suction is on the bottom part, and the return line is connected as shown in Figure 3.4. It is worth to mention that a pipe extension was installed inside the tank to minimize the turbulence generated when the fluid is discharged; in spite of this, some air bubbles are still re-circulated through the flowloop. One further opportunity to optimize the system design is to install one additional interconnected tank to have independent suction and return containers, which emulates closer the pit system in a drilling rig. Alternatively, some kind of divider can be installed in the current tank to allow air bubbles to be released before the fluid spills over to the suction compartment.

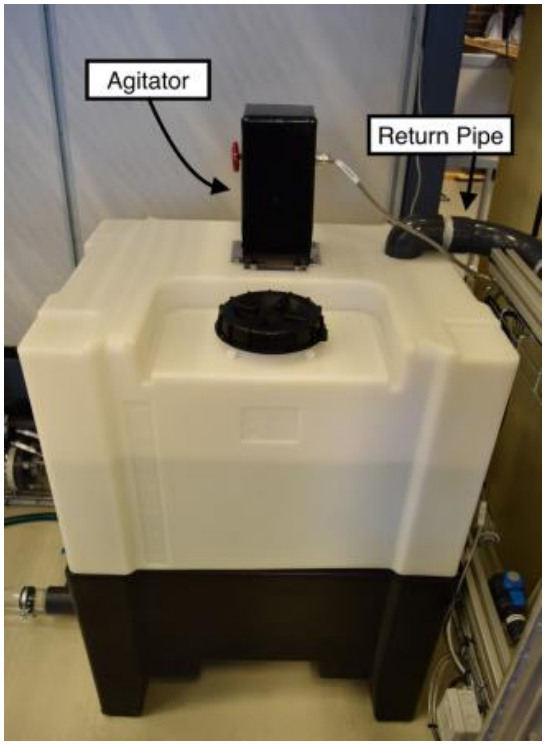

Figure 3.4. Rectangular tank used in the flowloop setup [12]

The pump is a mono progressing cavity screw pump with a maximum output of 95 liters per minute, see Figure 3.5. It was selected because of its ability to pump at very low rates, relatively low pressure pulses, and because of positive experiences from past projects in the laboratory [12]. A magnetic flow meter is used to accurately measure the volumetric flow delivered by the pump. In addition, a pressure sensor is installed close to the pump outlet to monitor the pump pressure which is limited to 2 bar [12].

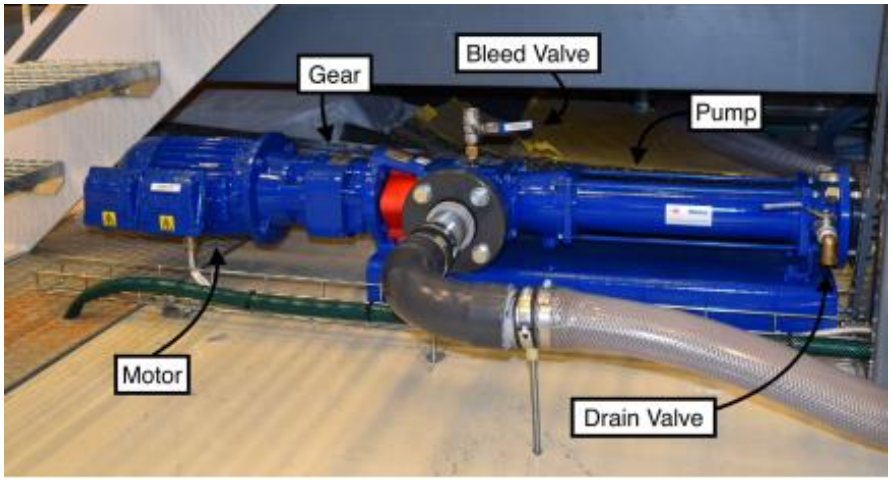

Figure 3.5. Mono progressing cavity pump, type C1XKS81RMA [12]

Two differential pressure sensors are installed as illustrated in Figure 3.2. The distance between the sensors in the horizontal and vertical sections is the same, 3.5m. The sensor used in the horizontal section has a measuring range of 6 - 600 mbar, whereas the one in the vertical section has a higher range of 16 - 1600 mbar to measure the additional gravitational pressure losses [12].

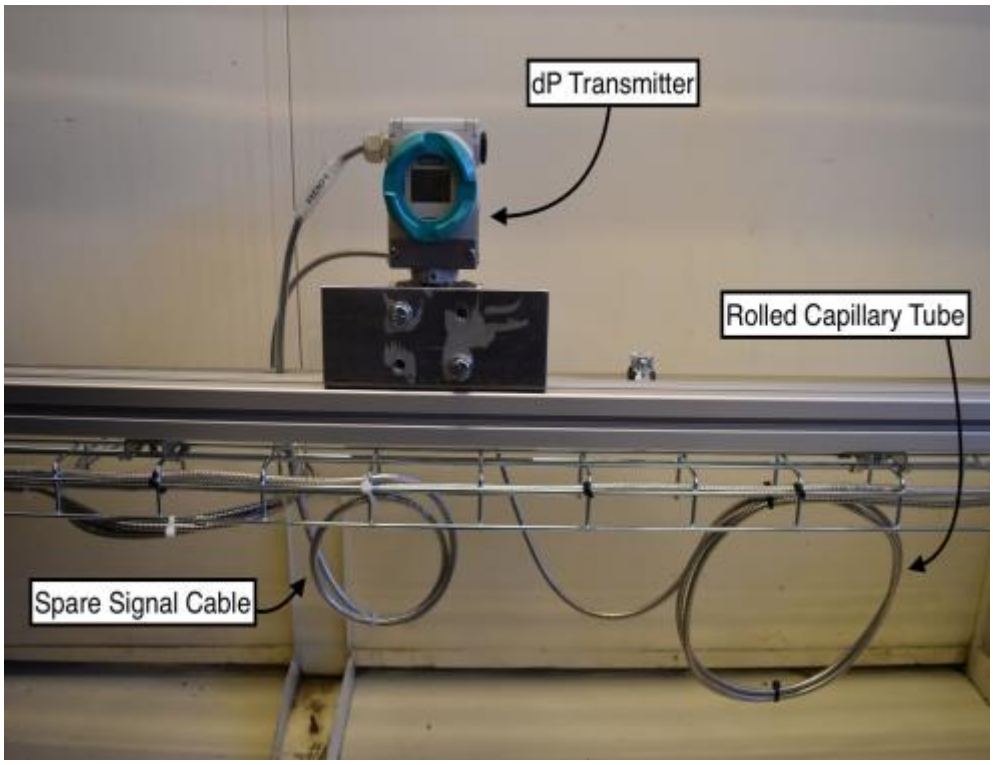

Figure 3.6. Differential pressure sensor mounted in the horizontal section of the flowloop [12]

The interface between the instrumentation and the dedicated computer is established via a communication card type NI PCIe-6321 *Multifunction Data Acquisition Device*; the details of the connections and configuration can be accessed in the reference herein provided [12]. MATLAB® and Simulink® are used for data acquisition and processing; the results to be presented in Chapter 4 of this thesis have been obtained from the MATLAB® and Simulink® tools designed for the control system. A flow chart of the data acquisition system is presented in Figure 3.7.

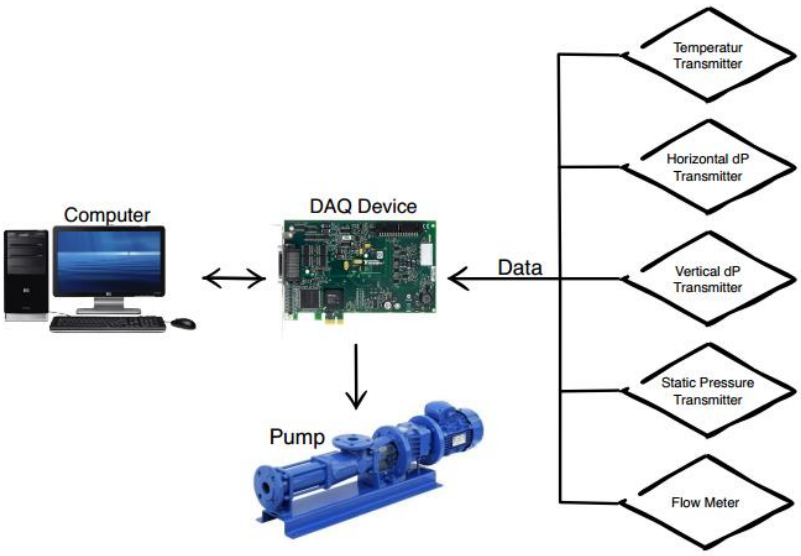

Figure 3.7. Flow chart of the data acquisition system [12]

Figure 3.8 shows the main window in Simulink®. Desired flow rate can be set with a constant varying from 0 - 90 liters per minute. Based on the set-point and the measurements from the flow meter, a PI-controller is actively regulating the pump. It is also possible to select a ramp function, where the pump rate is increasing linearly over time to a maximum [12].

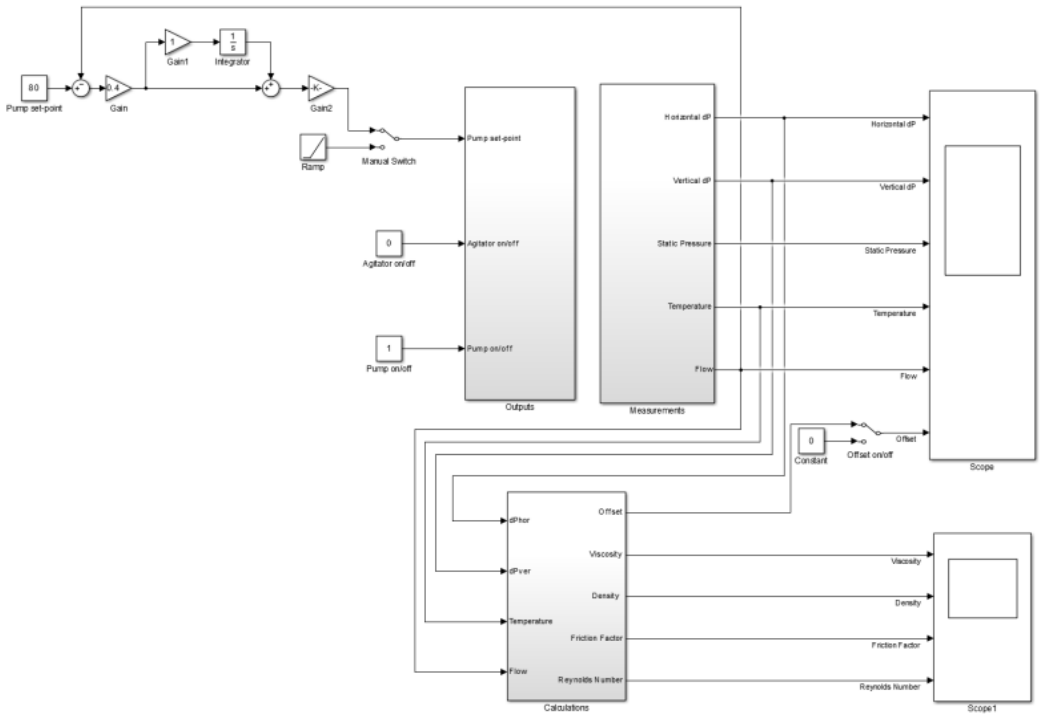

Figure 3.8. Main user interface in Simulink® [12]

Figure 3.9 shows how the *Multifunction Data Acquisition Device* receives signals from the sensors and how this information is then received by Simulink®. Each sensor installed in the flowloop setup has an associated Low-Pass filter that aids to the data processing.

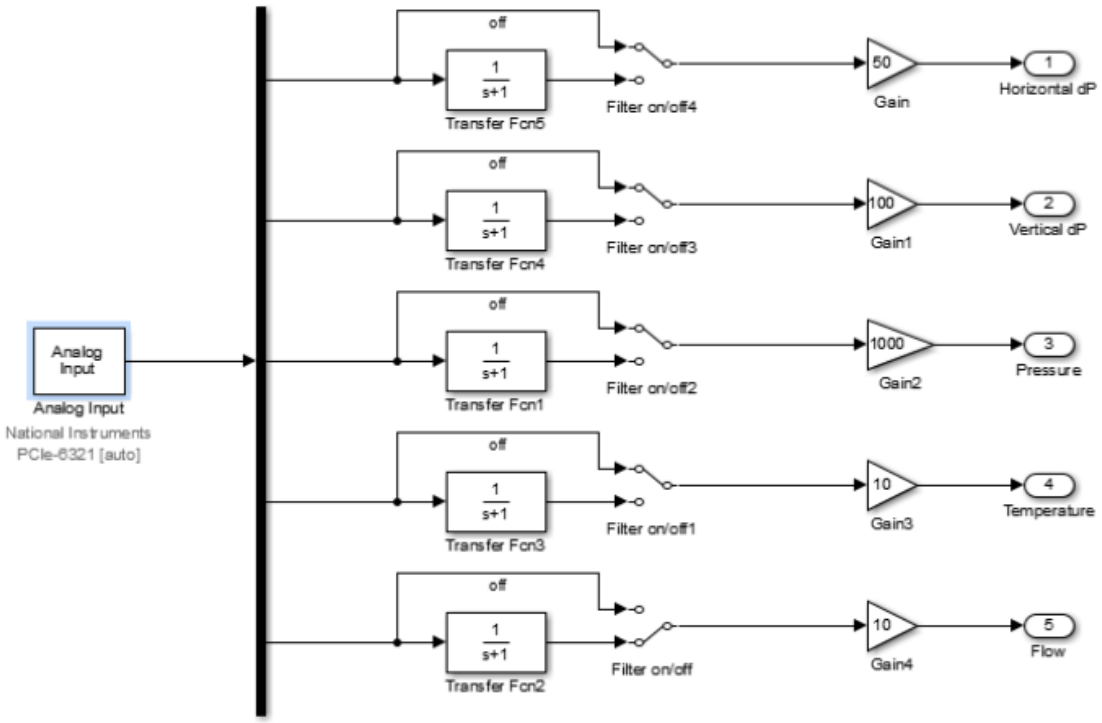

Figure 3.9. Simulink® diagram shows data transferring and processing from the sensors [12]

3.3 Drilling Fluid Hydraulics

Once the rheological properties of a fluid have been determined using the testing procedures discussed in subsection 2.3, and subsequently modeled to predict flow behavior according to the concepts presented in subsection 2.4, it is possible then to perform the hydraulics calculations necessary to determine what the effect of the fluid will be on the overall pressures in the system. The central notion that has to be fully comprehended by those involved in a drilling operation, is that of *pressure losses*. From the drilling optimization perspective, we are particularly interested in the total pressure losses in the system (pump pressure), pressure losses across the bit, and pressure losses in the annulus (ECD).

This experimental study uses the concept of *pressure losses* as the starting point to determine density and viscosity of the fluid in the system. This section is intended to provide an introduction to better understanding the algorithm used in the automated measurement of drilling fluid properties using the instrumented standpipe concept.

3.3.1 Flow Regimes

In 1883, Osborne Reynolds conducted experiments with various liquids flowing through glass tubes. He introduced a dye into the flowing stream at various points. He found that when the flow rate was relatively low, the dye he introduced formed a smooth, thin, straight streak down the glass. There was essentially no mixing of the dye and liquid. This type of flow in which all the fluid motion is in the direction of flow is called *laminar flow* [10].

Reynolds also found with relatively high flow rates, no matter where he introduced the dye it rapidly dispersed throughout the pipe. A rapid, chaotic motion in all directions in the fluid caused the crosswise mixing of the dye; this type of flow is called *turbulent flow*. Reynolds showed further that under some circumstances, the flow can alternate back and forth between being laminar and turbulent; when that happens, it is called *transitional flow*. Therefore, we can describe a fluid's flow as being either laminar, turbulent, or transitional [10].

In *laminar* flow, a Newtonian fluid flowing in a circular pipe moves as concentric layers as shown in Figure 3.10. Each layer represents a different *ring* of velocity vectors, meaning that the fluid velocity is dependent of the position in the cross-section of the pipe.

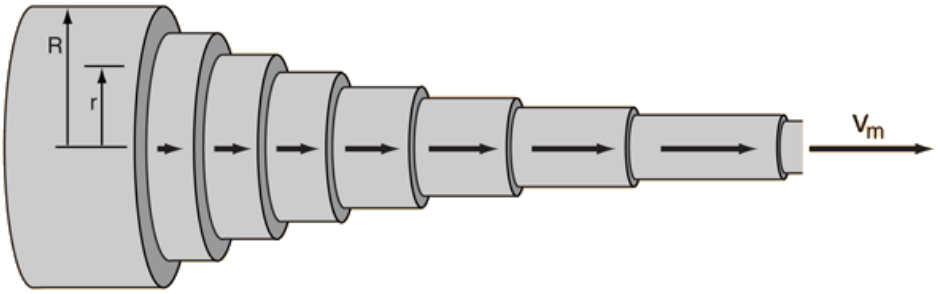

Figure 3.10. Three-dimension view of laminar flow in a pipe for a Newtonian Fluid [10]

The variation of velocity as a function of position is better illustrated in a two-dimensional representation of the fluid flow in the pipe. A typical velocity profile of a Newtonian fluid is shown in Figure 3.11. The flow profile is in the form of a parabola or bullet shape. The rate of change of velocity with distance (shear rate) is the slope of the velocity profile at any point in the pipe. At the pipe wall, the slope of the velocity profile is parallel to the pipe wall and has an infinite slope (maximum). In the center of the pipe, the slope of the velocity profile is perpendicular to the pipe wall and has a zero slope (minimum) [1]. Considering that for a Newtonian fluid, the shear stress and shear rate are directly proportional, the shear stress is also maximum at the wall and zero at the center of the pipe.

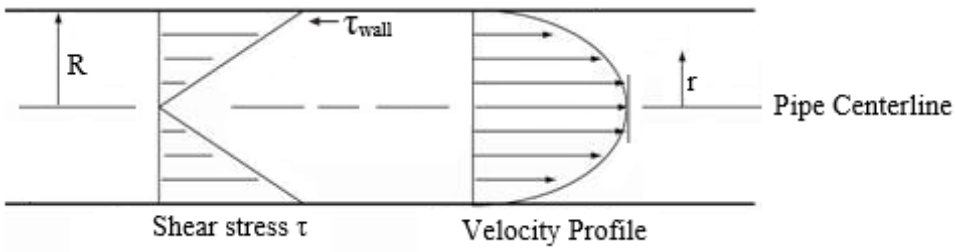

Figure 3.11. Two-dimension view of laminar flow in a pipe for a Newtonian Fluid

It is prudent at this point to introduce some additional definitions that will be used at the end of this Chapter and that are related to the discussion presented above. The following has been taken from [13] and originally referenced to [14]. In fully developed laminar flow, each fluid particle moves at a constant axial velocity along a streamline and the velocity profile remains unchanged in the flow direction. There is no motion in the radial direction, and thus the velocity component in the direction normal to flow is everywhere zero. There is no acceleration since the flow is steady and fully developed [14].

Now, consider a ring-shaped differential volume element of radius *r*, thickness *dr*, and length *dx*, oriented coaxially with the pipe, as shown in Figure 3.12 [14].

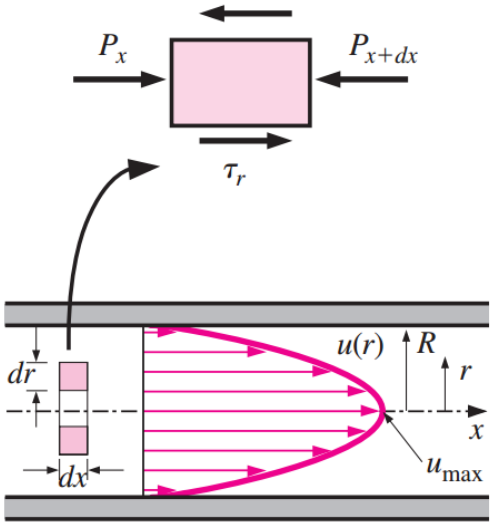

Figure 3.12. Free-body diagram of a ring-shaped differential fluid element [14]

In fully developed laminar flow, the volume element involves only pressure and viscous effects and thus the pressure and shear forces must balance each other. The pressure force acting on a submerged plane surface is the product of the pressure at the centroid of the surface and the surface area. A force balance on the volume element in the flow direction gives [14]:

$$(2\pi r \cdot \delta r \cdot P)_x - (2\pi r \cdot \delta r \cdot P)_{x+dx} + (2\pi r \cdot \delta x \cdot \tau)_r - (2\pi r \cdot \delta x \cdot \tau)_{r+dr} = 0 \qquad (3.1)$$

This indicates that in fully developed laminar flow in a horizontal pipe, the viscous and pressure forces balance each other. Dividing by $2\pi \cdot dr \cdot dx$ and rearranging [14]:

$$r \cdot \left(\frac{P_{x+dx} - P_x}{\delta x}\right) + \frac{(r \cdot \tau)_{r+dr} - (r \cdot \tau)_r}{\delta r} = 0 \qquad (3.2)$$

Taking the limit as $dr, dx \rightarrow 0$, gives

$$r \cdot \frac{\delta P}{\delta x} + \frac{\delta (r \cdot \tau)}{\delta r} = 0 \qquad (3.3)$$

Rearranging, we obtain that [13]

$$\frac{\delta P}{\delta x} \cdot r \cdot \delta r = - \tau \cdot \delta r \qquad (3.4)$$

Integrating with respect to *r*, we get

$$\tau = -\frac{\delta P}{2 \cdot \delta x} \cdot r \tag{3.5}$$

The equality must hold for any value of *r* and *x*. Consider now the element of radius *R* and length *dx* in the fully developed region, as shown in Figure 3.13 below [13]:

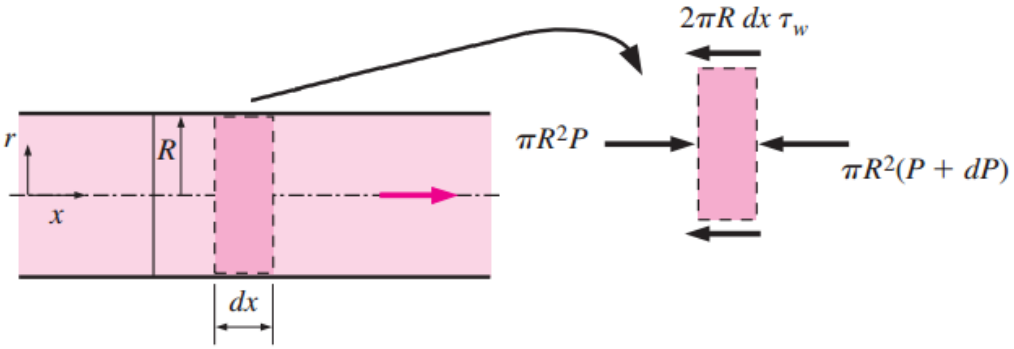

Figure 3.13. Free-body diagram of a fluid disk element in fully developed laminar flow [14]

The force balance in the disk element is given by

$$\left(\pi \cdot R^2 \cdot P\right) - \pi \cdot R^2 \cdot (P + \delta P) - (2\pi \cdot R \cdot \delta x \cdot \tau_w) = 0 \tag{3.6}$$

Simplifying

$$\frac{\delta P}{\delta x} = -\frac{2 \cdot \tau_w}{R} \tag{3.7}$$

Where τ_w is the shear stress at the wall, which is constant since the viscosity and the velocity profile are constants in the fully developed laminar flow in a horizontal pipe. Thus, we have the following:

$$\tau_w = -\frac{\delta P}{2 \cdot \delta x} \cdot R \tag{3.8}$$

Combining Equations 3.5 and 3.8, we finally get this expression for fully developed laminar flow:

$$\frac{\tau}{\tau_w} = \frac{r}{R} \tag{3.9}$$

In the case of laminar flow of *Non-Newtonian fluids*, the difference lies on the fact that the velocity profile depends upon the relationship between shear stress and shear rate; this can be clearly illustrated referring to the effect of the Power Law index *n* on the relationship between shear stress and shear rate presented in Figure 2.13. Accordingly, the effect of the Power Law index *n* is extended to the velocity profile of Non-Newtonian fluids in laminar flow as shown in Figure 3.14. The flattening of the velocity profile implies that the fluid velocity is higher over a larger area of the pipe, which results in a higher sweep efficiency and better ability of a fluid to carry larger particles, and consequently yielding an improved hole cleaning.

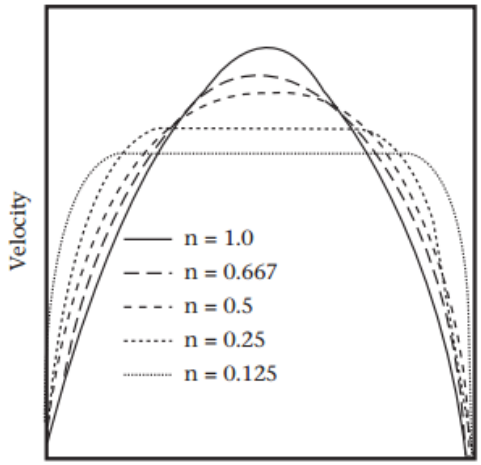

Figure 3.14. Effect of Power Law index *n* on the velocity profile of Non-Newtonian fluids [1]

Turbulent flow occurs when a fluid is subject to random, chaotic shearing motions that result in local fluctuations of velocity and direction, while maintaining a mean velocity parallel to the direction of flow. Only near the walls a thin layer of orderly shear exists; thus, the velocity profile is very steep near the walls, but essentially flat elsewhere [10] as shown in Figure 3.15. The schematic also portrays *transitional flow*, which occurs when the flow is not fully laminar nor completely turbulent.

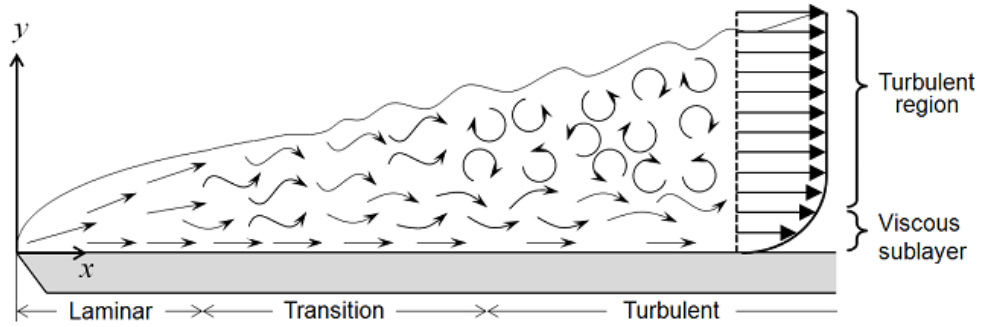

Figure 3.15. Two-dimension view of transitional and turbulent flow in a pipe section [15]

3.3.2 Determination of Flow Regime

The flow regime is determined using a dimensionless parameter known as Reynolds number. This factor takes into consideration the fluid properties and the geometry of the flow conduit. The general definition is given by the following expression.

$$Re = \frac{\rho \cdot \nu \cdot D}{\mu} \tag{3.10}$$

Where:

Re	Reynolds number [dimensionless]
ρ	Fluid density [kg/m^3]
ν	Average fluid velocity [m/s]
D	Pipe diameter [m]
μ	Fluid viscosity [Pa·s]

The calculations performed in this experimental study follow the guidelines suggested by the *API Recommended Practice 13D Recommended Practice on the Rheology and Hydraulics of Oil-well Drilling Fluids* [9], where the flow regimes are defined based on the following values of the Reynolds number.

- $Re < 2100$ Laminar flow
- $2100 < Re < 4000$ Transitional flow
- $Re > 4000$ Turbulent flow

3.3.3 Pressure Loss Calculation for Newtonian Fluids

Different factors determine the *pressure losses* in a system, i.e. fluid density and viscosity, geometry and roughness of the flow conduit, changes in elevation, distance that the fluid has to travel, etc. It is generally accepted, that the *total pressure losses* in a system are given by three different physical components: *frictional*, *hydrostatic*, and *kinetic* effects. This is expressed as:

$$(\Delta P)_{Total} = (\Delta P)_{Frictional} + (\Delta P)_{Hydrostatic} + (\Delta P)_{Kinetic} \tag{3.11}$$

As previously stated, the concept of pressure losses is the starting point to determine density and viscosity of the fluid using the instrumented standpipe concept. The kinetic effects are neglected as the pipe diameter is constant in the setup, thus this effect will not be further pursued in this text.

The concept of *frictional pressure losses* derives from the resistance experienced by fluids flowing through pipes caused by friction against the pipe wall. The frictional pressure loss is determined from the Darcy-Weisbach equation given below.

$$(\Delta P)_{Frictional} = \frac{f \cdot L \cdot \rho \cdot \nu^2}{2 \cdot D} \tag{3.12}$$

Where:

f	Friction factor [dimensionless]
L	Pipe length [m]
ρ	Fluid density [kg/m^3]
ν	Average fluid velocity [m/s]
D	Pipe diameter [m]

It is worth to introduce an additional definition used to determine the average fluid velocity based on the measured parameters in the flowloop setup, namely pump rate and cross-sectional area:

$$\nu = \frac{Q}{A} \tag{3.13}$$

Where:

Q	Pump rate [m^3/s]
A	Pipe cross-sectional inner area [m^2]

The calculation of the friction factor *f* depends on the flow regime and the conditions of the surface of the wall pipe given by the pipe roughness. Once the flow regime has been determined based on the Reynolds number as described in the previous subsection, the expression to determine the friction factor can be selected. The friction factor in *laminar flow* for a Newtonian fluid is given by the following expression:

$$f = \frac{64}{Re} \tag{3.14}$$

In *turbulent flow*, the friction factor is not only a function of the Reynolds number, it also depends on whether it is a smooth or rough pipe. Generally, in turbulent flow, the friction in the wall becomes larger, since the velocity profile is more uniform causing a larger velocity fall-off towards the pipe wall [13]. Several models have been proposed to determine the friction factor in turbulent flow, the solution used in this experimental study is the one developed by Professor S.E. Haaland of the Norwegian University of Science and Technology in 1983, it is expressed as follows:

$$\frac{1}{\sqrt{f}} \approx -1.8 \cdot \log_{10}\left[\left(\frac{\varepsilon/D}{3.7}\right)^{1.11} + \frac{6.9}{Re}\right] \tag{3.15}$$

Where:

ε	Absolute pipe roughness
D	Pipe diameter
ε / D	Relative pipe roughness

The second component of the total pressure losses expression is the *hydrostatic* effect. They are also commonly referred to as *gravitational pressure losses* and depend on the fluid density and the vertical distance that the fluid has to travel. The calculation is not a function of viscosity; hence the following expression is applicable to both Newtonian and Non-Newtonian fluids.

$$(\Delta P)_{Hydrostatic} = \rho \cdot g \cdot \Delta h \tag{3.16}$$

Where:

ρ	Fluid density [kg/m^3]
g	Gravitational constant [m/s^2]
Δh	Vertical distance [m]

3.3.4 Pressure Loss Calculation for Non-Newtonian Fluids

Additional considerations have to be made in order to determine the *total pressure losses* for Non-Newtonian fluids. As previously noted, the *hydrostatic* component is not a function of the fluid viscosity, thus it can be calculated using Equation 3.16. Now, for the *frictional pressure losses* we start the analysis from the same Darcy-Weisbach model given in Equation 3.12, but we introduce a generalized Reynolds number that is only valid for Power Law fluids, and which was first put forward by Metzner and Reed [16]:

$$Re_{PL} = \frac{\rho \cdot v \cdot D_{eff\text{-}PL}}{\mu_a} \tag{3.17}$$

Given that

$$D_{eff\text{-}PL} = \frac{4n}{3n + 1} \cdot D \tag{3.18}$$

and

$$\mu_a = K \cdot \left(\frac{8 \cdot v}{D_{eff\text{-}PL}} \right)^{n - 1} \tag{3.19}$$

Where:

Re_{PL}	Reynolds number for Power Law fluids
v	Average fluid velocity
$D_{eff\text{-}PL}$	Effective pipe inner diameter for Power Law fluids
n	Power Law index
μ_a	Apparent viscosity
K	Power Law consistency index

We need to make a further consideration to replicate closer the real behavior of a drilling fluid; as discussed in section 2.4.2 and referring particularly to Figure 2.15, most drilling fluids behave like a Modified Power Law Fluid, thus the effect of the yield stress (the force required to initiate flow) has to be taken into consideration. The model presented by Madlener, Frey, and Ciezki (2009) addressed this consideration by formulating a generalized Reynolds number valid for Herschel-Bulkley fluids. The equations are given as follows [17]:

$$Re_{HB} = \frac{\rho \cdot v \cdot D_{eff\text{-}HB}}{\mu_a} \tag{3.20}$$

Given that

$$D_{eff\text{-}HB} = \frac{4n_a}{3n_a + 1} \cdot D \tag{3.21}$$

and

$$\mu_a = K \cdot \left(\frac{8 \cdot \nu}{D_{eff\text{-}HB}} \right)^{n_a - 1} \tag{3.22}$$

The generalized flow index is given by

$$n_a = \frac{n \cdot K \cdot \left(\frac{8\nu}{D} \right)^n}{\tau_o + K \cdot \left(\frac{8\nu}{D} \right)^n} \tag{3.23}$$

We obtain the following

$$Re_{HB} = \frac{\rho \cdot D^n \cdot \nu^{(2-n)}}{\frac{\tau_o}{8} \cdot \left(\frac{D}{\nu} \right)^n + K \cdot \left(\frac{3n_a + 1}{4n_a} \right)^n \cdot 8^{(n-1)}} \tag{3.24}$$

Where:

Re_{HB}	Reynolds number for Herschel-Bulkley fluids
$D_{eff\text{-}HB}$	Effective pipe inner diameter for Herschel-Bulkley fluids
τ_o	Yield stress

Once the appropriate expression to determine the Reynolds number for Herschel-Bulkley fluids has been defined, we can finally describe the flow regime in the pipe based on the guidelines given for Newtonian fluids in subsection 3.3.2. Using the same definitions given for Newtonian fluids, we can then estimate the corresponding friction factor for the given flow regime as per the expressions below. Finally, the friction factor *f* can be substituted in the Darcy-Weisbach model given in Equation 3.12 to calculate the *frictional pressure losses* for Non-Newtonian Herschel-Bulkley fluids.

$$f = \frac{64}{Re_{HB}} \tag{3.25}$$

or

$$\frac{1}{\sqrt{f}} \approx -1.8 \cdot \log_{10} \left[\left(\frac{\varepsilon / D_{eff\text{-}HB}}{3.7} \right)^{1.11} + \frac{6.9}{Re_{HB}} \right] \tag{3.26}$$

3.3.5 Rabinowitsch-Mooney Equation

The Rabinowitsch-Mooney Equation permits to calculate viscosity of a Non-Newtonian Herschel-Bulkley fluid in laminar flow by converting flow rate to shear rate [18]. The following section describes the model that will be used at the end of this Chapter to calculate viscosity of Non-Newtonian fluids in laminar flow analyzed in the flowloop setup.

Consider one-directional flow of fluid through a pipe with radius *R*, see Figure 3.16. As previously stated, a fluid flowing in laminar flow in a circular pipe moves as concentric layers where each layer represents a different ring of velocity vectors.

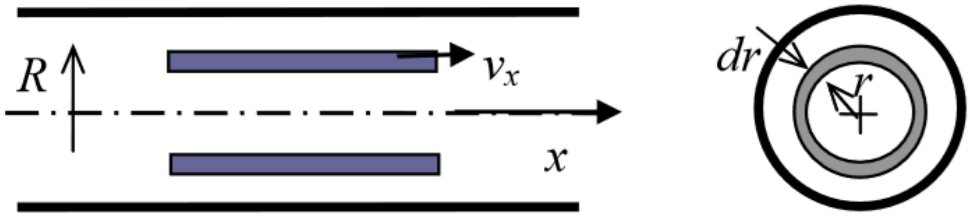

Figure 3.16. Schematic of one-directional flow of fluid through a pipe with radius *R* [19]

Now, the volumetric flow rate passing through one of this rings of width *δr* is given by the following expression [19]:

$$\delta Q = 2\pi \cdot r \cdot \delta r \cdot \nu \tag{3.27}$$

Integrating on the entire cross-section, the flow rate through the pipe is given by:

$$Q = 2\pi \cdot \int_0^R \nu \cdot r \cdot \delta r \tag{3.28}$$

Integrating by parts we obtain:

$$Q = 2\pi \cdot \left\{ \left[\frac{r^2 \cdot \nu}{2} \right]_0^R + \int_0^R \frac{r^2}{2} \cdot \left(-\frac{\delta \nu}{\delta r} \right) \cdot \delta r \right\} \tag{3.29}$$

Providing there is no slip at the pipe wall, the first term in Equation 3.29 vanishes, and we obtain:

$$Q = -\pi \int_0^R r^2 \cdot \left(\frac{\delta \nu}{\delta r} \right) \cdot \delta r \tag{3.30}$$

Now, from the definition of shear rate presented in Equation 2.2, we can generalize the expression for a fluid flowing in a circular pipe as follows:

$$\gamma = \frac{\delta v}{\delta r} \tag{3.31}$$

Thus, Equation 3.30 can be rewritten as:

$$Q = -\pi \int_0^R r^2 \cdot \gamma \cdot \delta r \tag{3.32}$$

If the fluid is time-independent and homogeneous, the shear stress τ is a function of shear rate only. The inverse also holds true, the shear rate γ, is a function of shear stress only [19]; and the variation of shear stress τ with respect to r is known from the previously derived Equation 3.9, which can be reformulated as follows:

$$r = \frac{\tau}{\tau_w} \cdot R \tag{3.33}$$

Combining Equations 3.32 and 3.33, we obtain:

$$Q = -\pi \int_0^{\tau_w} \frac{\tau^2 \cdot R^2}{\tau_w{}^2} \cdot \gamma \cdot \frac{\tau_i}{\tau_w} \cdot \delta\tau \tag{3.34}$$

Simplifying

$$Q = -\frac{\pi \cdot R^3}{\tau_w{}^3} \cdot \int_0^{\tau_w} \tau^2 \cdot \gamma \cdot \delta\tau \tag{3.35}$$

The shear rate γ, is now a function of shear stress τ instead of r. Now, Equation 3.35 can be expressed as follows:

$$\frac{Q}{\pi \cdot R^3} = -\frac{1}{\tau_w{}^3} \cdot \int_0^{\tau_w} \tau^2 \cdot \gamma \cdot \delta\tau \tag{3.36}$$

The left-hand side of Equation 3.36 can be written in terms of the flow characteristics as follows:

$$\frac{Q}{\pi \cdot R^3} = \frac{v \cdot A}{\pi \cdot R^3} = \frac{2 \cdot v}{D} \tag{3.37}$$

Thus, we can reformulate Equation 3.36 as:

$$\frac{8 \cdot v}{D} \cdot \tau_w{}^3 = -4 \cdot \int_0^{\tau_w} \tau^2 \cdot \gamma \cdot \delta\tau \tag{3.38}$$

For flow in a pipe, the shear rate γ is negative so the integral in Equation 3.38 becomes positive. For a given relationship between shear stress τ and shear rate γ, the value of the integral depends only on the value of shear stress in the pipe wall τ_w. Thus, for both Newtonian and Non-Newtonian fluids, the flow characteristic $8 \cdot \nu / D$ is a unique function of the wall shear stress τ_w [19].

The shear rate γ can be removed from Equation 3.38 by differentiating with respect to the shear stress τ. Moreover, if a definite integral is differentiated with respect to the upper limit (τ_w), the result is the integrand evaluated at the upper limit. It is convenient first to multiply Equation 3.38 by τ_w^3 throughout, then differentiating with respect to τ_w to obtain [19]:

$$\left(3 \cdot \tau_w^{\,2} \cdot \frac{8 \cdot \nu}{D} \right) + \left[\tau_w^{\,3} \cdot \frac{\delta \left(\frac{8 \cdot \nu}{D} \right)}{\delta \tau_w} \right] = \left(4 \cdot \tau_w^{\,2} \cdot \gamma_w \right) \tag{3.39}$$

Solving Equation 3.39 with respect to wall shear rate γ_w

$$\gamma_w = \frac{8 \cdot \nu}{D} \cdot \left[\frac{3}{4} + \frac{1}{4} \cdot \frac{\tau_w}{\left(\frac{8 \cdot \nu}{D} \right)} \cdot \frac{\delta \left(\frac{8 \cdot \nu}{D} \right)}{\delta \tau_w} \right] \tag{3.40}$$

Now, based on the relation given below

$$\frac{\delta(\ln x)}{\delta x} = \frac{1}{x} \;\rightarrow\; \delta(\ln x) = \frac{\delta x}{x} \tag{3.41}$$

Combining Equations 3.40 and 3.41, the Rabinowitsch-Mooney Equation is given as follows:

$$\gamma_w = \frac{8 \cdot \nu}{D} \cdot \left[\frac{3}{4} + \frac{1}{4} \cdot \frac{\delta \left(\ln \frac{8 \cdot \nu}{D} \right)}{\delta \ln \tau_w} \right] \tag{3.42}$$

It can be reformulated as:

$$\gamma_w = \frac{8 \cdot \nu}{D} \cdot \left(\frac{3}{4} + \frac{1}{4 n_a} \right) = \frac{8 \cdot \nu}{D} \cdot \frac{3 n_a + 1}{4 n_a} \tag{3.43}$$

Where n_a is a generalized flow index given by [13]:

$$n_a = \frac{\delta \ln \tau_w}{\delta \left(\ln \frac{8 \cdot \nu}{D} \right)} \tag{3.44}$$

3.4 Algorithms to Calculate Fluid Properties

The following section describes in detail the algorithms used to calculate density and viscosity of the fluids examined in the flowloop setup. The sequential steps were translated into MATLAB® scripts in the Master's Thesis developed in 2016 [12] and 2017 [18]; however additional scripts were required and developed to address the caveats found in the approach for Non-Newtonian fluids suggested in these past works. The codes used to analyze the experimental results are presented in Appendix C of this document.

It is important to mention that additional offset functions were introduced to calibrate the experimental results to the theoretical values for Newtonian fluids, this will be discussed in detail in Chapter 4 of this thesis. For now, the reader is advised to approach this section purely as the theoretical steps to be followed in order to implement the instrumented standpipe concept in the automated measurement of drilling fluid properties. We start the discussion with the information set available from the experimental setup, and then we move into the specifics of the calculations for both Newtonian and Non-Newtonian fluids.

The information available from the flowloop setup is compiled in the following table. It is worth to emphasize that we have marked the parameters that are known and those that are measured and transmitted into MATLAB® by the data acquisition system.

Table 3.1. Information set available for the calculation of fluid properties

Parameter	Value		Notes
Pipe Length	L =	3.5 m	Known
Vertical Distance	Δh =	3.5 m	Known
Pipe Diameter	D =	24 mm	Known
Absolute Pipe Roughness	ε =	0.0015 mm	Assumed
Gravitational Constant	g =	9.81 m/s^2	Known
Pump rate	Q	variable	Measured
Vertical differential pressure	dP_{ver}	variable	Measured
Horizontal differential pressure	dP_{hor}	variable	Measured
Temperature	T	variable	Measured

3.4.1 Calculations for Newtonian Fluids

The first step is to calculate the fluid density based on the assumptions presented in section 3.1. The reader is advised to review the aforementioned fragment and the corresponding Figure 3.1 as a refreshment of the basic functioning of the instrumented standpipe concept. Given that the pipe characteristics, flow properties, and distance between sensors are the same in both the vertical and horizontal sections, we state the following:

$$(\Delta P)_{Hydrostatic} = dP_{ver} - dP_{hor} \tag{3.45}$$

Combining Equations 3.16 and 3.45, we obtain

$$\rho = \frac{dP_{ver} - dP_{hor}}{g \cdot \Delta h} \tag{3.46}$$

The parameters involved in Equation 3.46 are all known, thus the first fluid property, density, can be determined. Next, we move on to determine the fluid viscosity using the Darcy-Weisbach relation given in Equation 3.12; bear in mind the other basic assumption in our experimental study, namely, that the horizontal differential pressure in the flowloop setup is caused solely by frictional pressure losses. Therefore, we can rearrange Equation 3.12 to define the following:

$$f = \frac{2 \cdot D \cdot dP_{hor}}{L \cdot \rho \cdot v^2} \tag{3.47}$$

Now, from the basic definition given in Equation 3.13, and in terms of the known parameters, we can state that:

$$f = \frac{\pi^2 \cdot D^5 \cdot dP_{hor}}{8 \cdot L \cdot \rho \cdot Q^2} \tag{3.48}$$

All parameters in Equation 3.48 are known, thus, a friction factor can then be calculated and subsequently used to determine the adequate Reynolds number and flow regime. In order to do so, Equations 3.14 and 3.15 are rearranged as follows:

$$Re_{lam} = \frac{64}{f} \tag{3.49}$$

$$Re_{turb} \approx \frac{6.9}{10^{\left(\frac{1}{-1.8 \cdot \sqrt{f}}\right)} - \left(\frac{\varepsilon/D}{3.7}\right)^{1.11}} \tag{3.50}$$

Now, a question arises on which is the appropiate expression to determine the Reynolds number. The first step is to evaluate Equation 3.49 with the known value of friction factor found in Equation 3.48, if the resultant value is less than 2100, then Equation 3.49 was correctly selected; conversely, if the resultant value is more than 4000, Equation 3.50 has to be evaluated to find the correct Reynolds number. Once this is completed, we can finally calculate the fluid viscosity by rearranging Equation 3.10 as follows:

$$\mu = \frac{\rho \cdot \nu \cdot D}{Re} \tag{3.51}$$

3.4.2 Calculations for Non-Newtonian Fluids

For Non-Newtonian fluids, the determination of fluid density follows exactly the same procedure as for Newtonian fluids, thus Equations 3.45 and 3.46 shall be used to calculate the first fluid property. However, the procedure to compute fluid viscosity is entirely different; the method selected is a combination of the Rabinowitsch-Mooney Equation for laminar flow that was presented in subsection 3.3.5, and the Thomas (1960) correlation used to determine an adequate friction factor for turbulent flow, which is then used to calculate the fluid viscosity.

First, the same basic assumption holds true for Non-Newtonian fluids, namely, that the horizontal differential pressure in the flowloop setup is caused solely by frictional pressure losses. We start the discussion with the approach used for laminar flow which has been excerpted from [13]; once we have obtained the horizontal pressure losses $\Delta P(i)$ for different flow rates $Q(i)$ from the experimental runs in the flowloop (note that i refers to each flow rate data point), we can calculate the shear stress at the pipe wall $\tau_w(i)$ with Equation 3.8 which has been reformulated as follows,

$$\tau_w(i) = \frac{D \cdot dP_{hor}(i)}{4 \cdot L} \tag{3.52}$$

Then, to calculate the generalized flow index $n_{Laminar}$ for each horizontal differential pressure value, we have to establish two additional parameters [13]:

$$a(i) = \ln\left(\tau_w(i)\right) \tag{3.53}$$

and

$$b(i) = \ln\left(\frac{8 \cdot v(i)}{D}\right) \tag{3.54}$$

Furthermore, from the definition of the generalized flow index given in Equation 3.44, we can approximate the solution by the following expression:

$$n_{Laminar}(i) = \frac{a(i+1) - a(i)}{b(i+1) - b(i)} \tag{3.55}$$

Subsequently, with the approximated values of the generalized flow index, we can then compute the wall shear rate γ_w using Equation 3.43 as follows:

$$\gamma_w(i) = \frac{8 \cdot v(i)}{D} \cdot \frac{3n_{Laminar}(i) + 1}{4n_{Laminar}(i)} \tag{3.56}$$

Finally, we can calculate apparent viscosity in laminar flow by combining Equations 3.52 and 3.56 to obtain the following basic definition [13]:

$$\mu_a(\mathrm{i}) = \frac{\tau_w(i)}{\gamma_w(i)} \tag{3.57}$$

During the experimental work, it was identified that the methodology above described is valid solely for laminar flow, further details of the analysis are provided in Chapter 4, but at this stage it suffices to list the procedure selected to describe the flow characteristics when the fluid flow is in the turbulent region. The reader may find convenient at this point to review the concepts developed in subsection 3.3.4.

Given that Equation 3.52 was developed exclusively for fully developed laminar flow, it is no longer applicable to model the fluid characteristics in the turbulent region, thus, we require a way to correlate the information obtained from the experimental runs in the flowloop setup with the concepts that have been presented so far. The solution selected was to use of a numerical *shooting* method to try to approximate the solution by finding the adequate friction factor that models more accurately the horizontal pressure losses recorded with the experimental setup.

The first step is to determine a generalized flow index $n_{Turbulent}$ for each pump rate value using Equation 3.23 which has been reformulated as follows:

$$\mathrm{n_{Turbulent}(i)} = \frac{\mathrm{n \cdot K \cdot \left(\frac{8 \cdot v(i)}{D} \right)^n}}{\tau_o + \mathrm{K \cdot \left(\frac{8 \cdot v(i)}{D} \right)^n}} \tag{3.58}$$

Note that *n*, *K*, and τ_o are calculated from the rheological readings obtained with the Fann® 35 Viscometer based on the definitions given in Equations 2.11, 2.12, and 2.13, respectively. Then, we shall recall two additional definitions introduced in Equations 3.21 and 3.56, which have been correspondingly rewritten as follows:

$$\mathrm{D_{eff\text{-}HB}(i)} = \frac{4\mathrm{n_{Turbulent}(i)}}{3\mathrm{n_{Turbulent}(i)} + 1} \cdot \mathrm{D} \tag{3.59}$$

and

$$\gamma_w(\mathrm{i}) = \frac{8 \cdot v(\mathrm{i})}{D} \cdot \frac{3\mathrm{n_{Turbulent}(i)} + 1}{4\mathrm{n_{Turbulent}(i)}} \tag{3.60}$$

In order to calculate the fluid viscosity using Equation 3.57, there is one additional piece of information that is required, namely, the shear stress at the pipe wall $\tau_w(i)$, but as previously mentioned, this can no longer be determined with Equation 3.52. Thus, at this point, we make use of a numerical method to approximate the solution; starting by *guessing* one initial value of $\tau_w(i)$ in order to calculate an initial *guessed* viscosity at each pump rate. Hence, we can reformulate Equation 3.57 as follows:

$$\mu_{a\ guess}(i) = \frac{\tau_{w\ guess}(i)}{\gamma_w(i)} \tag{3.61}$$

Then, by combining Equations 3.59 and 3.61 with the definition of Reynolds number, we obtain that:

$$Re_{HB\ guess}(i) = \frac{\rho(i) \cdot v(i) \cdot D_{eff\text{-}HB}(i)}{\mu_{a\ guess}(i)} \tag{3.62}$$

Now, based on the calculated value of the Reynolds number, we can define the flow regime corresponding to the initial *guessing* of $\tau_w(i)$. We recall from subsection 3.3.2 the following:

- $Re_{HB\ guess} < 2100$ Laminar flow
- $2100 < Re_{HB\ guess} < 4000$ Transitional flow
- $Re_{HB\ guess} > 4000$ Turbulent flow

Henceforth, we are now able to select the adequate expression to determine the friction factor for those particular flow characteristics. First, recalling Equation 3.14 for the laminar region we know that:

$$f(i)_{Laminar} = \frac{64}{Re_{HB\ guess}(i)} \tag{3.63}$$

Furthermore, we have mentioned earlier that different models to calculate the friction factor for Non-Newtonian fluids in turbulent flow were analyzed; further details of the comparison are described in Chapter 4, but for the sake of the present explanation, it is sufficient to state that the Thomas (1960) correlation was selected as the best approximation. The expression is as follows:

$$\frac{1}{\sqrt{f(i)_{Turbulent}}} = \frac{4.0}{n_{Turbulent}(i)} \cdot \log\left[Re_{HB\ guess}(i) \cdot f(i)_{Turbulent}^{\,1 - \frac{n_{Turbulent}(i)}{2}}\right] - 0.4 \cdot n_{Turbulent}(i) \tag{3.64}$$

One more challenge became apparent, how to combine the friction factor correlations in order to get a smooth transition from laminar to turbulent flow regions. The solution was to include a weight function in the MATLAB® scripts, and by trial and error, find the most adequate combination of values that would yield the best approximation of the fluid viscosity; refer to Appendix C for details of how this was implemented in MATLAB®.

Once the adequate expression to determine the friction factor is selected, and the corresponding result is computed, the next step is to calculate the pressure loss associated to the estimated friction factor using the Darcy-Weisbach model given in Equation 3.12 which has been rewritten as:

$$\Delta P_{guess}(i) = \frac{f(i)_{Laminar/Turbulent} \cdot L \cdot \rho(i) \cdot \nu(i)^2}{2 \cdot D} \tag{3.65}$$

Now, we can compare the *estimated* horizontal pressure losses with the values *recorded* with the flowloop setup in order to calculate the *error* of the approximation:

$$error\ (i) = \left|\Delta P_{guess}(i) - \Delta P_{flowloop}(i)\right| \tag{3.66}$$

If the *error* is greater than a certain *tolerance* value, the process is restarted by selecting a new *guessing* of the shear stress at the pipe wall $\tau_w(i)$, and repeating the calculations from Equations 3.61 to 3.66 until the *tolerance* value is met. The *bisection* method was selected to solve the numerical approximation of the problem. Refer to Appendix C for details of how this was implemented in MATLAB®.

Once the numerical approximation of the friction factor is solved, and the final generalized Reynolds number is defined, Equation 3.20 can be reformulated to obtain the apparent viscosity of a Non-Newtonian Herschel-Bulkley fluid in turbulent flow as follows:

$$\mu_a(i) = \frac{\rho(i) \cdot \nu(i) \cdot D_{eff\text{-}HB}(i)}{Re_{HB}(i)} \tag{3.67}$$

From the previous discussion, the question arises on how to compare the *Apparent Viscosity* results obtained with the flowloop setup to the rheological values generated with the rotational viscometer. The answer lies on the relationship presented in Chapter 2 Equation 2.5, which can be reformulated in a more general form as:

$$\mu_a = k \cdot f \cdot \frac{\theta}{\omega} \tag{3.68}$$

Where:

k	Viscometer overall instrument constant [dyne-sec/cm^2]
f	Viscometer torsion spring factor
θ	Viscometer dial reading
ω	Viscometer rotational speed

The values of *k* and *f* depend upon the selection of the rotor-bob-torsion spring combination; for the standard R1-B1-F1 used in this experimental study, the product of both factors equals *300*, hence the form of the expression presented in Equation 2.5. For any other rotor-bob-torsion spring combination, refer to the Instruction Manual provided in the relevant reference [4]. Thus, for our purposes, Equation 2.5 can be used to calculate *Apparent Viscosity* from the rotational viscometer readings, the relationship is listed again below.

$$\mu_a = 300 \cdot \frac{\theta}{\omega} \tag{3.69}$$

Additionally, it is recommended to further extend the comparison of the experimental results to the *Apparent Viscosity* values calculated from the rheological models presented in subsection 2.4.2. The following expressions are derived from the general form of each of the models given in Equations 2.7, 2.10 and 2.13 respectively, by dividing each side of the aforementioned expressions by the shear rate γ, which ultimately translates into the basic definition of viscosity given in Equation 2.1. Furthermore, the description of each of the parameters involved in the expressions is listed again for convenience of the reader.

Bingham Plastic model

$$\mu_a = \frac{\tau_o}{\gamma} + \mu_p \tag{3.70}$$

where

$$\mu_p \text{ (cP)} = \theta_{600} - \theta_{300} \tag{3.71}$$

and

$$\tau_o \left(\text{lb}/100\text{ft}^2\right) = \theta_{300} - \mu_p \tag{3.72}$$

Power Law model

$$\mu_a = K \cdot \gamma^{n-1} \tag{3.73}$$

Herschel-Bulkley model

$$\mu_a = \frac{\tau_o}{\gamma} + K \cdot \gamma^{n-1} \tag{3.74}$$

Where

$$n = 3.32 \cdot \log \frac{\theta_{600}}{\theta_{300}} \tag{3.75}$$

$$K = \frac{5.11 \cdot \theta_{600}}{1021^n} \tag{3.76}$$

A wary reader may identify that Equations 3.75 and 3.76 are presented in a different form compared to what was originally introduced in Equations 2.11 and 2.12, respectively; this is because in this experimental study we have standardized the calculation of the Power Law index *n* and the Power Law consistency index *K* to adhere to the guidelines suggested by the *API Recommended Practice 13D Recommended Practice on the Rheology and Hydraulics of Oil-well Drilling Fluids* for fluid flow calculations inside a pipe [8].

Thus, with the values calculated from both the basic relationship of the rotational viscometer, and the rheological models, a comparison table can be constructed similar to the one shown below. The relevant Equation numbers are listed for ease of reference.

Table 3.2. Comparison table of apparent viscosity values

	Eq. 2.3		Eq. 2.4	Eq. 3.69	Eq. 3.74	Eq. 3.67
				Viscometer	**H-B**	**Flowloop**
ω (rpm)	γ (sec^{-1})	θ (deg)	τ ($lb/100ft^2$)	μ_a (cP)	μ_a (cP)	μ_a (cP)
600	1021					
300	511					
200	340					
100	170					
6	10					
3	5					

The discussion presented in this Chapter provided the reader with the details upon which the experimental results to be shown in Chapter 4 have been obtained. I shall dedicate the remainder of this text to present the findings of the experimental runs conducted with the flowloop setup. The reader is advised to review the information included in Appendix C to understand how the algorithms to calculate fluid properties were deployed in MATLAB®, this will aid to better comprehend the presentation and discussion of results in the forthcoming section.

Chapter 4

Experimental Study Results and Analysis

The objective of this section is to provide a detailed explanation of how the experimental study was conducted, the results obtained, and the suggested framework upon which this study should continue to be developed in future works. The first part of the Chapter is dedicated to validating again the accuracy of the flowloop setup and theoretical models for Newtonian fluids; then we move into the description of the Non-Newtonian fluids analyzed, to finally provide a thorough explanation of the testing results and analysis obtained for Non-Newtonian fluids.

4.1 Newtonian Fluids

The evaluation of properties of Newtonian fluids was included in this study as a necessary reference benchmark prior to investigate the accuracy of the flowloop setup on determining properties of Non-Newtonian fluids. The parameters recommended in the Master's Thesis developed in 2017 [18] were used as starting point for the configuration of the data acquisition system in Simulink® and MATLAB®.

It was identified that no standard procedure was in place to operate the flowloop setup nor to collect data for the subsequent analysis; thus, before moving any further, I shall list the steps followed in this study which should be considered hereafter as the recommended standard procedure to ensure repeatability and comparability of future works using the flowloop setup.

1. Fill up the tank with 90 liters of fluid and set the pump controller to *Local* mode.
2. Start up the pump manually at approximately 50% of the output capacity.
3. Stage up the pump rate to 90 lpm and circulate until the entire setup is filled with fluid.
4. The horizontal section of the return pipe will have some air trapped, this can be removed by increasing and decreasing the pump rate manually until most of it has been released.

5. Stop the pump manually and switch the pump controller to *Remote* mode.
6. Set a sample time in MATLAB® using the following command *sample_time = 0.01*
7. Using the Simulink® interface set the pumping rate to 90 lpm, start up the pump and circulate for 10 minutes before collecting any data.
8. Prepare a spreadsheet similar to the one shown in Table D.1 to collect the measured data.
9. Stop the pump through the Simulink® interface.
10. Set the pump rate to 90 lpm, start up the pump and circulate for 60 seconds, the pump rate will overshoot at first, but it should stabilize after 3-5 seconds, stop the pump.
11. Run the MATLAB® script named *measure_viscosity*.
12. Using the relevant MATLAB® command, plot *pump rate vs time* to verify that the pump output has been stable throughout the sample period. The user should be warned that for pump rates lower than 10 lpm, the controller is unstable as shown in Figure 4.1, hence no data shall be collected for this low flow rates.

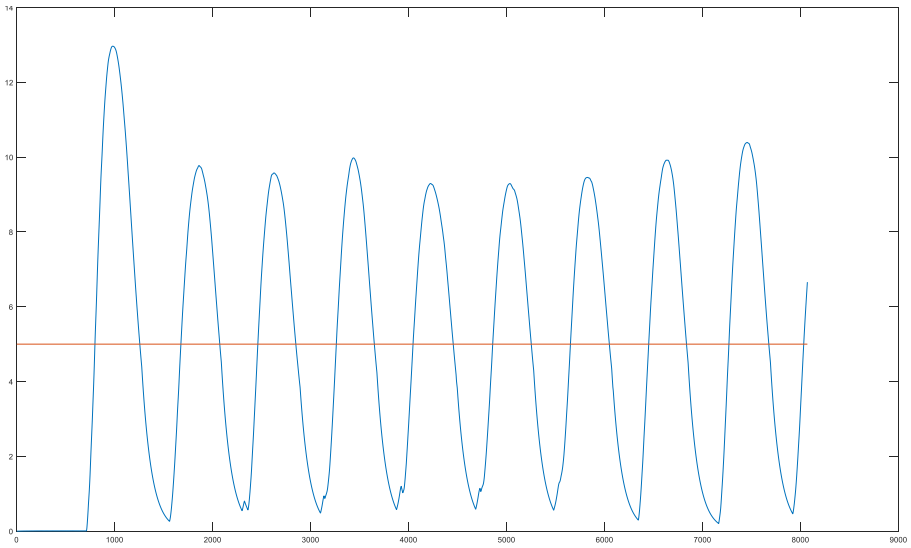

Figure 4.1. Pump rate oscillations circulating water at 5 lpm in the flowloop

13. Once the pump rate stability has been verified, use the relevant MATLAB® commands to calculate the mean values of pump rate, horizontal differential pressure, and vertical differential pressure.
14. Record the three mean values in the spreadsheet as shown in Table D.1.
15. Repeat steps 10 – 14 every 2 lpm in decreasing order until reaching 10 lpm. Note: the repeatability of the results in decreasing and ascending order has been assessed, so this is an arbitrary suggestion to collect the flowloop data.

The preceding standard procedure was used throughout the entire experimental study to ensure comparability of the results obtained. As previously pointed out, the first step was to calibrate the flowloop measurements using water, the measured values are presented in Appendix D Table D.1. Figure 4.2 displays the measured values of horizontal and vertical differential pressures at pump rates varying from 10 – 90 lpm.

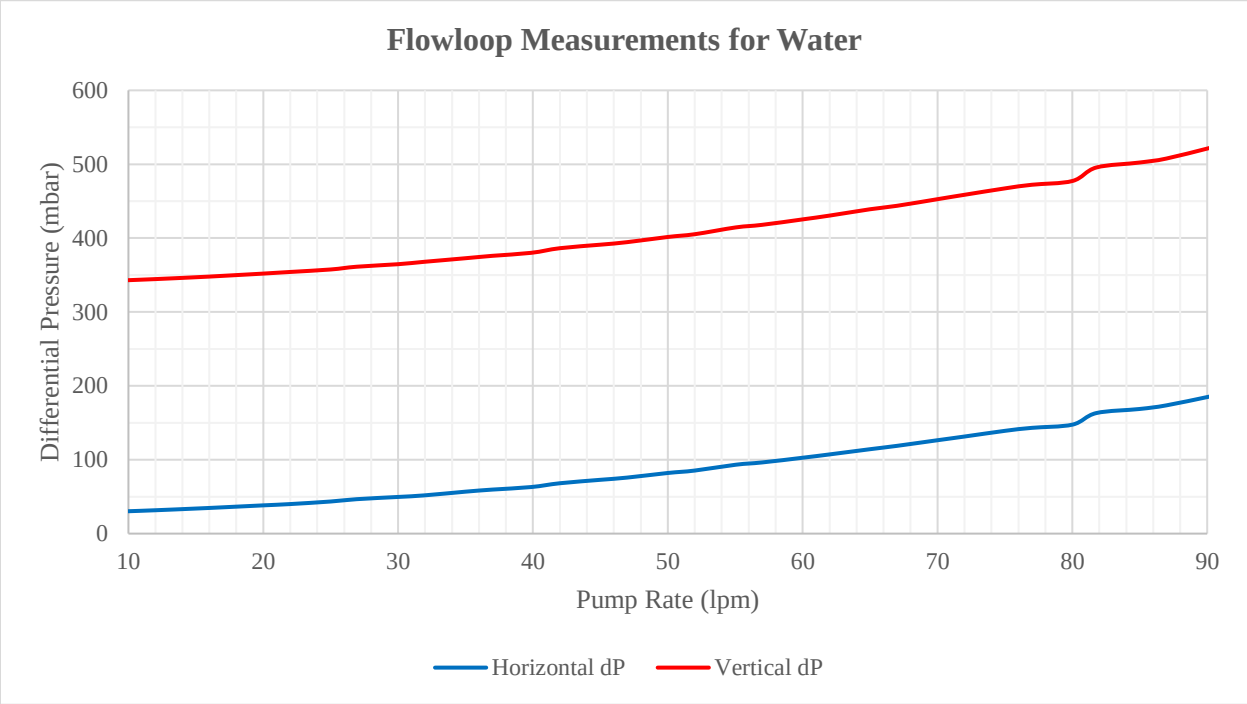

Figure 4.2. Measured differential pressure values when circulating water

It is important here to highlight a fact that will play a crucial role later in the discussion of the results of Non-Newtonian fluids. Considering the theoretical values of viscosity and density of water, and the geometrical characteristics of the pipe, all the measurements recorded in Table D.1 fall into the turbulent flow region as per the definition presented in subsection 3.3.2. Unfortunately, the current flowloop setup does not allow to investigate the accuracy of the laminar flow models discussed in subsection 3.4.1, as the pump output is unstable at flow rates lower than 10 lpm.

Following the guidelines provided in the Master's Thesis developed last year [18], an offset correction function is needed to calibrate the measurements of the flowloop setup. The calibration is based on the variations of the hydrostatic pressure losses as shown in Figure 4.3. The theoretical value is constant at any given pumping rate (blue curve), and the measured value (red curve) is given by Equation 3.45 as the difference between the vertical and horizontal differential pressure measurements from the flowloop. Thus, as clearly exhibited in Figure 4.3, there is a difference at each pumping rate between the theoretical and measured values, this difference is the basis to generate an offset function depending on the flow rate.

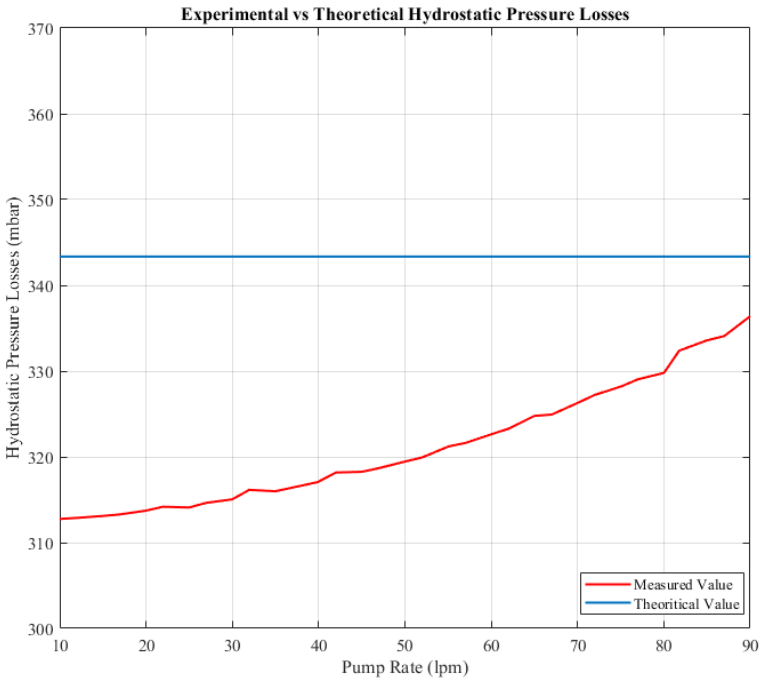

Figure 4.3. Experimental vs theoretical hydrostatic pressure losses

The offset values at each pump rate are then plotted as shown in Figure 4.4 (red curve), and a sextic polynomial function is used in the regression model. The generated function is subsequently used in MATLAB® to correct the values of the hydrostatic pressure losses at each pump rate.

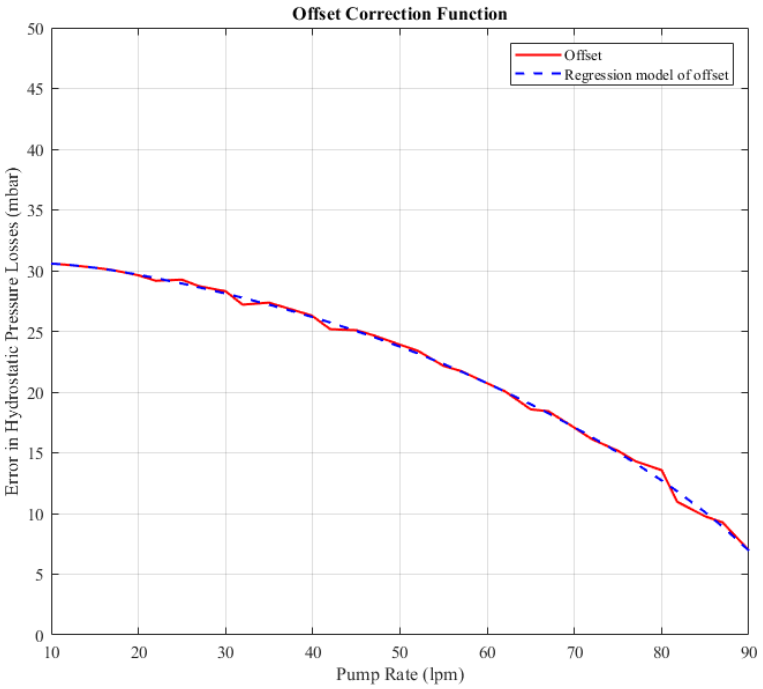

Figure 4.4. Offset correction function for hydrostatic pressure losses

After adding the offset correction function to the measured hydrostatic pressure losses, the density of water in the flowloop is calculated with Equation 3.46, the results for each pump rate are presented in Figure 4.5 (red curve). The accuracy of the estimated density is acceptable, but the results can still be improved by the inclusion of a low-pass filter to attenuate the signals with the higher frequencies, thus the final estimated water density is depicted by the dashed black curve in Figure 4.5.

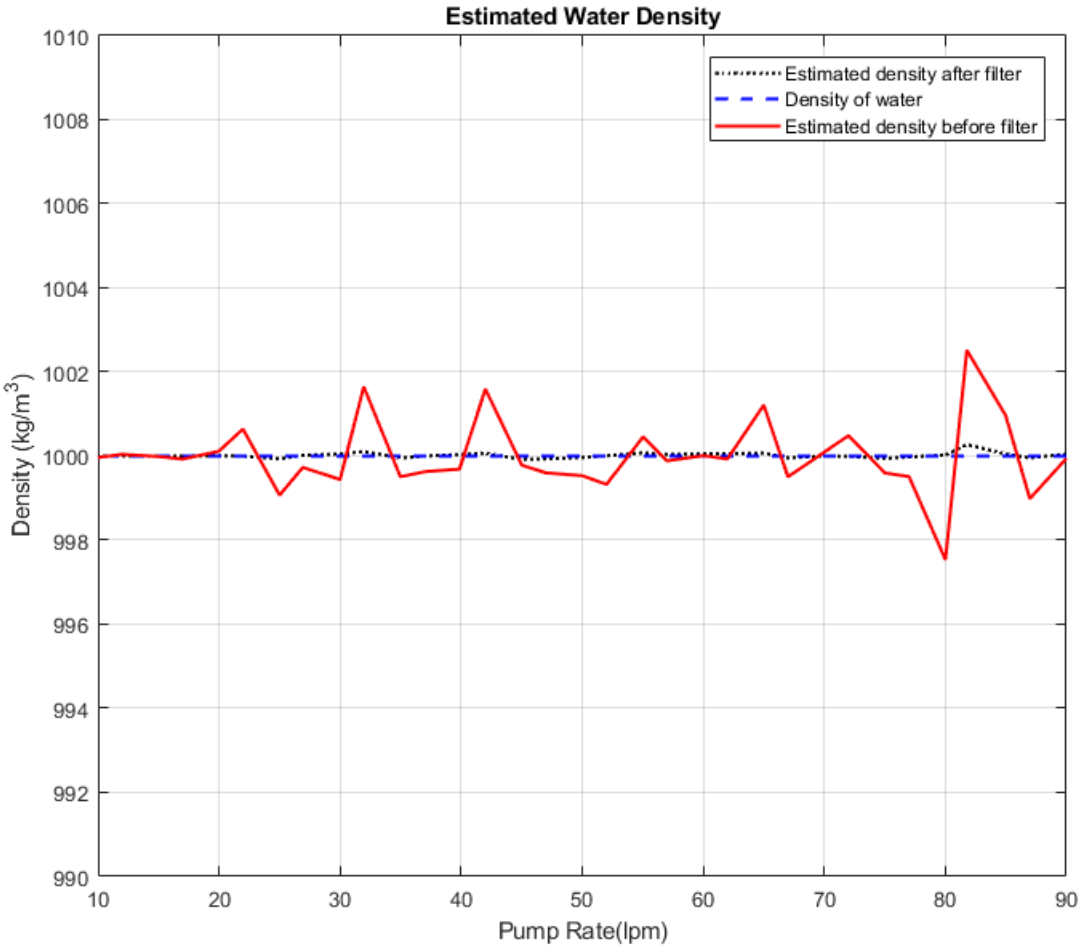

Figure 4.5. Estimated water density from flowloop measurements

Based on the results presented above, the model to estimate density of Newtonian fluids in turbulent flow using the flowloop measurements is validated. Now, the estimation of fluid viscosity starts by calculating the corresponding friction factor for each given pump rate using Equation 3.48. Once the adequate Reynolds number is estimated, the fluid viscosity is finally calculated using Equation 3.51. The results of the estimated viscosity of water for pump rates varying from 10 – 90 lpm are presented in Figure 4.6.

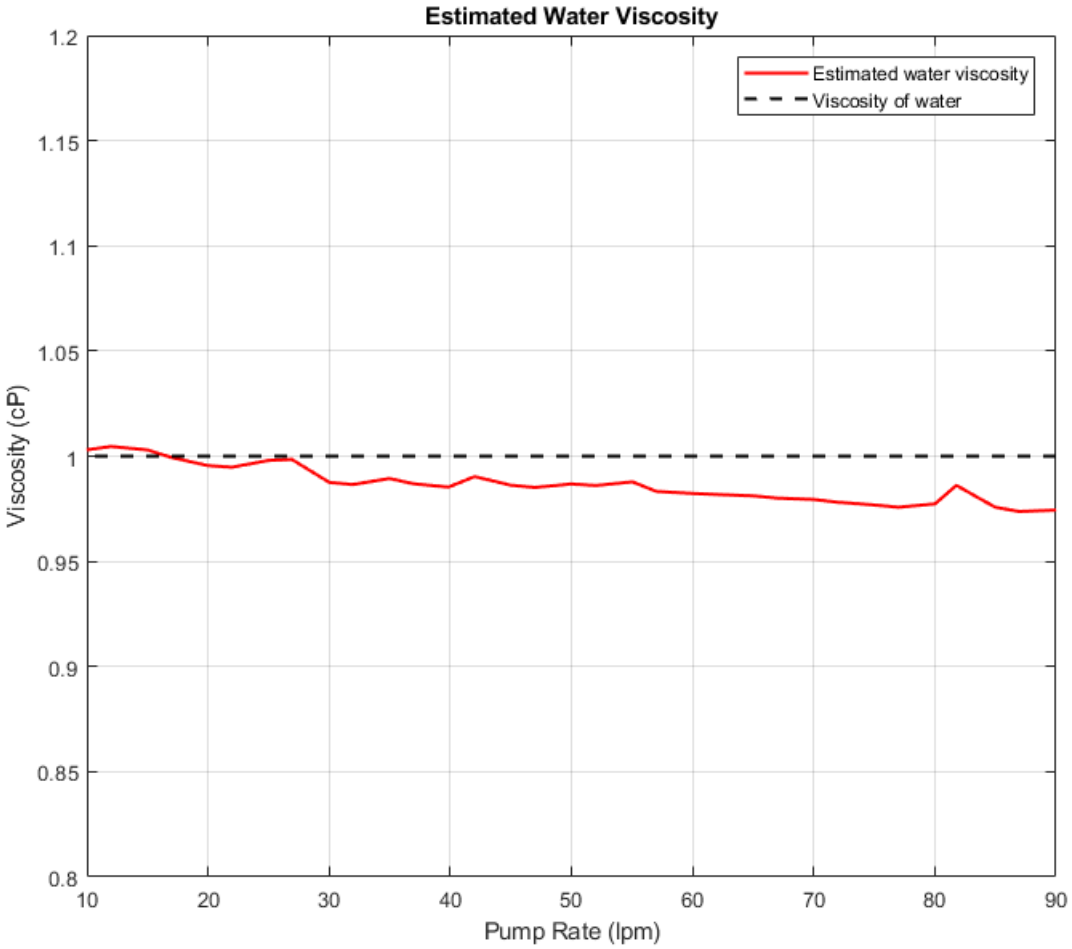

Figure 4.6. Estimated water viscosity from flowloop measurements

The estimated water viscosity is within an acceptable margin, a maximum relative error of 2.5% that in absolute terms translates into merely 0.025 cP, yields in practical terms an accurate enough estimation of fluid viscosity. We shall acknowledge that the viscosity estimation is not as accurate as the estimated density, this could be caused by factors that are difficult to define in a precise fashion, for instance, the pipe roughness. Similarly, we should bear in mind that the determination of friction factors of Newtonian fluids in turbulent flow as given by the Haaland model in Equation 3.15, is based on an empirical correlation that ultimately affects the exactness of the viscosity estimation.

The above discussion concludes the calibration of the flowloop setup using water. It was identified that the study of Newtonian fluids had to be expanded to validate the applicability of the offset correction function to densities different to that of water; for that purpose, sodium chloride brine was selected as the most viable option from the availability and safety standpoints. The flowloop measured values of 1.105 SG NaCl brine are presented in Appendix D Table D.1. Likewise, Figure 4.7 and Figure 4.8, depict the estimated density and viscosity of 1.105 SG NaCl brine, respectively, using the same offset correction function generated for water.

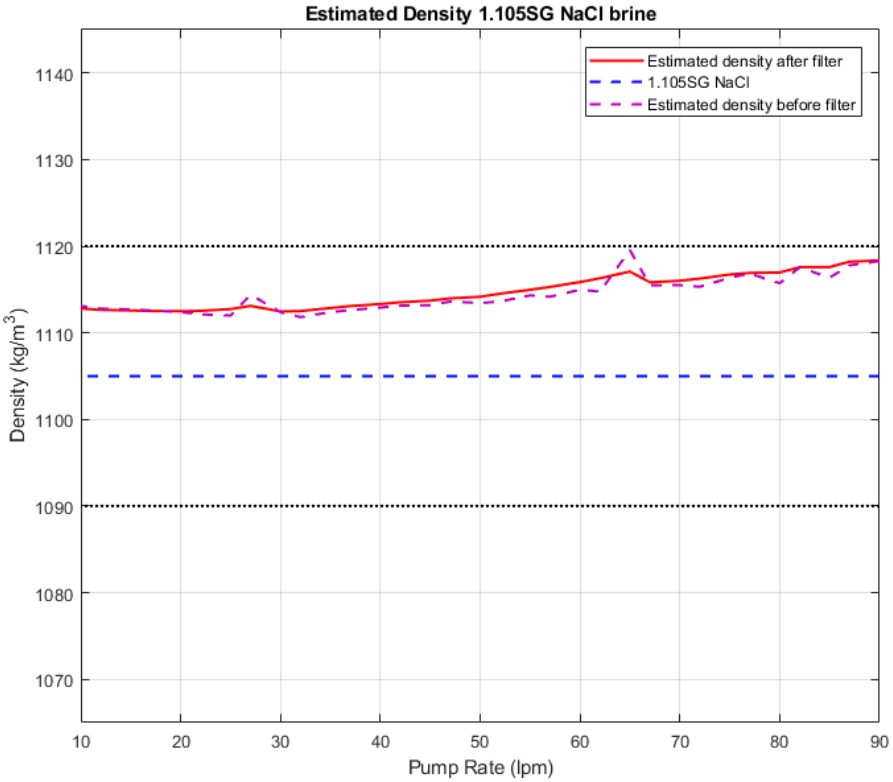

Figure 4.7. Estimated density of 1.105 SG NaCl brine from flowloop measurements

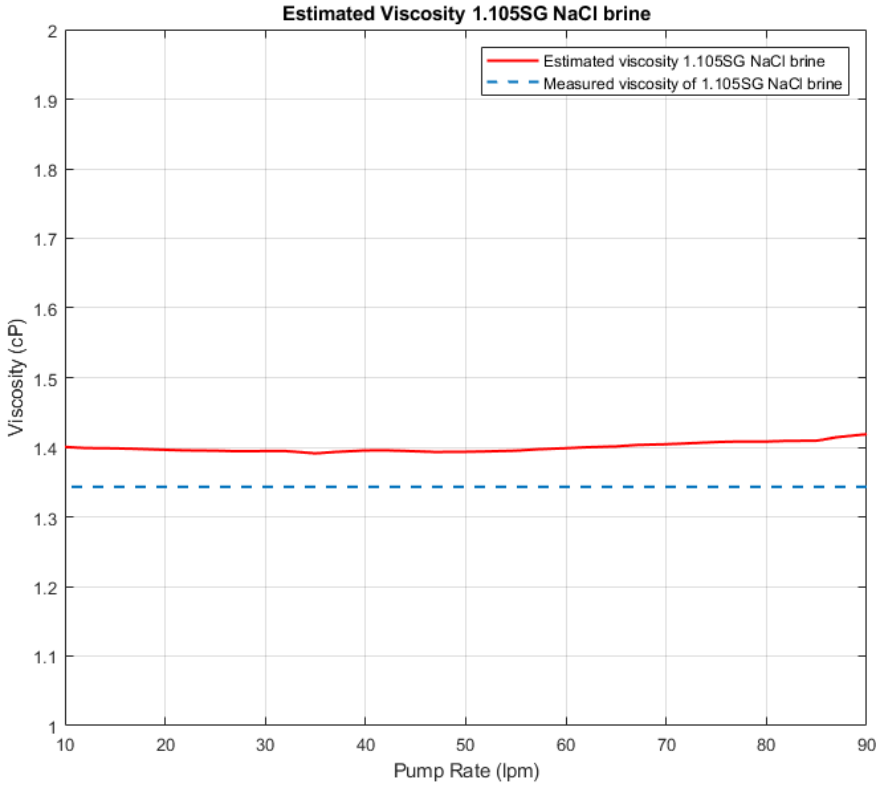

Figure 4.8. Estimated viscosity of 1.105 SG NaCl brine from flowloop measurements

The density of the sodium chloride brine was measured in the Analytical Laboratory at UiS using an Anton Paar density meter at 20 °C, the recorded value was 1105 kg/m^3. The estimated density with the flowloop setup, as illustrated in Figure 4.7, gives a maximum error of 0.014 SG which is within an acceptable tolerance for the purpose of this investigation.

The theoretical viscosity of 1.105 SG NaCl brine was obtained from the literature in [21], the nearest measured value in that study is reported as 1.34 cP at 20 °C; thus, the estimated viscosity presented in Figure 4.8 is within an acceptable margin, with a maximum relative error of 5% that in absolute terms renders only 0.07 cP.

Despite the fact that the estimated values are within an acceptable tolerance, the results are not as accurate as previously obtained with water, which leads to conclude that the offset correction function is variable and the applicability for any other fluid density has to be carefully evaluated. The latter assertion is demonstrated when plotting the calculated offset for 1.105 SG NaCl brine against the polynomial function generated in the regression model of the water measurements, as shown in Figure 4.9. Further investigation is needed to develop a generalized offset correction function for the flowloop setup at UiS, but that is beyond the scope of this thesis.

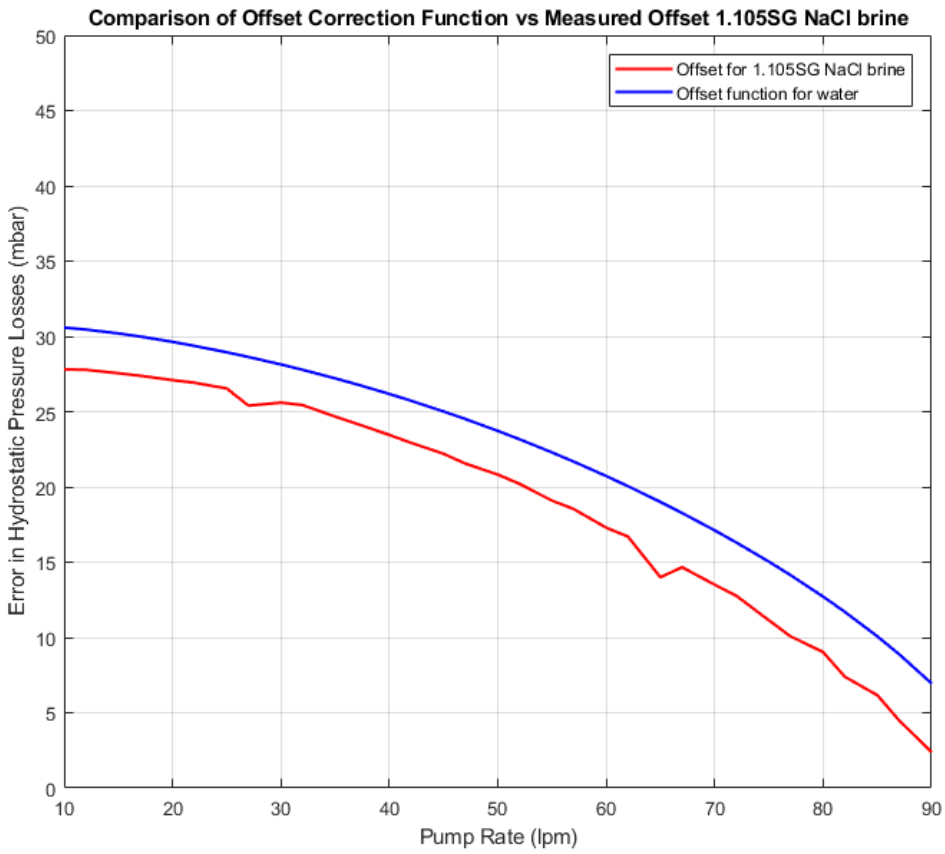

Figure 4.9. Offset correction function vs measured offset of 1.105SG NaCl brine

4.2 Non-Newtonian Fluids

The next stage in this experimental study was to analyze the applicability of the instrumented standpipe concept to determine the properties of Non-Newtonian fluids. We shall start the discussion by understanding the fluids utilized in the experimental runs. Given the limitations of the current setup at UiS, it was decided to continue using the fluids selected in the Master's Thesis developed last year [18], namely a solids-free Xantham Gum Polymer (XCD) water-based mud system. The selection of the Non-Newtonian fluid type is constrained by the disposal of the slurry and the pump being unable to handle fluids with high-solids content.

One of the main caveats of the past work was the development of foam in the flowloop setup; the excessive presence of bubbles in the system led to dramatic underestimations of the fluid density. Furthermore, these air bubbles could erode the internal components of the pump if the problem is not addressed appropriately. Thus, the first step was to select the adequate fluid formulation to prevent the appearance of bubbles in the fluid; the following table summarizes the additives used in this experimental study.

Table 4.1. Non-Newtonian fluid formulation

Additive	Concentration	Notes
Magnesium Oxide (MAGOX)	0.25 ppb	pH buffer
Xantham Gum Polymer (XCD)	Variable	Viscosifier
NULLFOAM	0.5 %vol	Defoamer

A Fluids Engineer would probably argue that the presented formulation is an over-simplification of a water-based mud system, but again, it is fundamental to understand that the present study intends to set the basis upon which further and more complex investigations of the applicability of the instrumented standpipe concept can be developed. The formulation presented in Table 4.1 included two additional additives to improve the performance of the slurry, namely, a pH buffer and a defoamer; the former is added to effectively buffer alkalinity to a maximum pH of 10.0 in order to allow the XCD polymer to fully yield, and the latter is added to prevent foaming in water-based drilling fluids. The concentrations used were obtained from the recommended values endorsed by the supplier (Schlumberger M-I SWACO).

The order of addition is reflected in the sequence presented in Table 4.1. For future reference, the author considers prudent to include a recommended procedure to mix the slurry at the UiS Drilling Fluids Laboratory that would aid in the standardization of the test and comparability of results. The recommended procedure is as follows:

1. As described in subsection 4.1, each experimental run shall be performed with 90L of fluid; thus, six individual batches of 15L each should be mixed one at a time. It is preferable to start the mixing early in the morning to proceed with the flowloop runs in the afternoon of the same day; albeit, we have verified the stability of the fluid formulation after 72 hours in the tank, it is advisable to adhere to this schedule to eliminate any possible variations.
2. Start by filling up a 5gal bucket with 15L of tap water. In very rare cases, the water hardness might be high enough to prevent the XCD polymer to fully yield, if you suspect that the rheological readings are significantly lower than expected after mixing the first batch, test the tap water for calcium and magnesium and define if any treatment is needed.
3. Place the bucket into the overhead mixer. Start up the mixer and slowly increase the speed until a vortex forms without spilling any fluid out of the bucket.
4. Add 0.25ppb (10.7g) of Magnesium Oxide (MAGOX) and stir for 10min.
5. Depending on the formulation to be mixed, weigh up the adequate amount of XCD polymer and slowly add it to the bucket. It is vital here that the polymer is added as slow as possible to avoid the presence of fisheyes (chunks of undissolved polymer). As the polymer is added, the speed of the overhead mixer will have to be adjusted. Once all polymer has been added, stir for 10min.
6. Finally, add 0.5%vol (75ml) of NULLFOAM and stir for 10min.
7. Carefully pour the slurry into the flowloop tank. Repeat all steps until the six individual batches of 15L each are completed and proceed with the recommended testing procedure described in subsection 4.1.

The mixing procedure above described was followed throughout the remainder of this experimental study. In order to verify the applicability of the mathematical models for different fluid viscosities, five different formulations were selected to be tested using the flowloop setup. The only variable component is the concentration of viscosifier (XCD), thus the reader should intuitively understand that the higher the XCD concentration, the more viscous the fluid is. The following table encompasses the fluid formulations analyzed in this Master's Thesis work.

Table 4.2. Fluid formulations mixed at the UiS Drilling Fluids Laboratory

	Formulation 1	Formulation 2	Formulation 3	Formulation 4	Formulation 5
Additive	Concentration	Concentration	Concentration	Concentration	Concentration
MAGOX	0.25 ppb	0.25 ppb	0.25 ppb	0.25 ppb	0.25 ppb
XCD	2 g/liter	3 g/liter	4 g/liter	5 g/liter	6 g/liter
NULLFOAM	0.5 %vol	0.5 %vol	0.5 %vol	0.5 %vol	0.5 %vol

As previously stated, the first issue that had to be addressed was the presence of foam in the flowloop setup that led to underestimations of the fluid density in the Master's Thesis developed last year. Thus, once the pipes were filled with fluid, the system was circulated for 20 minutes at maximum pump rate (90 lpm) in order to verify whether the fluid was foaming or not. A visual check demonstrated that no bubbles in the system were generated, as clearly seen in the pictures presented below.

(a) Without defoamer 2017 [18] (b) With defoamer 2018

Figure 4.10. Addressing foam generation in the Non-Newtonian fluid formulation

The visual evidence presented above corresponds to the formulation mixed with 3 g/liter of XCD polymer; it was selected for comparability purposes with the referenced document [18], although similar checks were conducted for all the formulations listed in Table 4.2. The inclusion of NULLFOAM (defoamer) in the fluid recipe proved to be an effective solution to deal with the foaming issues faced in the previous work.

In addition to the visual comparison presented above, it is sensible to document the improvement in the fluid density calculations generated with Equations 3.45 and 3.46. For illustrative purposes, the results of the 3 g/liter XCD formulation are compared with the correspondent output generated last year; the density calculations of the remaining fluid formulations will be discussed later in this section. Figure 4.11 has been excerpted from [18], it depicts the severe underestimation of the fluid density due to the presence of foam in the flowloop setup; when this output is compared to the results obtained in Figure 4.12, it is clear that by eliminating the foam in the system, the density estimations are within an acceptable tolerance when compared with the laboratory measurements using the pressurized mud balance (1.00 SG at 15 °C).

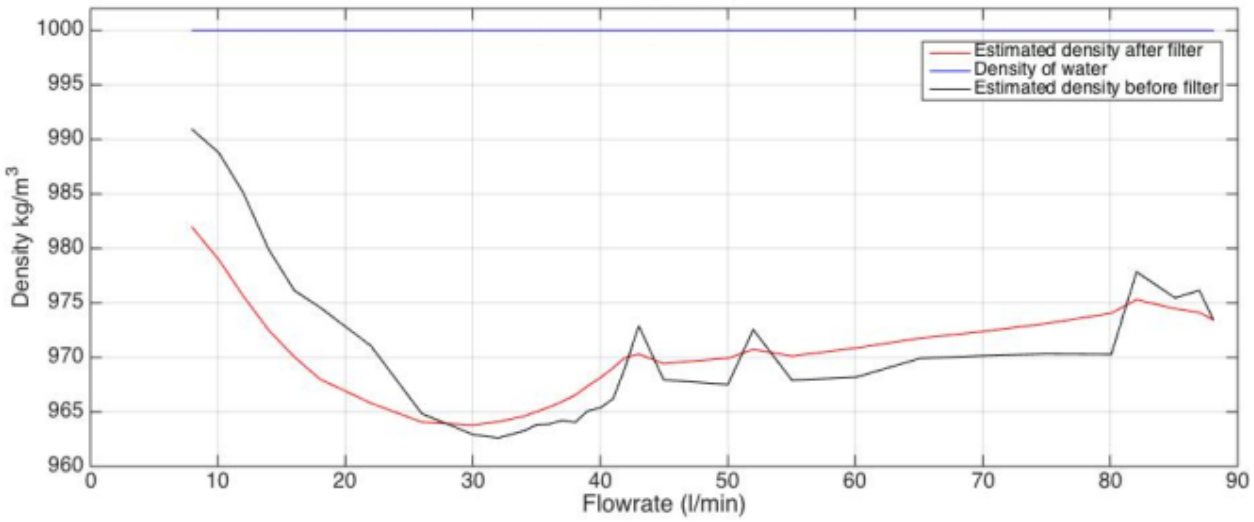

Figure 4.11. Underestimation of fluid density caused by the presence of foam in the flowloop [18]

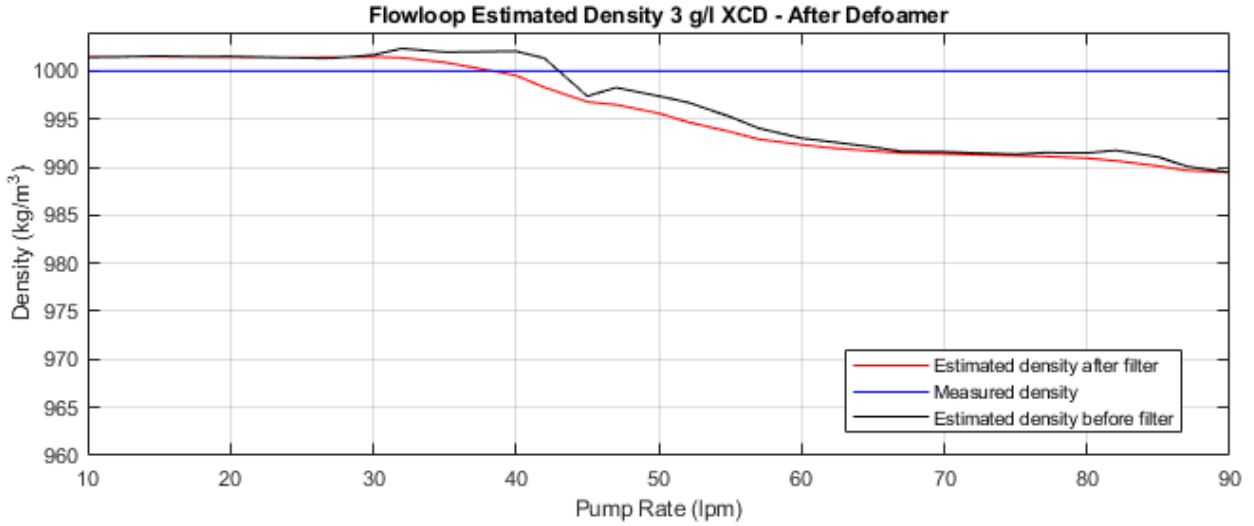

Figure 4.12. Fluid density estimation after the addition of defoamer to the formulation

In the comparison presented above, it is evident that the inclusion of a defoamer in the fluid formulation resulted in a significant improvement in the accuracy of the fluid density estimations. Once this first issue was resolved, the rest of the formulations were tested; we shall start a thorough discussion of the results by presenting first the density calculations for each of the fluids mixed and will later proceed with the issues encountered in the viscosity determination and how these were addressed.

For convenience of the reader, we shall start the discussion by briefly refreshing on the procedure followed to obtain the results presented in the following figures. The vertical and horizontal mean pressure losses at different pump rates measured with the flowloop setup are presented in Appendix D Table D.2 Part A and Table D.3 Part B.

Using Equation 3.46 and the relevant data set, we obtain the fluid density estimations at each pumping rate, which have been corrected using the same offset correction function presented in Figure 4.4. Finally, the results are improved by introducing a low-pass filter to attenuate the signals with the higher frequencies, hence the final estimated fluid density is depicted by the red curve in each of the figures presented below.

The density of each of the formulations was measured in the UiS Drilling Fluids Laboratory using a previously calibrated pressurized mud balance, the recorded values were close to 1000 kg/m^3 at room temperature (approximately 15 °C). We have arbitrarily set an acceptable tolerance of ± 0.015 SG for the density results, this is portrayed by the black curves in the following figures.

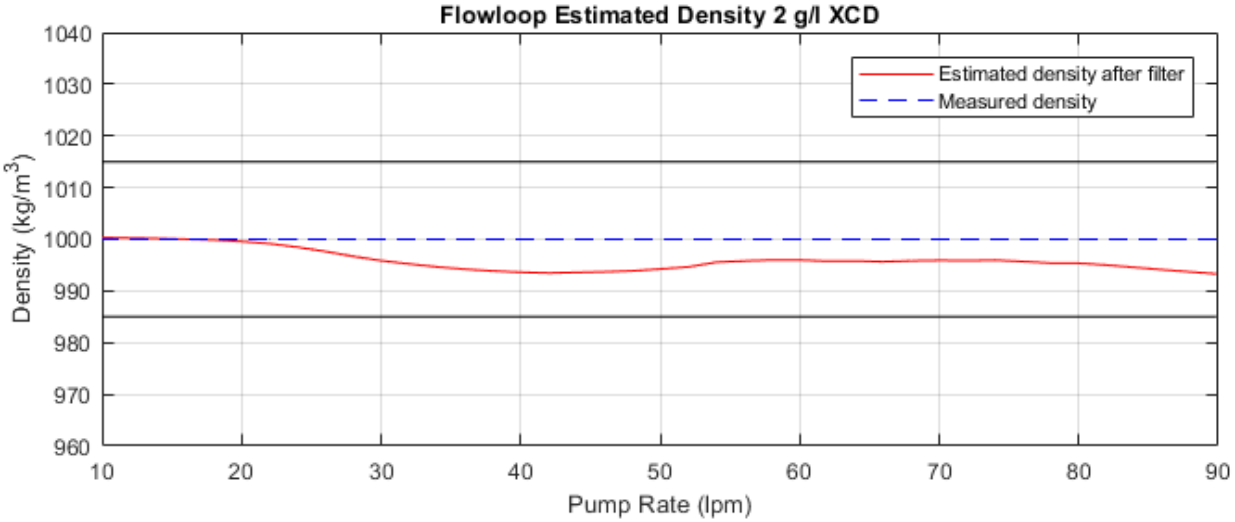

Figure 4.13. Estimated density of Formulation 1 from flowloop data

The estimated density of Formulation 1 using the flowloop setup, as illustrated in Figure 4.13, gives a maximum error of 0.007 SG which is within an acceptable tolerance for the purpose of this investigation.

The estimated density of Formulation 2 using the flowloop setup, as illustrated in Figure 4.14, gives a maximum error of 0.01 SG which is within the acceptable tolerance of this study.

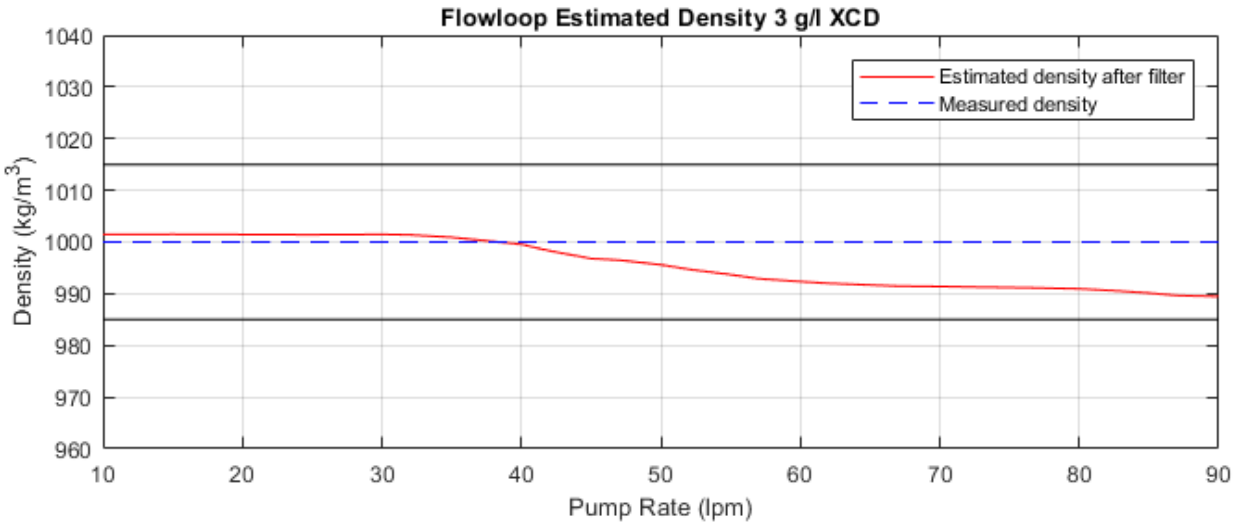

Figure 4.14. Estimated density of Formulation 2 from flowloop data

The estimated density of Formulation 3 using the flowloop setup, as illustrated in Figure 4.15, gives a maximum error of 0.028 SG which is undoubtedly not accurate enough. Two possible explanations to this mismatch are that (1) the offset correction function presented in Figure 4.4 is also viscosity-dependent and thus not applicable to each case; another hypothesis is that (2) since the flowloop setup is not air-tight, air could enter and remain undetected in the system, and given that the fluid is more viscous, it would not be able to escape when pumping at high rates, henceforth the underestimation of fluid density at higher flowing rates.

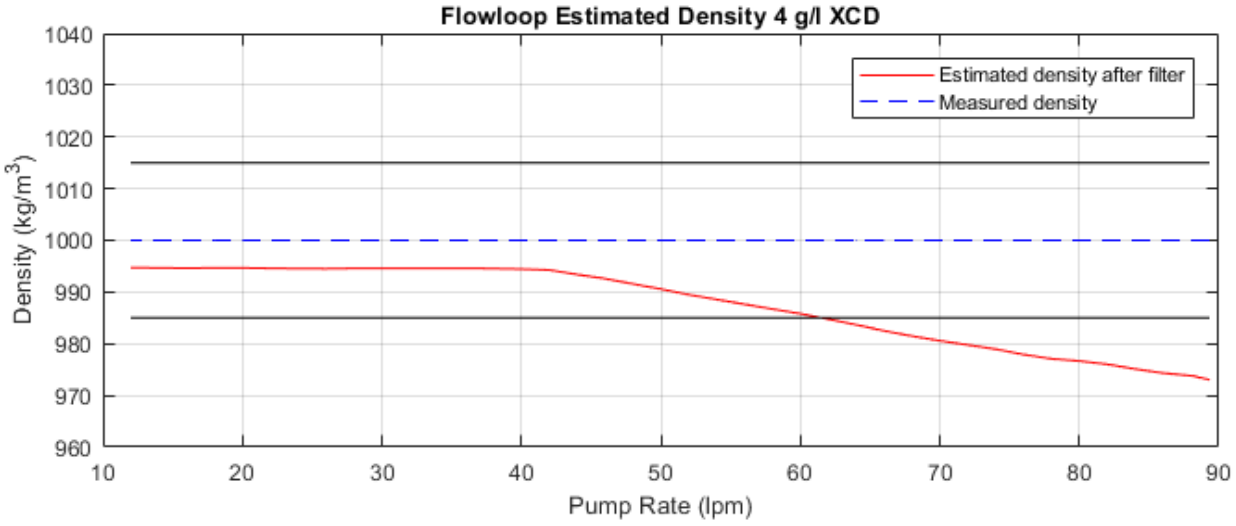

Figure 4.15. Estimated density of Formulation 3 from flowloop data

Similar inaccuracies are found when analyzing the data collected for Formulations 4 and 5, depicted in Figures 4.16 and 4.17 respectively, although the degree of mismatch is lower than that of Formulation 3. There is not a clear trend that indicates what the origin of this error might be, but we could argue that if hypothesis (2) presented above would be correct, we would expect the opposite behavior, namely, the mismatch would increase as the viscosity increases. Thus, we shall discard the idea that air bubbles are causing the underestimation of fluid density at high pump rates, and we shall investigate further the dependency on viscosity of the offset correction function generated with water measurements that was presented in Figure 4.4.

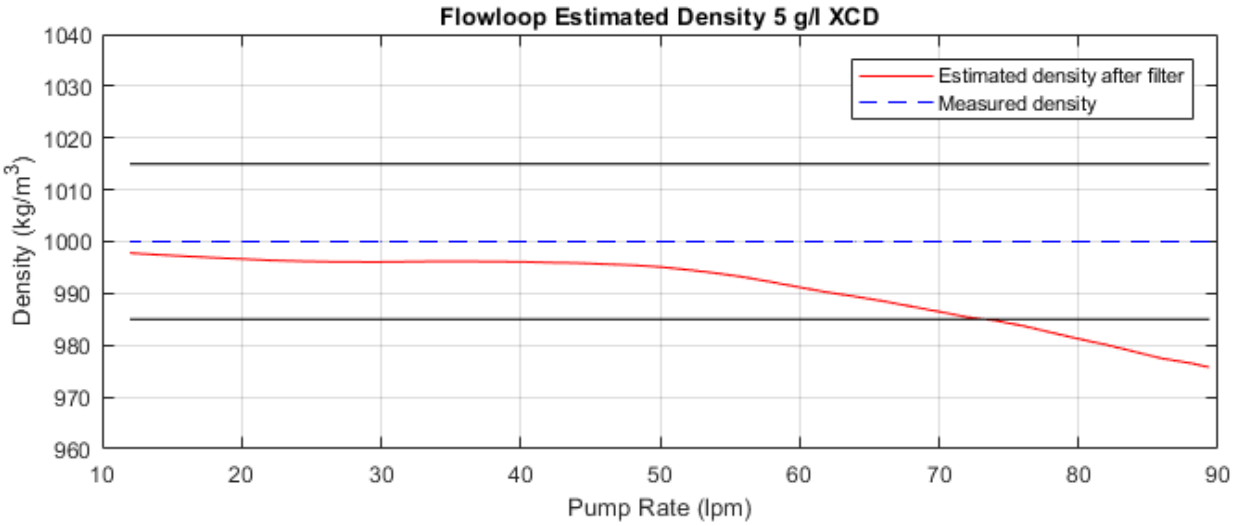

Figure 4.16. Estimated density of Formulation 4 from flowloop data

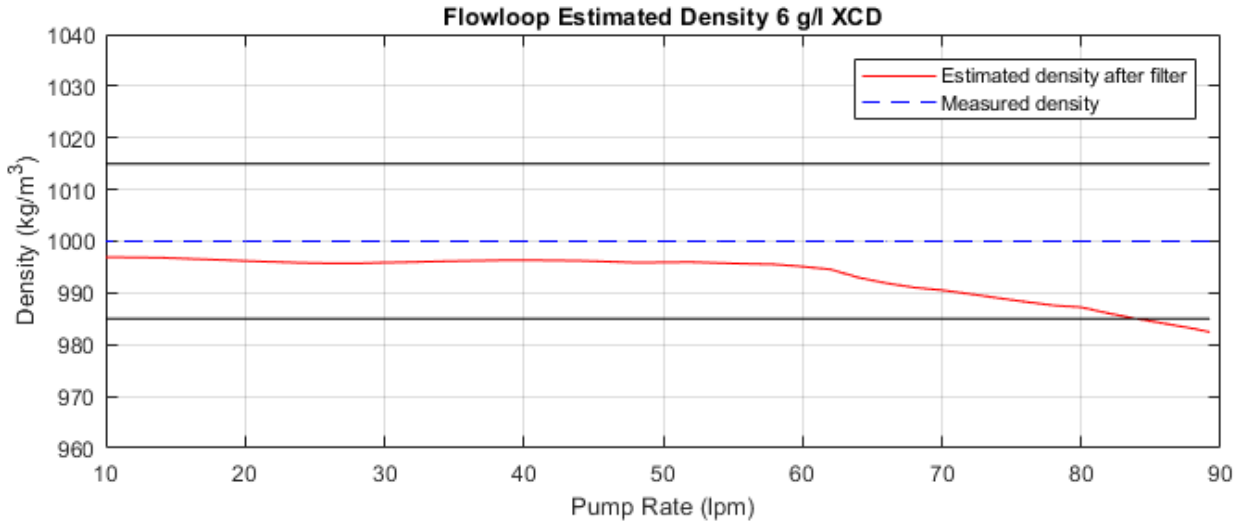

Figure 4.17. Estimated density of Formulation 5 from flowloop data

In order to analyze further the effect of viscosity on the offset correction function, we shall compare the polynomial function generated in the regression model of the water measurements with the measured offsets of Formulations 3 and 4, as shown in Figures 4.18 and 4.19, respectively.

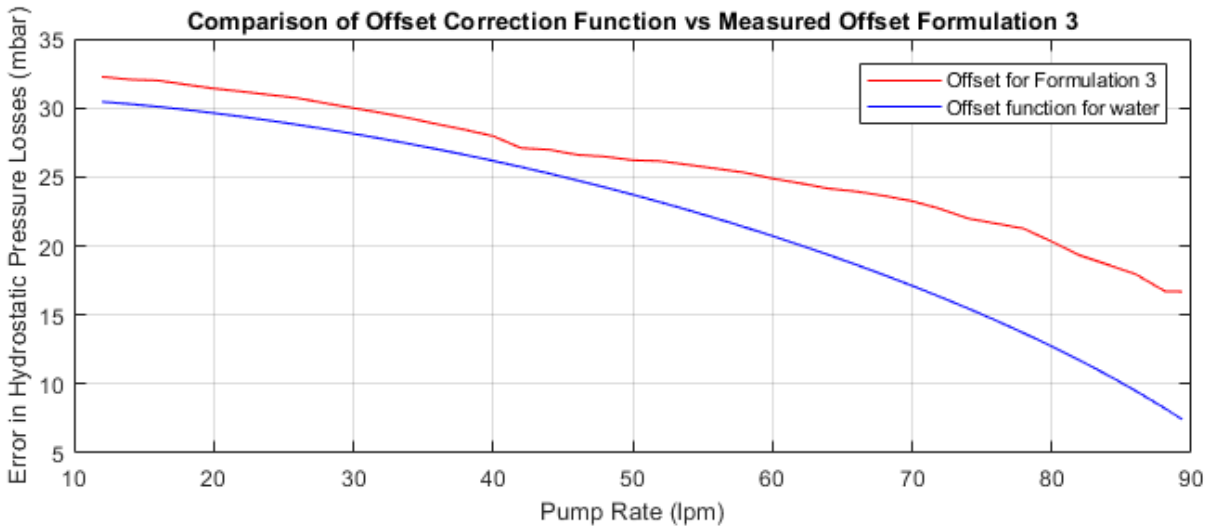

Figure 4.18. Offset correction function vs measured offset of Formulation 3

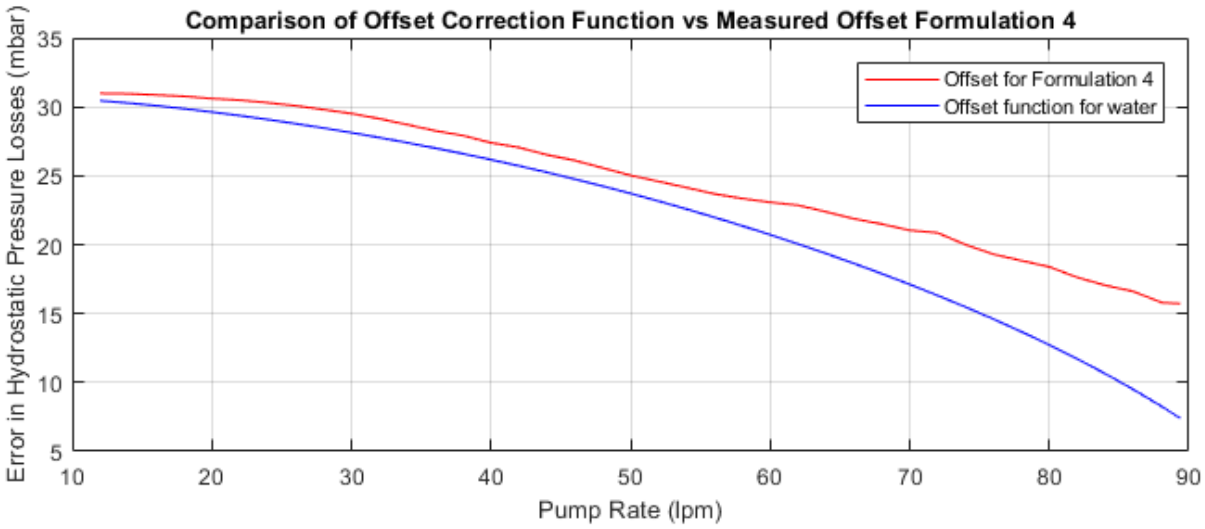

Figure 4.19. Offset correction function vs measured offset of Formulation 4

Similar to the findings generated for Newtonian fluids of densities different to that of water, illustrated in Figure 4.9, we cannot generalize an offset correction function, given that the variances are dependent on both density and viscosity. Consequently, until we do not find a solution to this issue, the estimations of fluid density using the flowloop setup are mere approximations of the actual values. Once again, that is beyond the scope of this thesis.

Now, we shall turn our attention to the modelling of fluid viscosity. It is convenient to start the discussion by presenting the rheological readings obtained with the Fann® Model 35 Viscometer. It is important to point out that the readings presented below were collected at room temperature (approximately 15 °C), and they were verified by double-checking one sample with multiple viscometers at the UiS Drilling Fluids Laboratory. The samples of each formulation were collected from the flowloop tank after circulating the system for 20 minutes, the stability of the rheology was verified after 72 hours in the tank. Table 4.3 presents a composite of the rheological characterization of the five formulations obtained with the Fann® Model 35 Viscometer.

Table 4.3. Fann® Model 35 Viscometer readings of each of the fluid formulations

Speed	Formulation 1	Formulation 2	Formulation 3	Formulation 4	Formulation 5
600	10	16.5	20	27.5	31.5
300	7.5	12.5	16.5	23	26
200	6.5	11	14.5	20	23
100	5	9	12	16.5	19.5
6	2	4.5	6	9.5	12
3	1.5	4	5	8.5	11

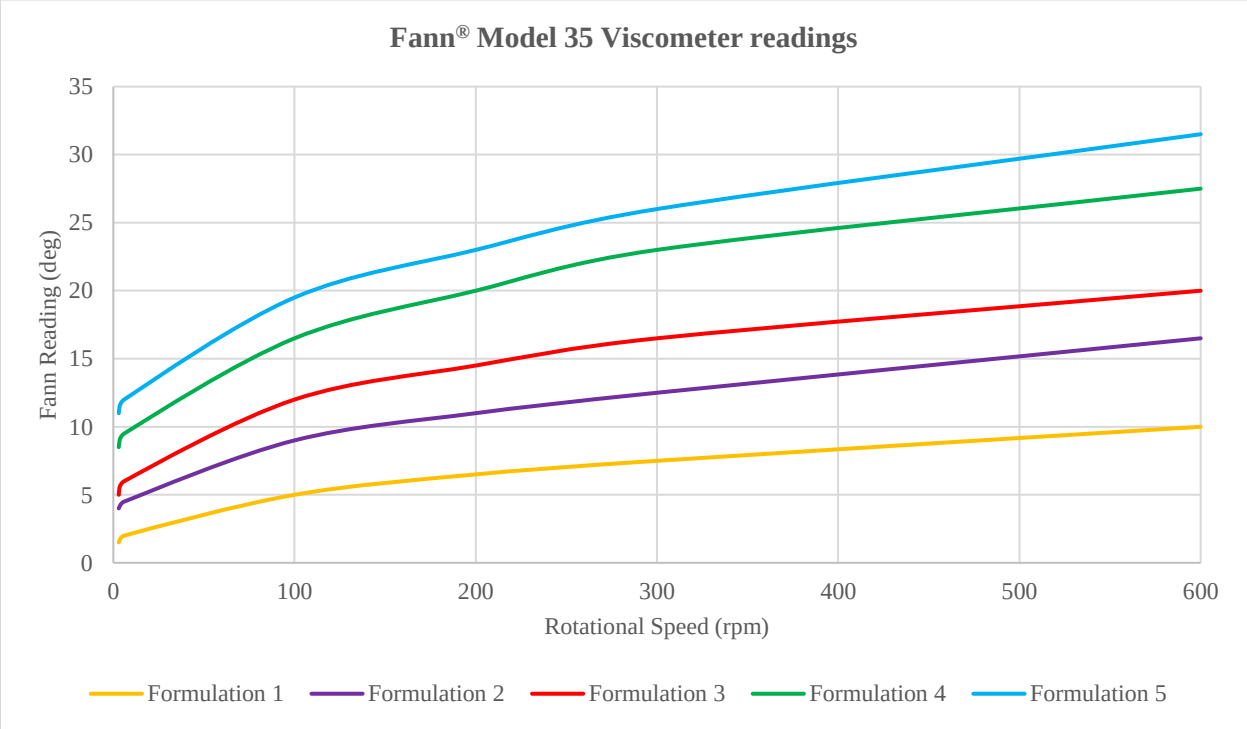

Figure 4.20. Comparison of Fann® Model 35 Viscometer readings

Let us elaborate further on the fluid characterization that can be done based on the data set presented above. First, we shall consider Formulation 3 to develop the ideas that will be fundamental to understand the forthcoming discussion on the limitations encountered to model adequately the fluid viscosity based on the flowloop data. Figures 4.21 and 4.22 have been generated with MudWare® ver. 3.0, a Schlumberger M-I SWACO proprietary software in the public domain that is easily accessible on their website.

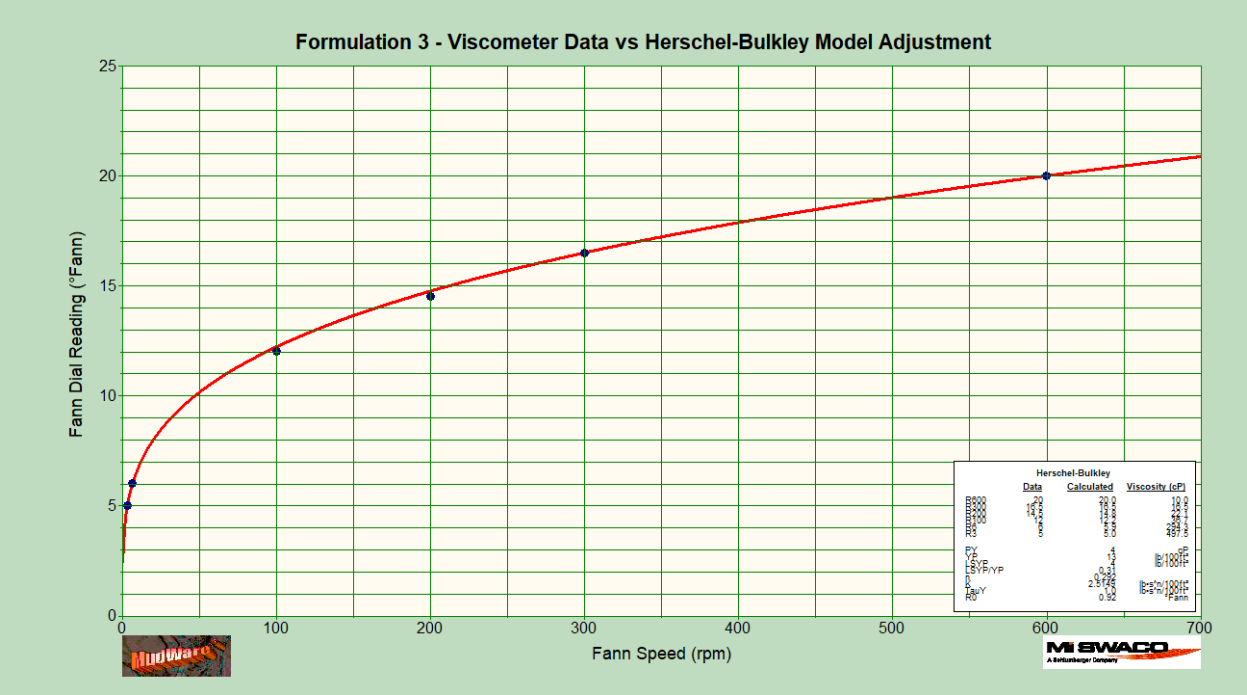

Figure 4.21. Viscometer data vs Herschel-Bulkley model adjustment of Formulation 3

In Figure 4.21, we have plotted the Fann® Model 35 Viscometer readings (blue points) along with the calculated values (red curve) obtained with the equations of the Herschel-Bulkley rheological model presented in subsection 2.4.2. Note that the data is presented in a linear scale where the dimensions are the Fann® rotational speed (rpm) and the Fann® readings (°Fann®).

Subsequently, this data can also be translated into the form presented in Figure 4.22 by using the basic definitions introduced in Equation 2.3 and Equation 3.66. Bear in mind that the data is now shown in a log-log scale where the dimensions are shear rate (sec^{-1}) and viscosity (cP). Similar plots were generated for each of the five formulations based on the data set presented in Table 4.3.

Figure 4.23 is a composite of the shear rate vs Herschel-Bulkley viscosity calculations generated for all the fluids tested in the UiS Drilling Fluids Laboratory.

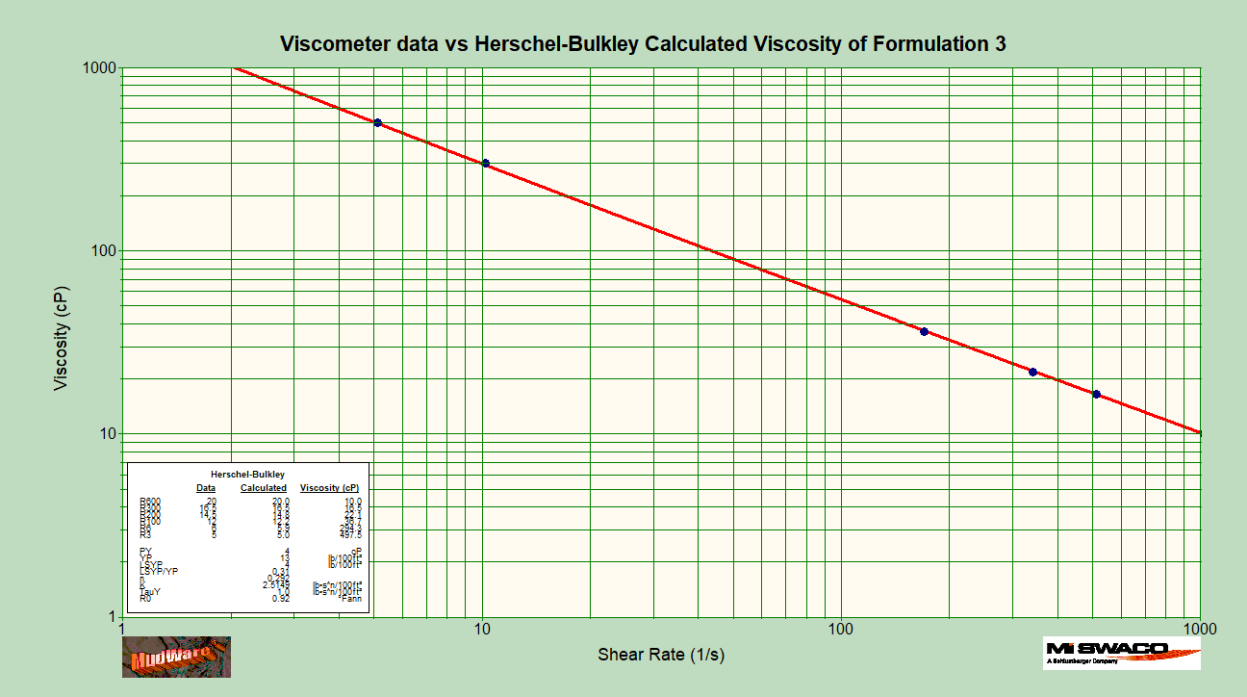

Figure 4.22. Viscometer data vs Herschel-Bulkley calculated viscosity of Formulation 3

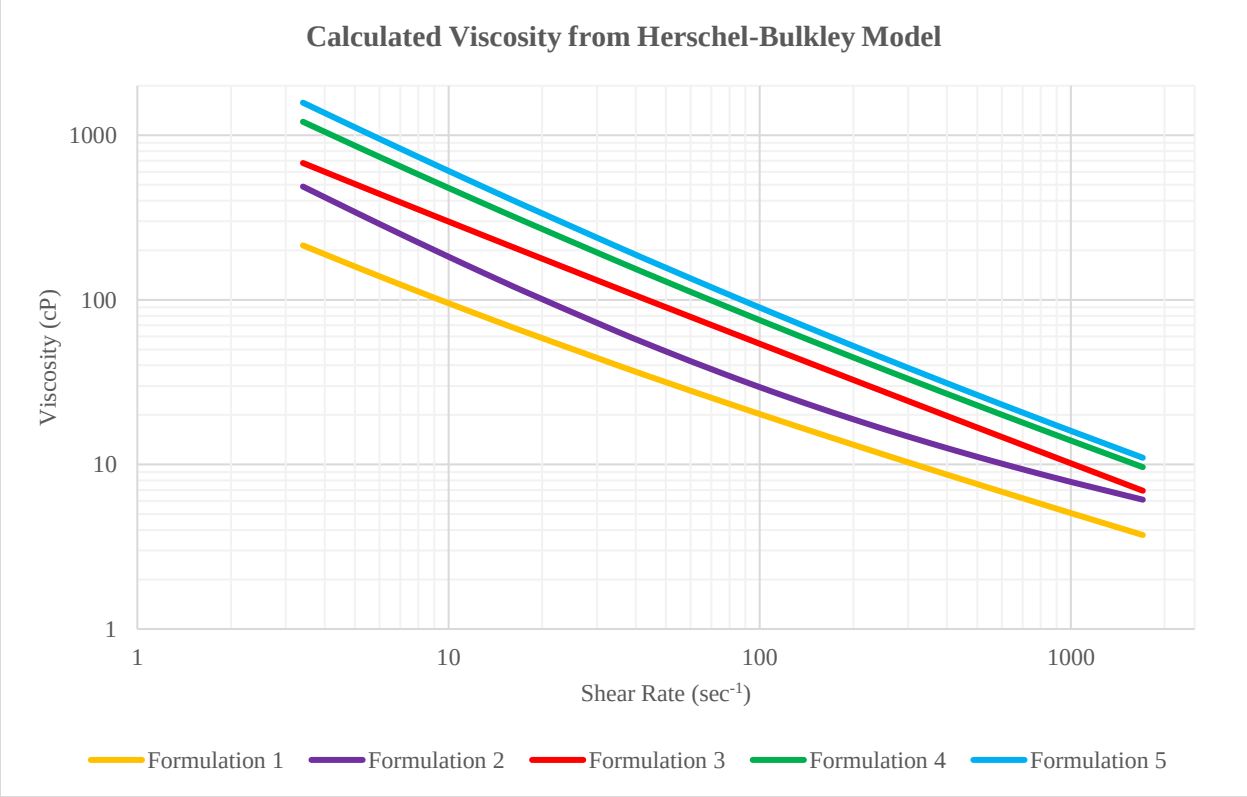

Figure 4.23. Composite of calculated viscosity using the Herschel-Bulkley model

Once we have presented the information portrayed in Figure 4.23, we move forward to introduce the calculated viscosities obtained from the flowloop measurements. The reader might find convenient at this point to review the procedure described in subsection 3.4.2. We shall point out that the Master's Thesis developed last year [18] recommends to use of the Rabinowitsch-Mooney Equation to model the fluid viscosity based on the horizontal pressure losses recorded with the flowloop setup. Thus, our starting point was to calculate the fluid viscosity with the procedure defined in Equations 3.52 through 3.57.

For illustrative purposes, we continue the discussion using Formulation 3 to demonstrate the findings. When the Rabinowitsch-Mooney Equation is used to compute fluid viscosity based on the flowloop measurements, there is a clear mismatch of the calculated values (red points) when compared to the Herschel-Bulkley viscosities (blue curve) obtained from the Fann® Model 35 Viscometer readings, as clearly seen in Figure 4.24.

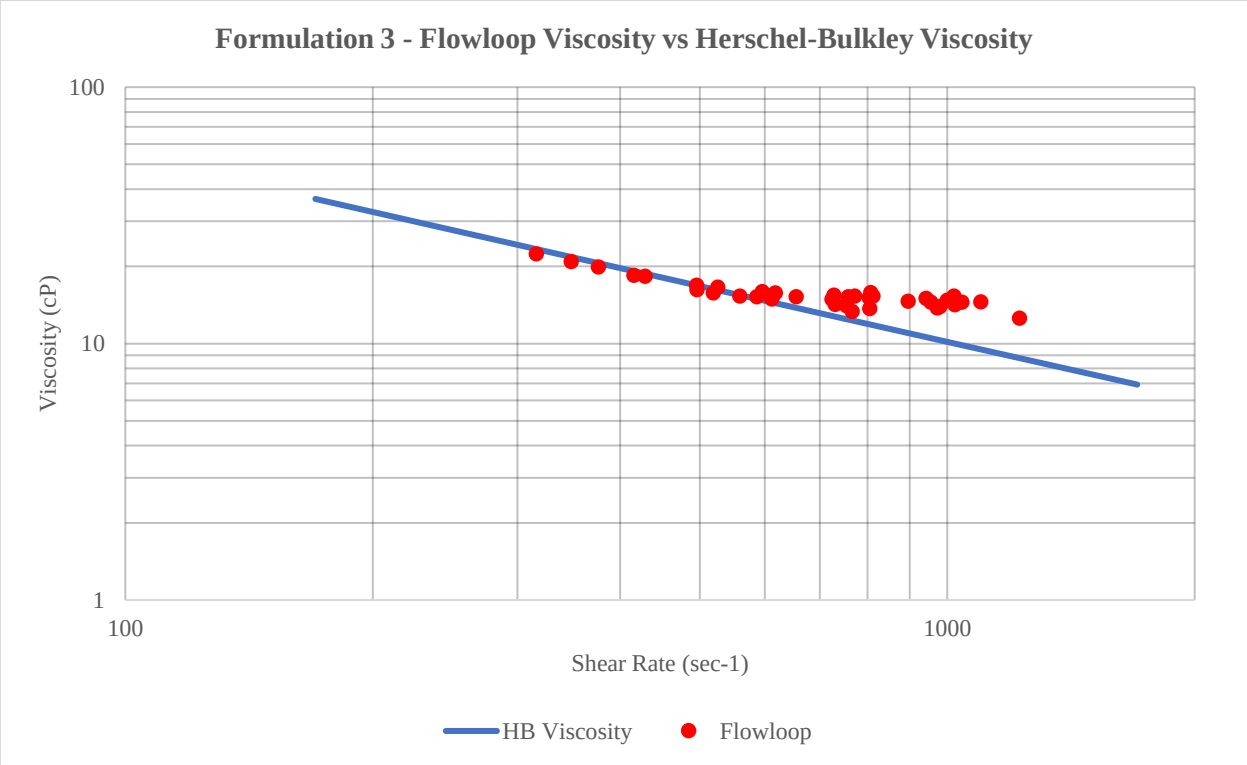

Figure 4.24. Formulation 3 – Initial flowloop Viscosity vs Herschel-Bulkley Viscosity

Now, observe that the calculated flowloop viscosities match the Herschel-Bulkley values until certain point at which the mismatch becomes clearly evident. We decided to investigate the effect of the flow regime in this behavior; thus, when plotting on the same chart the boundaries of laminar and turbulent flow regimes, a trend becomes evident. This hypothesis is illustrated in Figures 4.25 through 4.29 presented below.

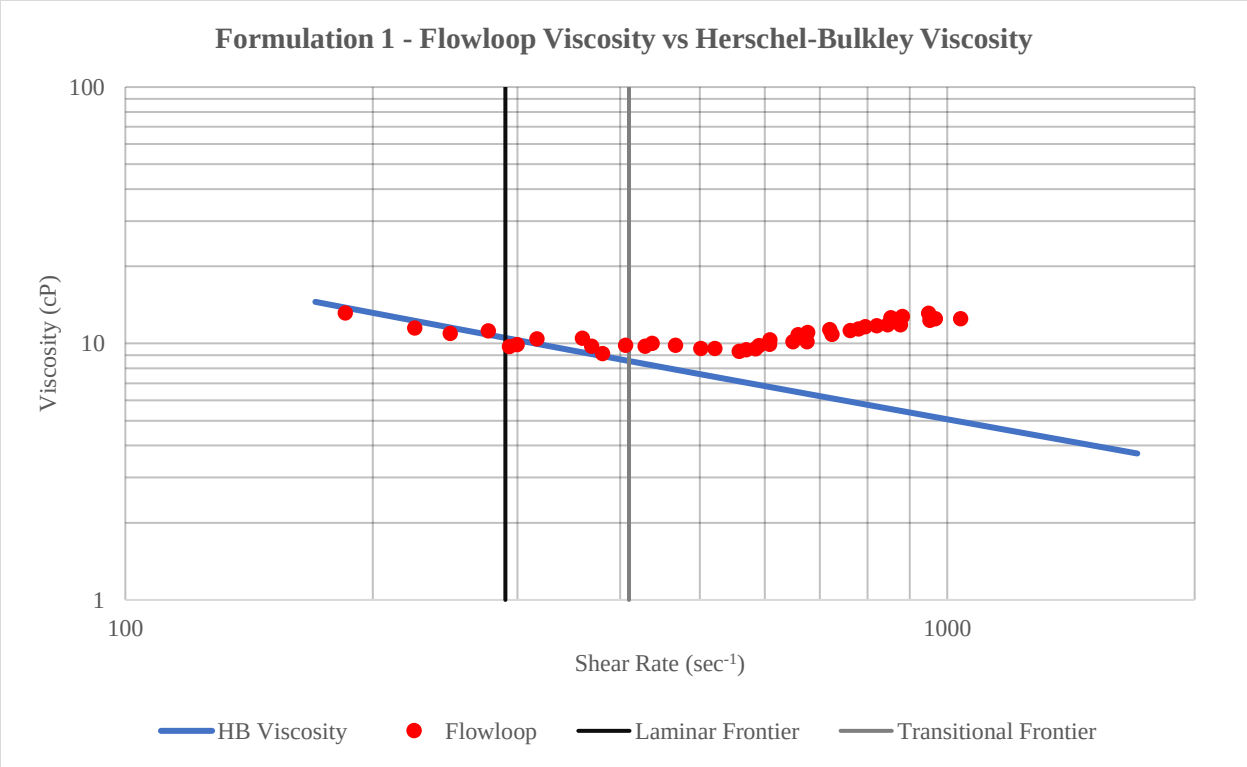

Figure 4.25. Formulation 1 - Flowloop Viscosity vs Herschel-Bulkley Viscosity

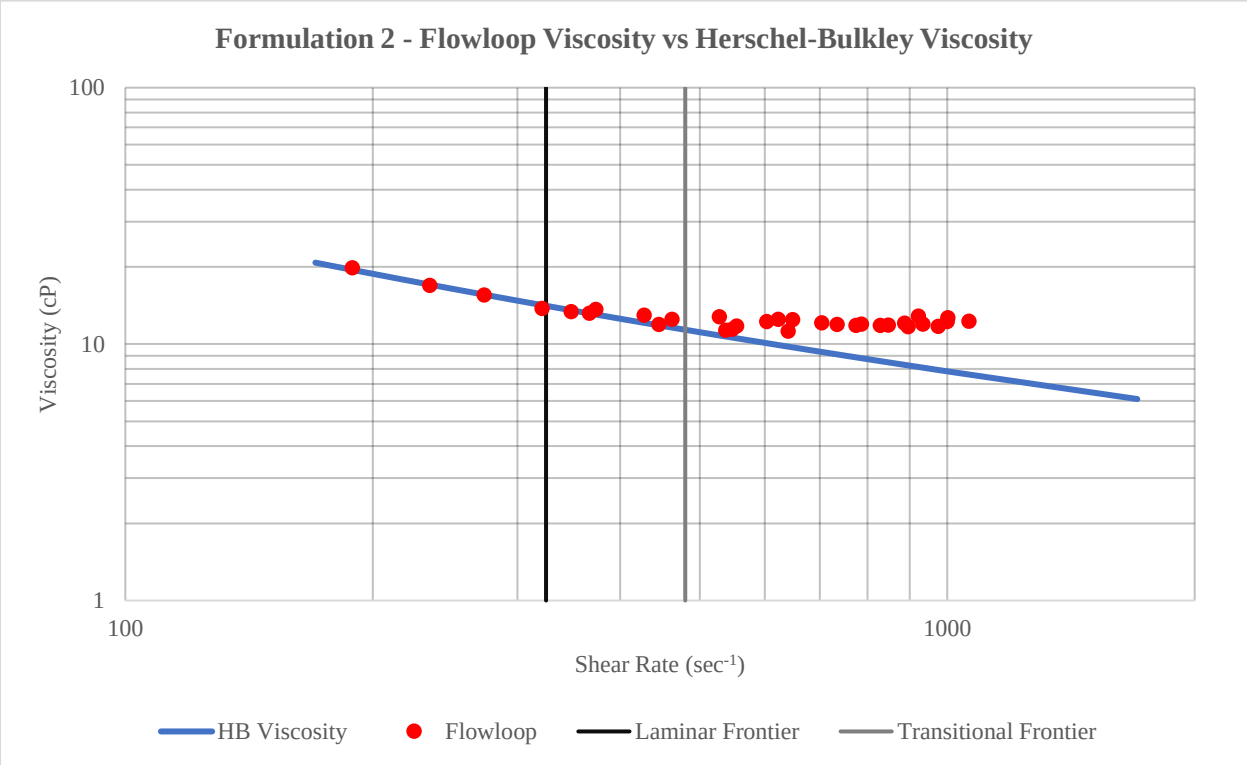

Figure 4.26. Formulation 2 - Flowloop Viscosity vs Herschel-Bulkley Viscosity

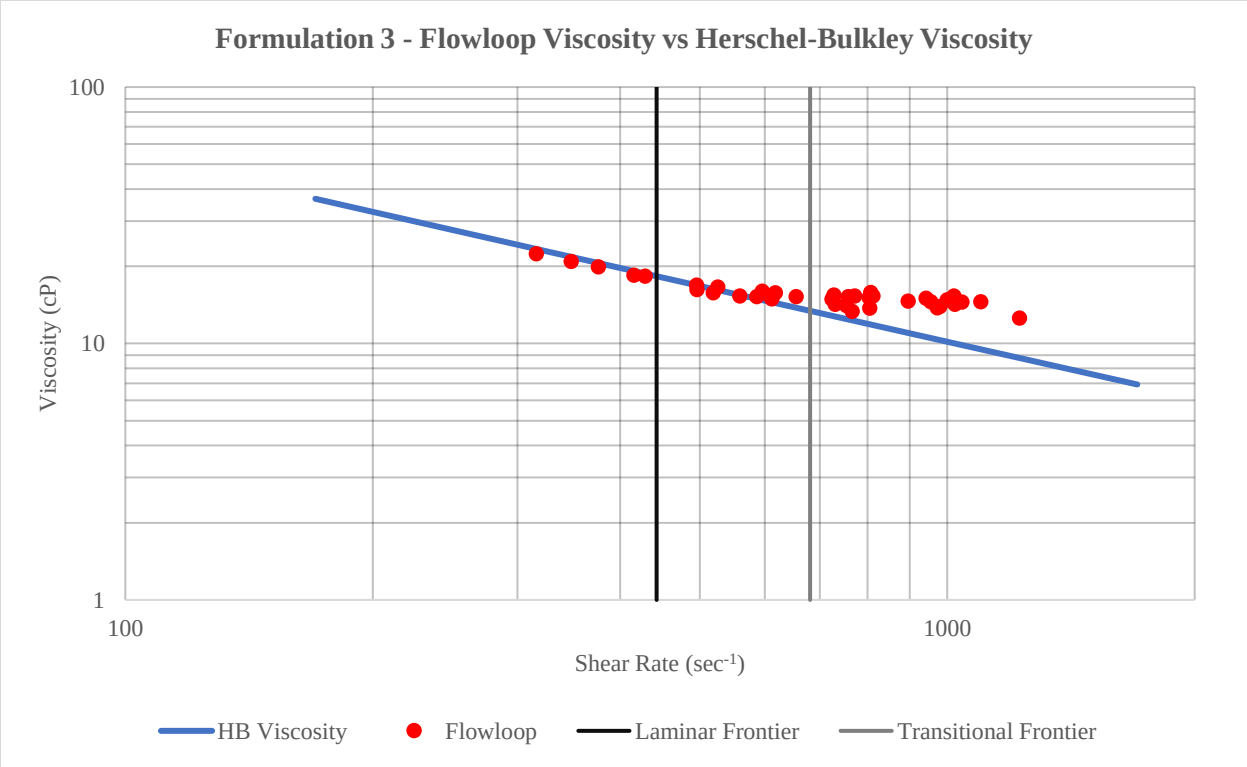

Figure 4.27. Formulation 3 - Flowloop Viscosity vs Herschel-Bulkley Viscosity

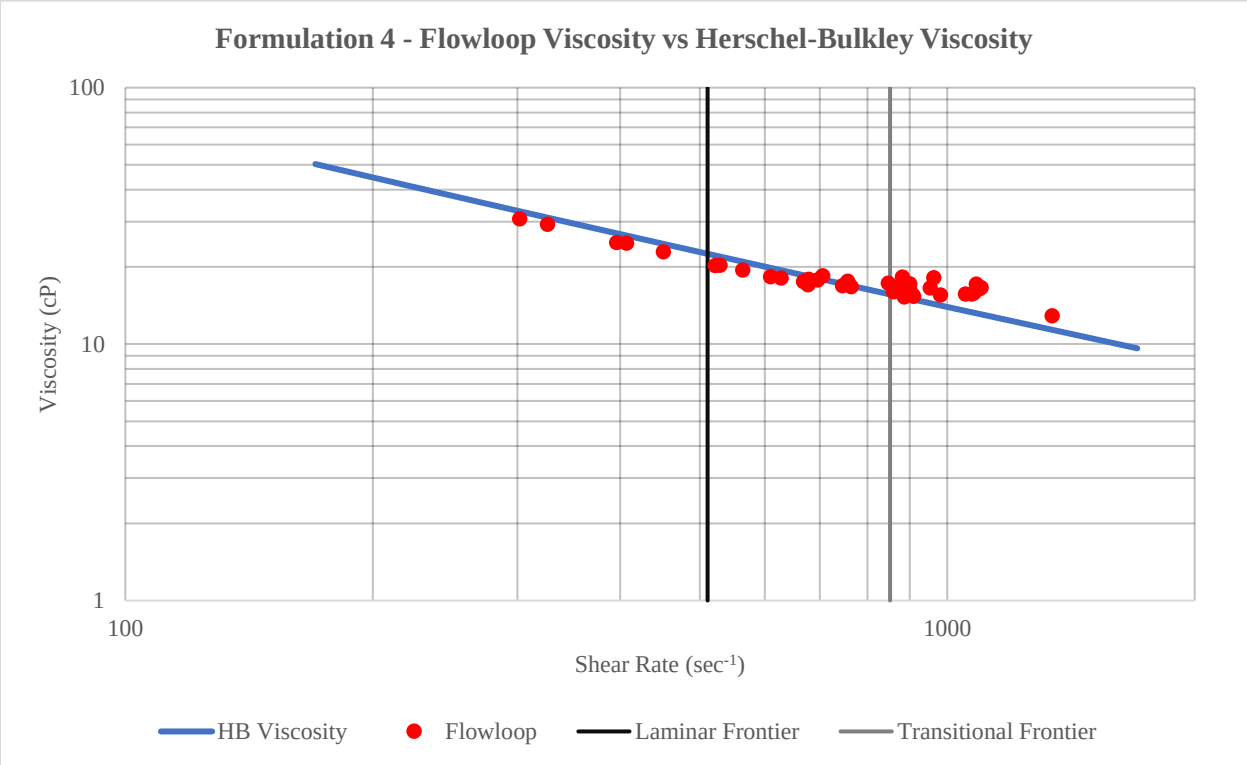

Figure 4.28. Formulation 4 - Flowloop Viscosity vs Herschel-Bulkley Viscosity

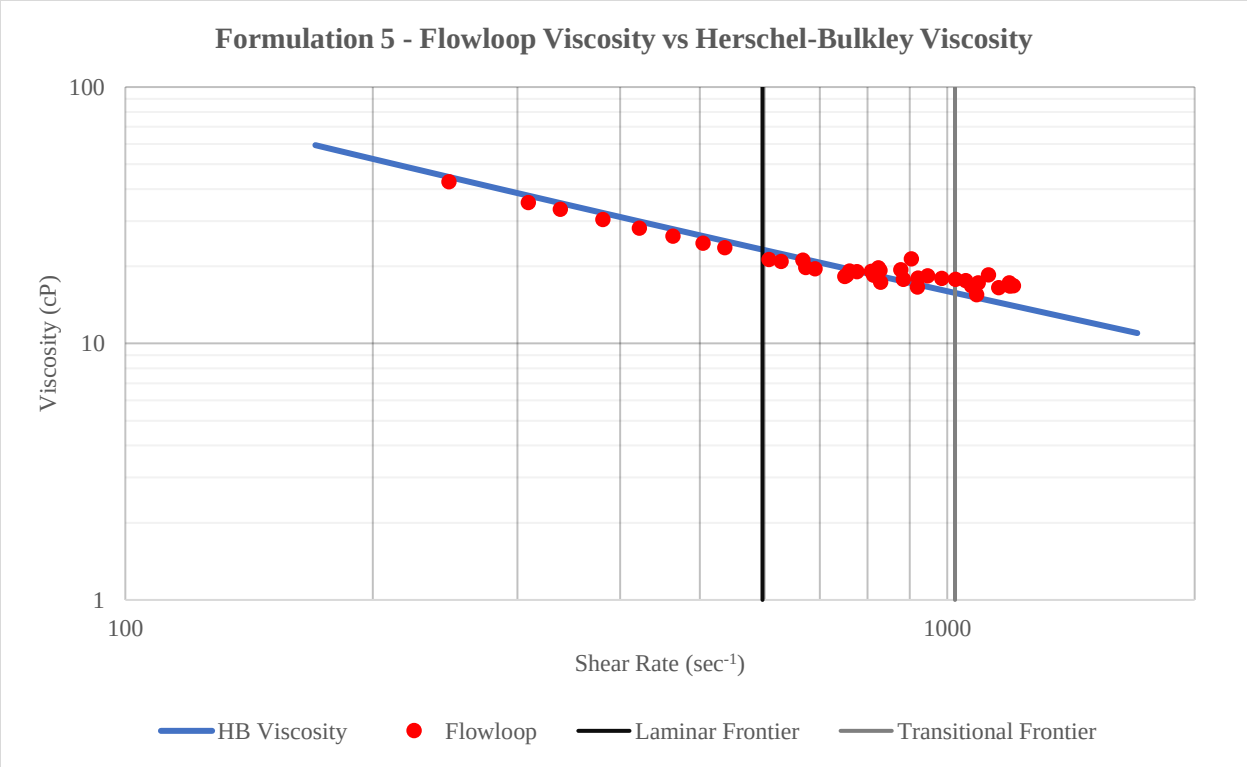

Figure 4.29. Formulation 5 - Flowloop Viscosity vs Herschel-Bulkley Viscosity

The difference between Figure 4.25 and Figure 4.29 is striking, the Rabinowitsch-Mooney Equation is not applicable to turbulent flow regime since Equation 3.52, used to determine the shear stress at the pipe wall τ_w, was developed for the geometry corresponding to a fully developed laminar flow. This explains why the mismatch is more severe in thinner fluids that develop turbulent flow at lower pump rates, and the discrepancies reported in the Master's Thesis developed last year [18].

Therefore, it was clear that an additional model was required to determine an adequate friction factor for turbulent flow, which would be subsequently used to calculate the fluid viscosity as described in subsection 3.4.2. Several models available in the literature were analyzed, they are presented in Table 4.4 [20] shown below.

Table 4.4. Friction factor correlations for Non-Newtonian fluids in turbulent flow [20]

Author	Year	Equation
Dodge & Metzner	1959	$\frac{1}{\sqrt{f(i)}} = \frac{4.0}{n_a(i)^{0.75}} \cdot \log\left[Re_{HB}(i)\cdot f(i)^{1-\frac{n_a(i)}{2}}\right] - \frac{0.4}{n_a(i)^{1.2}}$
Shaver & Merill	1959	$f(i) = \frac{0.079}{n_a(i)^5 \cdot Re_{HB}(i)^{\frac{2.63}{10.5^{n_a(i)}}}}$
Thomas	1960	$\frac{1}{\sqrt{f(i)}} = \frac{4.0}{n_a(i)} \cdot \log\left[Re_{HB}(i)\cdot f(i)^{1-\frac{n_a(i)}{2}}\right] - 0.4\cdot n_a(i)$
Clapp	1961	$\frac{1}{\sqrt{f(i)}} = \frac{4.53}{n_a(i)} \cdot \log\left[Re_{HB}(i)\cdot f(i)^{1-\frac{n_a(i)}{2}}\right] + \frac{2.69}{n_a(i)} + 0.68\cdot\left(5\cdot n_a(i) - \frac{8}{n_a(i)}\right)$
Trinh	1969	$\frac{1}{\sqrt{f(i)}} = \frac{4.06}{n_a(i)} \cdot \log\left[Re_{HB}(i)\cdot f(i)^{1-\frac{n_a(i)}{2}}\right] - \frac{2.78}{n_a(i)} + 2.16$
Hanks & Ricks	1973	$f(i) = \frac{0.0682\cdot n_a(i)^{-0.5}}{Re_{HB}(i)^{\frac{1}{1.87+2.39\cdot n_a(i)}}}$
Shenoy & Saini	1986	$\frac{1}{\sqrt{f(i)}} = 3.57 \cdot \log\left[\frac{Re_{HB}(i)^{\frac{1}{n_a(i)^{0.615}}}}{6.5^{\frac{1}{n_a(i)^{1+0.75\cdot n_a(i)}}}}\right]$
El-Eman et al	2003	$f(i) = \frac{n_a(i)}{\frac{(3.072-0.1433\cdot n_a(i))\cdot Re_{HB}(i)^{\frac{n_a(i)}{0.282-4.211\cdot n_a(i)}} - 0.00065}{4}}$

The different correlations presented in Table 4.4 were implemented in a MATLAB® script included in Appendix C. A comparison was performed in order to select the model that yields the best approximation of the Herschel-Bulkley fluid viscosity values. Figure 4.30 shows the comparison of the different models using the flowloop data of Formulation 5.

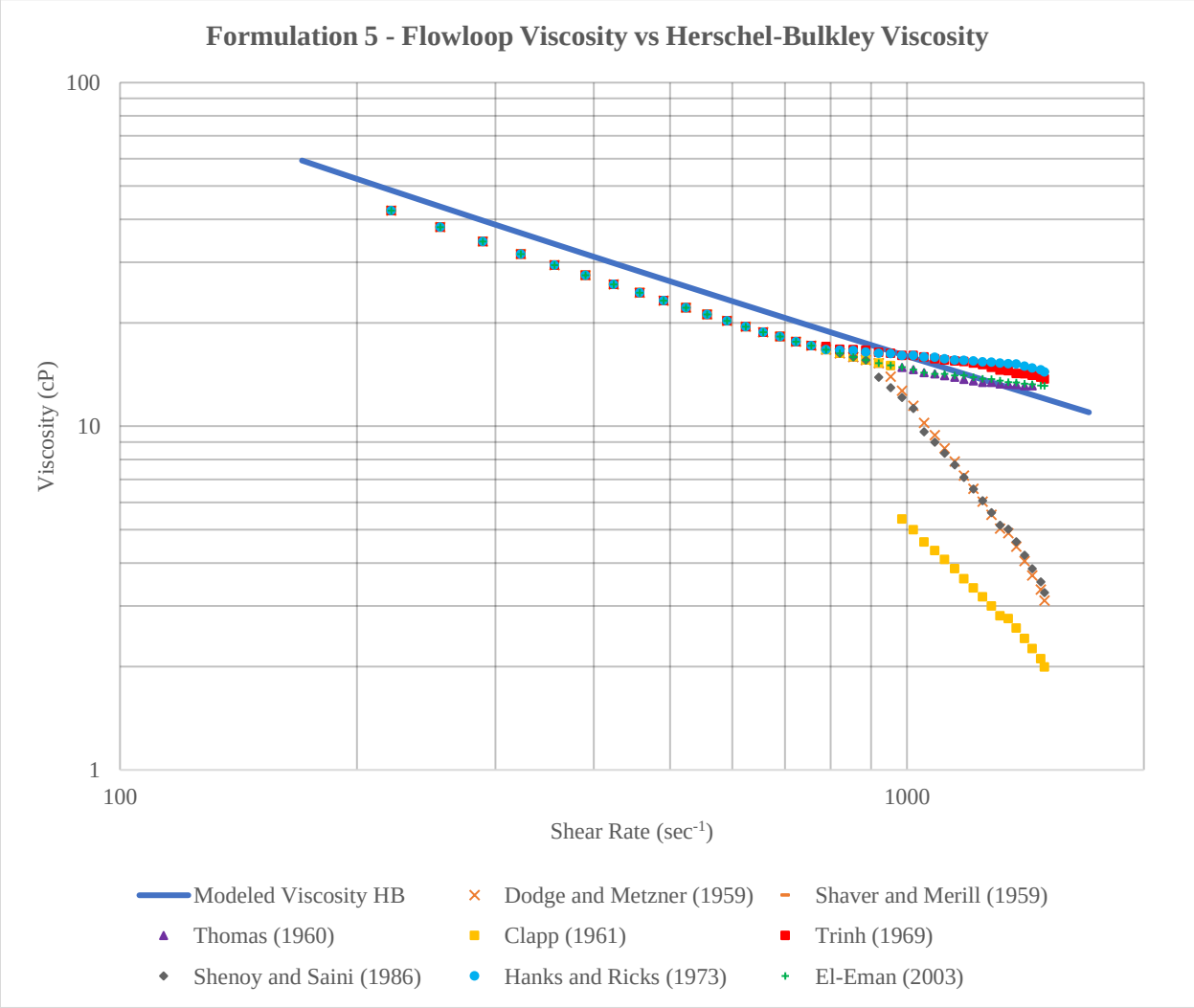

Figure 4.30. Comparison of the friction factor correlations for Non-Newtonian fluids in turbulent flow

Similar comparisons were performed for each of the formulations tested. After analyzing the results, the Thomas (1960) correlation, described in Equation 3.64 was selected as the most accurate approximation for the turbulent flow region. It is important to bring to the attention of the reader that not all the correlations presented in Table 4.4 were stable for all the flowloop datasets; we have decided to present the results obtained for Formulation 5 for illustrative purposes, but we shall also point out that the Thomas (1960) correlation was not only stable, but also yielded the best adjustment for each of the formulations tested in this study.

The figures to be presented next were generated based on the notions discussed above; they are the final estimations of the fluid viscosity using the data collected from the flowloop setup for each of the formulations analyzed in this experimental study. The blue curve depicts the Herschel-Bulkley fluid viscosities obtained from the Fann® Model 35 Viscometer readings, the red points are the viscosity values calculated using the Rabinowitsch-Mooney Equation, and the purple markers represent the fluid viscosities generated with the Thomas (1960) correlation.

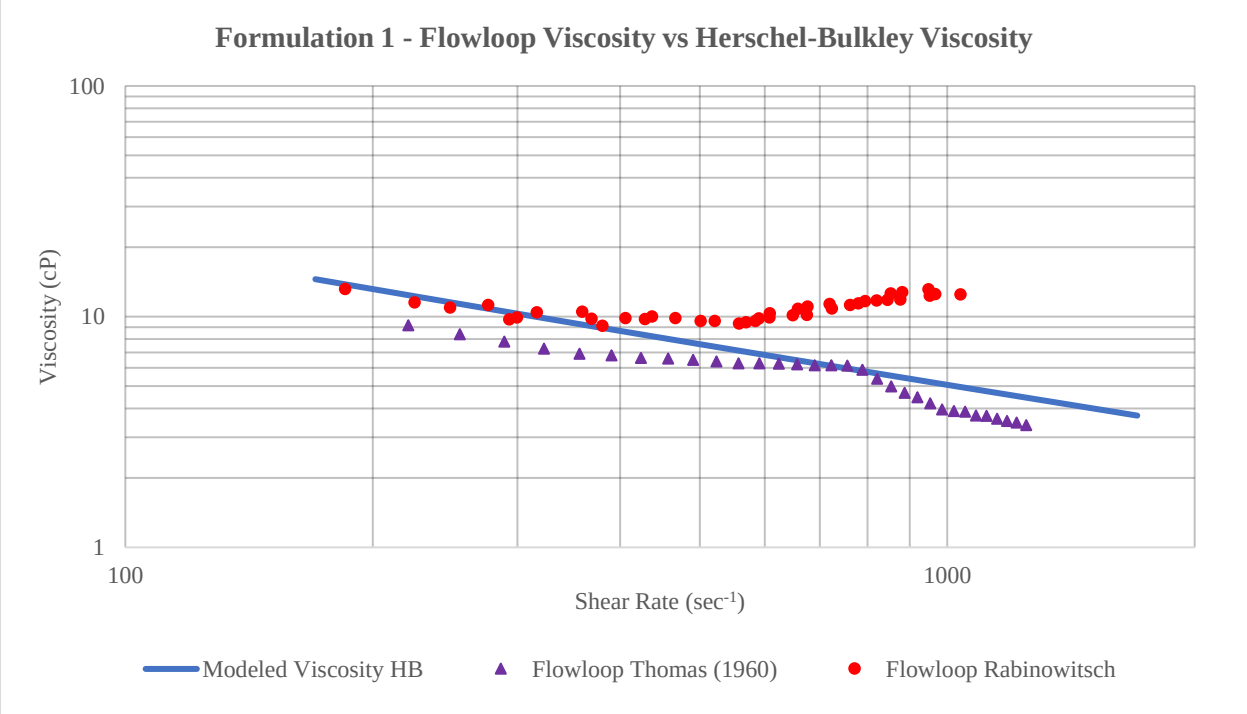

Figure 4.31. Formulation 1 - Comparison of Flowloop Viscosity vs Fann® 35 Viscosity

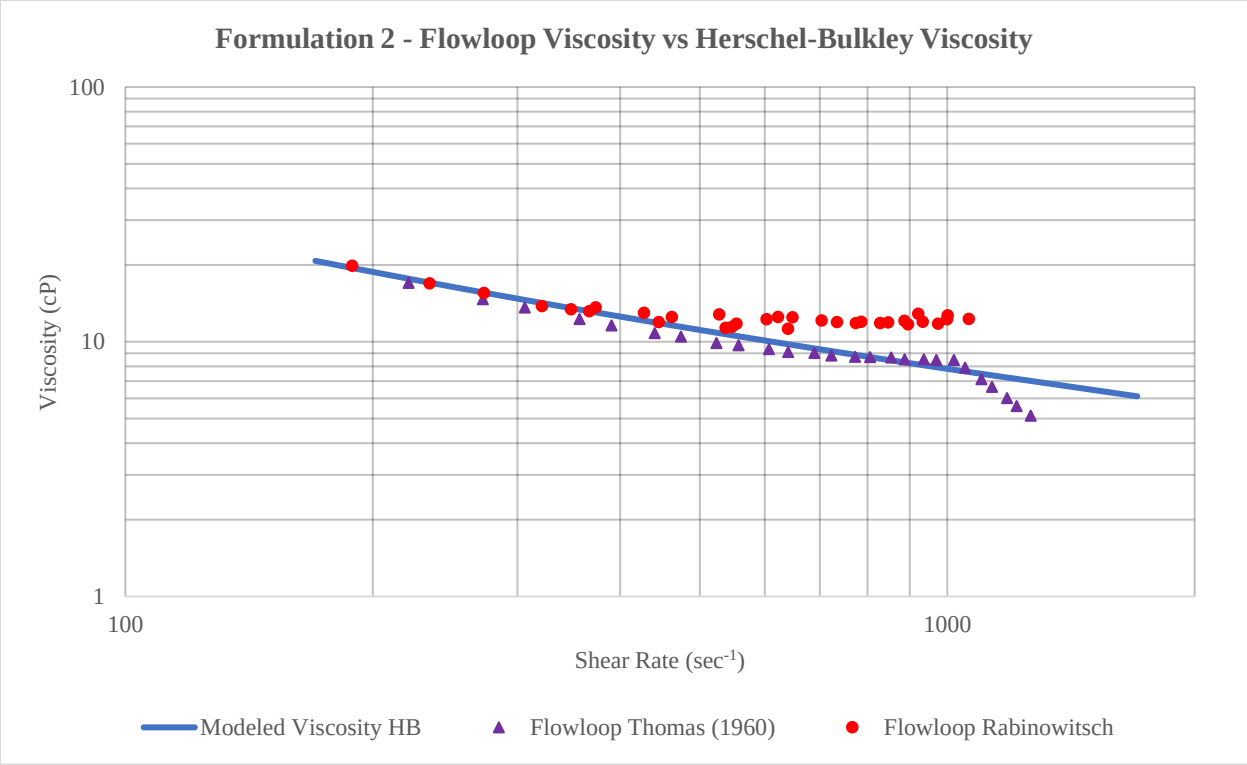

Figure 4.32. Formulation 2 - Comparison of Flowloop Viscosity vs Fann® 35 Viscosity

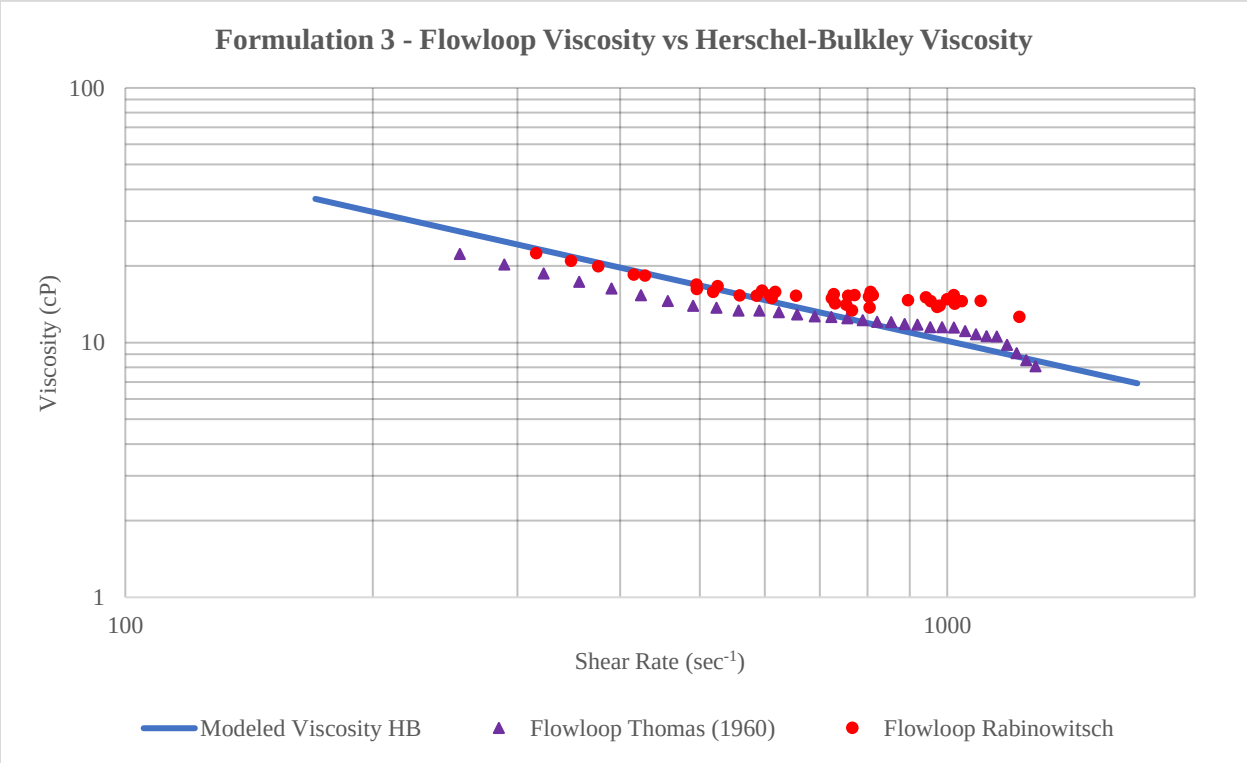

Figure 4.33. Formulation 3 - Comparison of Flowloop Viscosity vs Fann® 35 Viscosity

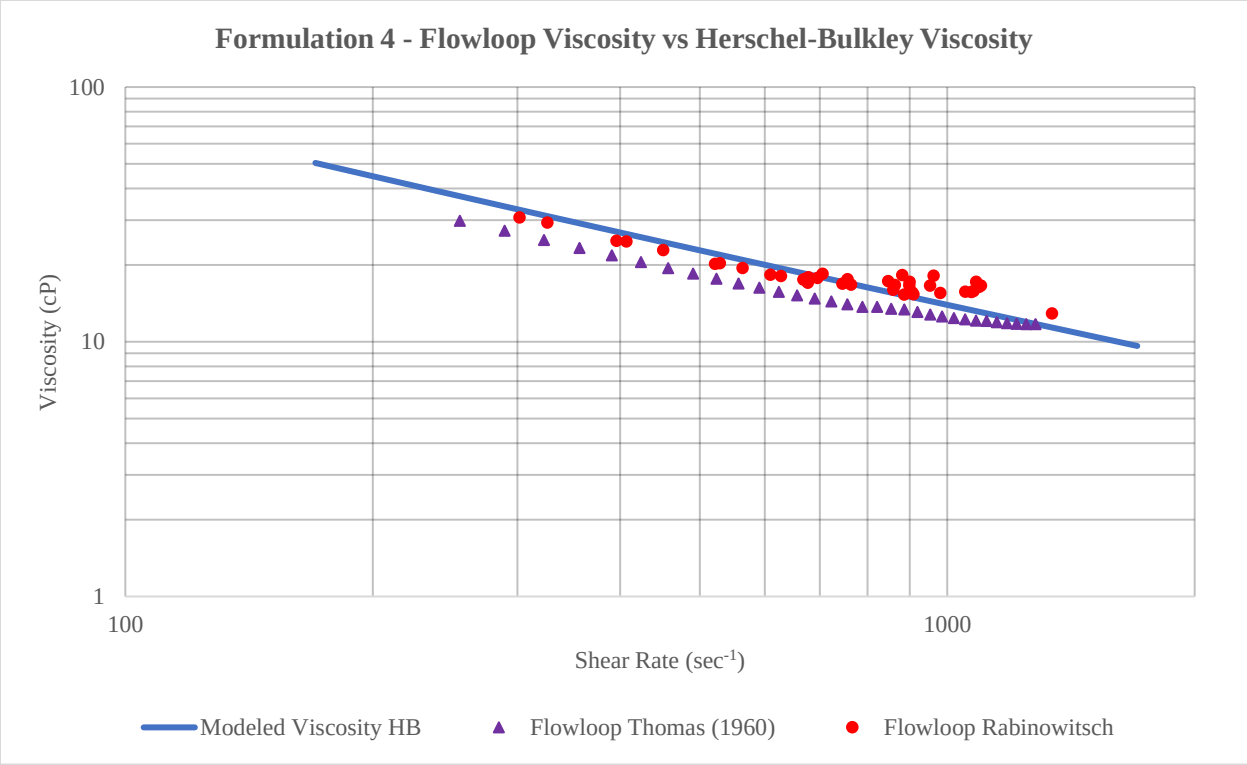

Figure 4.34. Formulation 4 - Comparison of Flowloop Viscosity vs Fann® 35 Viscosity

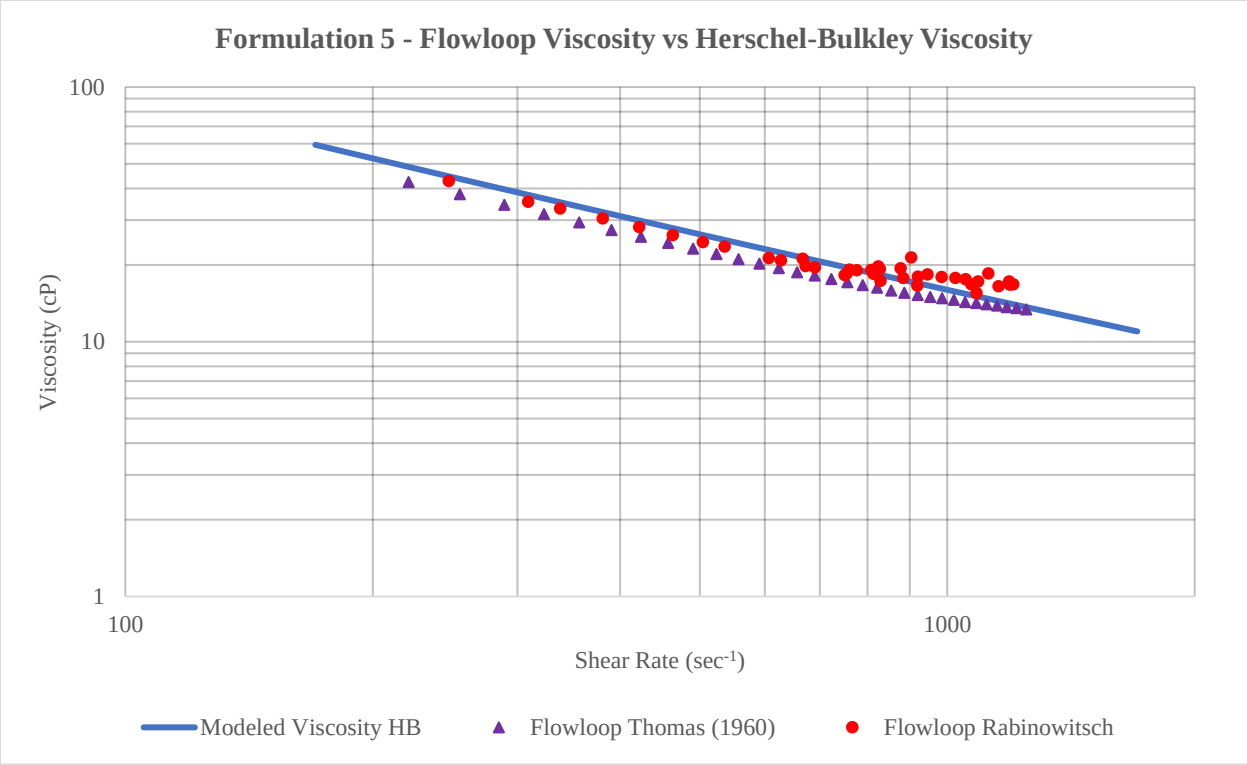

Figure 4.35. Formulation 5 - Comparison of Flowloop Viscosity vs Fann® 35 Viscosity

From the findings presented above we can draw some conclusions regarding the accuracy of the fluid viscosity estimations using the flowloop setup. First, the inclusion of the Thomas (1960) correlation improved the modelling of fluid viscosity in the turbulent flow region. Nevertheless, there is still a significant discrepancy that makes the estimated fluid viscosity values from the flowloop setup, of little use for practical purposes. On the positive side, we have experimentally verified the applicability of the Rabinowitsch-Mooney Equation for the laminar and transitional regions. Now, the fact that we have to select manually the values of the weight function by trial and error, makes it impossible to produce a generalized MATLAB® script to model any given fluid.

A future alternative to continue this work is to devise a way to combine both the Rabinowitsch-Mooney Equation for laminar and transitional flow regimes, and the Thomas (1960) correlation for turbulent flow. The model will have to define first the adequate flow regime and then select the suitable expression to calculate the fluid viscosity. The combination of both models could be an alternative to generate a more accurate approximation of the fluid properties.

A wary Fluids Engineer would argue that the rheological readings of Formulation 5 are more in accordance to the rheological profile of a typical drilling mud. Thus, it could be possible to validate the applicability of the estimation of fluid viscosity using the instrumented standpipe concept, by carrying out a statistical analysis of the geometry of the pipes in the surface connections of different drilling rigs, compared to the typical pumping rates used for drilling, in order to define whether the fluid is in most cases in laminar or transitional flow regimes when it travels through the standpipe. This could be a possible way to apply the Rabinowitsch-Mooney Equation in a practical way and could potentially be the subject of a future study.

Chapter 5

Conclusions and Recommendations

This experimental study concludes with a set of remarks that summarize the findings presented in the previous sections. First, we should point out that there is an inherent mismatch between the theoretical pressure differential values and the measured pressure losses recorded with the flowloop setup; these discrepancies are dependent on the pump rate, but further investigation showed that they are also dependent on the density and viscosity of the fluid in question; henceforth, it is not viable to generalize a calibration function based on the measurements of a particular fluid. This shortcoming is the single most critical issue that renders the estimations of fluid density and viscosity using the flowloop setup, rough approximations of the actual values.

With respect to the estimation of fluid viscosity, we have experimentally verified the applicability of the Rabinowitsch-Mooney Equation for the laminar and transitional flow regimes. Unfortunately, the modelling of turbulent flow faced significant caveats that were necessary to be addressed on a single case basis, thus, reducing the possibility of applying the concept in practice.

The foaming problems faced on the previous work were resolved by modifying the fluid formulations, this improvement resulted in a more accurate estimation of fluid density, nevertheless they are still not sufficiently precise due to the inadequate calibration function used to process the measurements collected in the flowloop setup.

It is in the personal opinion of the author that the automated measurement of drilling fluid properties using the instrumented standpipe concept has narrow chances of becoming a commercially applicable concept. Besides the aforementioned shortcomings of the mathematical models, there are still too many variables in play that would influence the accuracy of the pressure differential measurements, and the actual deployment of the idea would most likely require to modify the surface connections in the drilling rigs in order to have the conditions needed to apply the concept in practice.

Furthermore, there are several solutions already available in the market that provide a more detailed set of information in a more practical way; some service providers already supply fully automated fluid monitoring systems that are able to determine not only density and viscosity, but also the chemical composition of the fluid, particle size distribution, etc. Unless the approach to this research topic is revised, the author considers that there is little benefit to continue investigating further the applicability of the automated measurement of drilling fluid properties using the instrumented standpipe concept.

References

[1] M-I SWACO a Schlumberger Company (December 2006). *Drilling Fluids Engineering Manual*, Revision No. A-2.

[2] American Petroleum Institute (April 2014). *API Recommended Practice 13B-2 Recommended Practice for Field Testing Oil-Based Drilling Fluids*, 5th Edition.

[3] American Petroleum Institute (March 2009). *API Recommended Practice 13B-1 Recommended Practice for Field Testing Water-Based Drilling Fluids*, 4th Edition.

[4] Fann Instrument Company (January 2016). *Model 35 Viscometer Instruction Manual*, Manual No. 208878, Revision P.

[5] OFI Testing Equipment (April 2014). *Metal Mud Balance (Machined Balance) Instruction Manual*. Manual #115-00, Ver. 1.5.

[6] Fann Instrument Company (January 2015). *TRU-WATE™ Fluid Density Balance, Model 141 Instruction Manual*, Manual No. 100063065, Revision J.

[7] Fann Instrument Company (May 2013). *Marsh Funnel Viscometer Instructions*, Revision B.

[8] American Petroleum Institute (May 2003). *API Recommended Practice 13D Recommended Practice on the Rheology and Hydraulics of Oil-well Drilling Fluids*, 4th Edition.

[9] American Petroleum Institute (Sept 2017). *API Recommended Practice 13D Recommended Practice on the Rheology and Hydraulics of Oil-well Drilling Fluids*, 7th Edition.

[10] Baker Hughes (2006). *Drilling Fluids Reference Manual*, Revision 2006.

[11] Dahlem, A. (June 2013). *Automatic Adjustment of Drilling Fluid Properties*. Master's Thesis, Faculty of Science and Technology, University of Stavanger.

[12] Hjelm, O. Jøsang Nilsen, S., and Wærnes, T. (May 2016). *Automatic Evaluation of Drilling Properties and Construction of Laboratory Model*. Bachelor's Thesis. Faculty of Science and Technology, University of Stavanger.

[13] Sui, D. (2017). *Drilling Automation*. Lecture Notes (Not published), Faculty of Science and Technology, University of Stavanger.

[14] "Flow in Pipes" (2011). *Pipeflow_Intro*. Educational Material for MEK4450 Offshore Technology, University of Oslo. Available in https://www.uio.no/studier/emner/matnat/math/MEK4450/h11/undervisningsmateriale/modul-5/Pipeflow_intro.pdf

[15] COMSOL Group (July 2017). *COMSOL Multiphysics® software - Which Turbulence Model Should I Choose for My Computational Fluid Dynamics Application?*. Available in www.comsol.com/blogs/which-turbulence-model-should-choose-cfd-application.

[16] Metzner, A. B., and Reed, J. (December 1955). *Flow of Non-Newtonian fluids – Correlation of the laminar, transition and turbulent-flow regions.* AIChE Journal 434.

[17] Madlener, K., Frey, B., and H.K., C. (2009). *Generalized Reynolds Number for Non-Newtonian Fluids.* EDP Sciences.

[18] Følling, B. (June 2017). *Experimental Study on Automatic Evaluation of Drilling Fluid Properties*. Master's Thesis, Faculty of Science and Technology, University of Stavanger.

[19] Nguyen, Q. H. and Nguyen, N. D. (March 2012). *Incompressible Non-Newtonian Fluid Flows, Continuum Mechanics - Progress in Fundamentals and Engineering Applications.* InTech, DOI: 10.5772/26091. Available from https://www.intechopen.com/books/ continuum-mechanics-progress-in-fundamentals-and-engineering-applications

[20] Trinh, K. T. (December 2009). *The Instantaneous Wall Viscosity in Pipe Flow of Power Law Fluids: Case Study for a Theory of Turbulence in Time-Independent Non-Newtonian Fluids.* Institute of Food Nutrition and Human Health Massey University, New Zealand.

[21] Kestin, J. et.al. (1981). *Tables of the Dynamic and Kinematic Viscosity of Aqueous NaCl Solutions in the Temperature Range 20-150 °C and the Pressure Range 0.1-35 MPa.* Journal of Physical and Chemical Reference Data 10, 71. Division of Engineering, Brown University.

Appendix A

Determination of drilling fluid density using a pressurized mud balance [2]

1. Principle

1.1 The pressurized mud balance provides a more accurate method for determining the density of a drilling fluid containing entrained air or gas than does the conventional mud balance. The pressurized mud balance is similar in operation to the conventional mud balance, the difference being that the drilling fluid sample is placed in a fixed-volume sample cup under pressure.

1.2 The purpose of placing the sample under pressure is to minimize the effect of entrained air or gas upon drilling fluid density measurements. By pressurizing the sample cup, any entrained air or gas is decreased to a negligible volume, thus providing a drilling fluid density measurement more closely in agreement with that obtained under downhole conditions.

2. Apparatus

2.1 Any density-measuring instrument having an accuracy of ±0.01 g/ml or 10 kg/m^3 (0.1 lb/gal or 0.5 lb/ft^3). A pressurized mud balance is the instrument generally used for density determinations of pressurized drilling fluids. The pressurized mud balance is designed such that the drilling-fluid holding cup and screw-on lid, at one end of the beam, is balanced by a fixed counterweight at the other end, with a sliding-weight rider free to move along a graduated scale. A level-bubble is mounted on the beam to allow for accurate balancing. The instrument should be calibrated frequently with fresh water, e.g. bi-weekly or weekly. Fresh water should give a reading of 1.00 g/ml or 1000 kg/m^3 (8.345 lb/gal or 62.4 lb/ft^3) at 21 °C (70 °F). If it does not, adjust the balancing screw or the amount of lead shot in the well at the end of the graduated arm, as required. A calibration of the upper density should be performed as specified by the manufacturer, and done on a less frequent basis, e.g. annually.

2.2 Thermometer, with a range of 0 - 105 °C (32 - 220 °F) and an accuracy of ±1 °C (±2 °F).

3. Procedure

3.1 Measure the temperature of the drilling fluid and record.

3.2 Fill the sample cup of the pressurized mud balance to a level approximately 6.5 mm (0.25 in) below the upper edge of the cup.

3.3 Place the lid on the cup with the attached check-valve in the down (open) position. Push the lid downward into the mouth of the cup until surface contact is made between the outer skirt of the lid and the upper edge of the cup. Any excess drilling fluid will be expelled through the check-valve. When the lid has been placed on the cup, pull the check-valve up into the closed position, rinse off the cup and threads with water, and screw the threaded cap on the cup.

3.4 The pressurizing plunger is similar in operation to a syringe. Fill the plunger by submersing its end in the drilling fluid with the piston rod completely inside. Then draw the piston rod upward, thereby filling the cylinder with drilling fluid. This volume should be expelled with the plunger action and refilled with fresh drilling fluid sample to ensure that this plunger volume is not diluted with liquid remaining from the last clean-up of the plunger mechanism.

3.5 Push the nose of the plunger onto the mating O-ring surface of the cap valve. Pressurize the sample cup by maintaining a downward force on the cylinder housing in order to hold the check-valve down (open) and at the same time force the piston rod inside. A force of approximately 225 N (50 lb-force) or greater should be maintained on the piston rod.

3.6 The check-valve in the lid is pressure-actuated; when the inside of the cup is pressurized, the check-valve is pushed upward into the closed position. To close the valve, gradually ease up on the cylinder housing while maintaining pressure on the piston rod. When the check-valve closes, release pressure on the piston rod before disconnecting the plunger.

3.7 The pressurized drilling fluid sample is now ready for weighing. Rinse the exterior of the cup and wipe dry. Place the instrument on the knife edge. Move the sliding weight right or left until the beam is balanced. The beam is balanced when the attached bubble is centered between the two black marks. Read the density from one of the four calibrated scales on the arrow side of the sliding weight. As it is considered that the water density is 1 g/ml, the density can be read directly in units of grams per milliliter using specific gravity scale, pounds per gallon, and pounds per cubic foot, or as a drilling fluid gradient in pounds per square inch per 1000 feet.

3.8 To release the pressure inside the cup, reconnect the empty plunger assembly and push downward on the cylinder housing.

3.9 Clean the cup, lid, and pump assembly. Rinse thoroughly with water.

Appendix B

Determination of viscosity using a direct-reading viscometer [2]

1. Procedure

1.1 Place a sample of the drilling fluid in a thermostatically controlled viscometer cup. Leave enough empty volume (approximately 50 ml to 100 ml) in the cup for displacement of fluid due to the viscometer bob and sleeve. Immerse the rotor sleeve exactly to the scribed line. Measurements in the field should be made with minimum delay from the time of drilling fluid sampling. Testing should be carried out at either 50°C ± 1°C (120°F ± 2°F) or 65°C ± 1°C (150°F ± 2°F) for reference comparisons to historical data. Testing at a lower temperature, such as 4°C ± 1°C (40°F ± 2°F), is recommended for low temperature effects. The place of sampling should be stated in the report.

CAUTION — The maximum recommended operating temperature is 90°C (190°F). If it is necessary to test fluids above this temperature, a solid metal bob or a hollow metal bob with a completely dry interior should be used. Liquid trapped inside a hollow bob can vaporize when immersed in high-temperature fluid and cause the bob to explode.

1.2 Heat (or cool) the sample to the selected temperature. Use intermittent or constant shear at 600 RPM to stir the sample while heating (or cooling) to obtain a uniform sample temperature. After the cup temperature reaches the selected value, immerse the thermometer into the sample and continue stirring until the sample reaches the selected temperature. Record the temperature of the sample.

1.3 With the sleeve rotating at 600 RPM, wait for the viscometer dial reading to reach a steady value (the time required is dependent on the drilling fluid characteristics). Record the dial reading, θ_{600}.

1.4 Reduce the rotor speed to 300 RPM and wait for the dial reading to reach steady value. Record the dial reading θ_{300}.

1.5 Repeat the previous step for the following rotor speeds 200 RPM, 100 RPM, 6 RPM and 3 RPM. Record the dial readings θ_{200}, θ_{100}, θ_{6}, and $\theta_{3,}$ respectively.

1.6 Refer to equations 2.5 and 2.6 of this document for the calculations of Apparent and Plastic Viscosities.

Appendix C

MATLAB® Scripts

Newtonian Fluids Density and Viscosity Calculations

```
clear all
close all

Flowrate=xlsread ('JCMV_1.00sg_water.xlsx','C4:C36');
P_h=xlsread ('JCMV_1.00sg_water.xlsx','D4:D36');
P_v=xlsread ('JCMV_1.00sg_water.xlsx','E4:E36');

P_delta=P_v-P_h;
P_delta_t=1000*9.81*3.5/100*ones(length(P_h),1);

offset=P_delta_t-P_delta;

figure
plot(Flowrate, P_delta,'r',Flowrate, P_delta_t,'b')
grid
legend('true measurement','theoritical values')'
title('P_v-P_h')

p=polyfit(Flowrate, offset, 6)

offset_s=p(7)+p(6).*Flowrate+p(5).*Flowrate.^2+p(4).*Flowrate.^3+p(3).*Flowra
te.^4+p(2).*Flowrate.^5+p(1).*Flowrate.^6;

figure
plot(Flowrate, offset,'r',Flowrate, offset_s,'b')
legend('Offset','Regression model of offset')'

density_c=(P_delta+offset_s)/9.81/3.5*100;
grid

figure
plot(Flowrate, density_c,'r',Flowrate, density_c*0+1000,'b')
grid
legend('Estimated density','Density of water')'

density_c_l = lowpassFilter(density_c,1,10);

figure
plot(Flowrate, density_c_l,'r',Flowrate, density_c*0+1000,'b',Flowrate,
density_c,'k')
grid
legend('Estimated density after filter','Density of waterv','Estimated
density before filter')
```

```
mean(density_c_l)

density_f=density_c_l;

D=0.024;
A=pi/4*D^2;
e=10^-6;
L=3.5;
vel=Flowrate/60000/A;
vis=1.00*10^-3;
rho=1000;

f_e=P_h*100*2*D./density_f'/L./vel./vel;
load offset1.mat
p=p1;
offset_s=p(7)+p(6).*Flowrate+p(5).*Flowrate.^2+p(4).*Flowrate.^3+p(3).*Flowra
te.^4+p(2).*Flowrate.^5+p(1).*Flowrate.^6;

f_o=(P_h+offset_s)*100*2*D./density_f'/L./vel./vel;

Re_t=rho*D.*vel/vis;
for i=1:length(Re_t)
    if Re_t(i)<=2300
        f(i)=64/Re_t(i);
    else
       f(i)=1/(-1.8*log10((e/D/3.7)^1.11+6.9/Re_t(i)   ))^2;
    end
end

figure
plot(Flowrate, f_e,'r',Flowrate, f,'k',Flowrate, f_o,'b')
legend('estimated f before offset','true f','after offset')
grid

Re_e=64./f_o;
weight=0.01;
for i=1:length(Re_e)
    if Re_e(i)>2000
        Re_e(i)=6.9/(10^(-1/1.8./sqrt(f_o(i)))-(e/D/3.7)^1.11);
    end
    if Re_e(i)<2000&&Re_e(i)>1000
        Re_e(i)=weight*64/f_o(i)+(1-weight)*6.9/(10^(-1/1.8./sqrt(f_o(i)))-
(e/D/3.7)^1.11);
        temp=1;
    end
end

vis_e=vel.*density_f'*D./Re_e;
vis_e=lowpassFilter(vis_e,1,20)';
 min(vis_e)

figure
plot(Flowrate, vis_e,'r',Flowrate, vis_e*0+vis,'k')
```

Non-Newtonian Fluids Density and Viscosity Calculations

```
close all
clear all
clc

Flowrate=xlsread ('JCMV_6gl_XCD.xlsx','C4:C44');  %reads values from excel
sheet
P_h=xlsread ('JCMV_6gl_XCD.xlsx','D4:D44');
P_v=xlsread ('JCMV_6gl_XCD.xlsx','E4:E44');

load density_offset.mat
offset_s=p(7)+p(6).*Flowrate+p(5).*Flowrate.^2+p(4).*Flowrate.^3+p(3).*Flowra
te.^4+p(2).*Flowrate.^5+p(1).*Flowrate.^6;
P_delta=P_v-P_h; %delta P between horizontal and vertical diff. pressure
density_c=(P_delta+offset_s)/9.81/3.5*100; %Density after offset correction
grid

plot(Flowrate, density_c)
axis([10 90 980 1020])
grid
legend('Estimated Density')
xlabel('Flowrate (l/min)')
ylabel('Density (kg/m^3)')
title('Flowloop Estimated Density 6 g/l XCD')

%% viscosity

R=0.012;
D=2*R;
L=3.5;
Q=Flowrate/60000;
A=pi*R^2;
v=Q/A;
e=0.00015;

load offset1.mat
p=p1;
offset_s=p(7)+p(6).*Flowrate+p(5).*Flowrate.^2+p(4).*Flowrate.^3+p(3).*Flowra
te.^4+p(2).*Flowrate.^5+p(1).*Flowrate.^6;

DP=(P_h+offset_s)*10^2;

load coeff.mat

tau=2*R*DP/(4*L); %Wall shear stress 3g/l

% %Define y and x as in section 4.2.3
y=log(tau);
x=log(4*v/R); % 4v/R= (8u/D)
tolerance=100;
tau_guess=tau+3;
```

```
parameter.x=x;
parameter.t=tolerance;

for i=1:length(x)-1
    m(i)=n*K*(8*v(i)/D)^n/(Tau_0+K*(8*v(i)/D)^n);
    %     m(i)=.3;
    parameter.m=m(i);
    parameter.v=v(i);
    parameter.d=density_c(i);
    parameter.q=Q(i);
    parameter.dp=DP(i);
    tau(i)=bisec(0.1,tau_guess(i),parameter);

    r_w(i)=(3*m(i)+1)/4/m(i)*4*v(i)/R; % shear rate at wall
    vis_a(i)=(tau(i)/r_w(i))*1000; %Apparent viscosity for 6 g/l
    Deff(i)=4*m(i)/(3*m(i)+1)*D;
    Re(i)=density_c(i)*v(i)*Deff(i)/vis_a(i);

end

theta=[600 300 200 100 6 3]; %RPM
readings=[31.5 26 23 19.5 12 11];

shear_r=1.7023*theta; %shear rate
shear_s=1.067*readings*0.4788; %shear stress
vis_a1=(shear_s./shear_r)*1000; %apparent viscosity from drilling fluids
laboratory

% vis_a_l=lowpassFilter(vis_a,1,2);
figure
plot(shear_r, vis_a1,r_w,vis_a,'o');
title('Viscosity Comparison 6 g/l XCD')
xlabel('Shear rate (s^{-1})')
ylabel('Apparent Viscosity (cP)')
legend('Viscosity from Fann 35','Viscosity from Flowloop')
axis([0 1600 0 60])
grid
```

Additional Functions for Non-Newtonian Fluids Calculations

```
function p = bisec(a,b,parameter)

%Bisection method's procedure

if f(a,parameter)*f(b,parameter)>0
    disp('Wrong choice')
else
    err = abs(a-b);
    while err > 1e-7
        p = (a + b)/2;
        if f(a,parameter)*f(p,parameter)<0
            b = p;
        else
            a = p;
        end
        err = abs(a-b);
    end
end
```

```
function y=f(tau,parameter)

R=0.012;
e=0.00015;
L=3.5;

DP=parameter.dp;
gr=parameter.m;
v=parameter.v;
density=parameter.d;
Q=parameter.q;

a=0.001;
b=1-a;

r_w=(3*gr+1)/4/gr*4*v/R;
vis_a=tau/r_w; %Apparent viscosity for 3 g/l
Deff=4*gr/(3*gr+1)*2*R;
Re=density*v*Deff/vis_a;
%     f(i) = ff_d(e,Deff(i),gr(i),Re(i),f_guess);
if Re<=2300
    f=64/Re;
elseif 2300<Re && Re<4000

    %         f=1/(-1.8*log10((e/Deff/3.7)^1.11+6.9/Re))^2;
    %         f=abs(friction(gr,Re,Deff))*4;
    f1=friction(gr,Re,Deff)*4;
    f2=64/Re;
    f=a*f1+b*f2;
```

```
else
    %        f(i)=goudar_sonnad(e,D,Re(i));
    f=friction(gr,Re,Deff)*4;
end

dpdx = dpdx_dp(f,density,Q,R)*L;
y=dpdx-DP;


-----------------------------------------------------------------------------------------------------------

function [f_dp] = ff_d(roughness,D_eff_dp,n_star_dp,Re_g_dp,f_guess)

if Re_g_dp<2300

    f_dp = 64/Re_g_dp;
else

tol = 0.001;

x0 = f_guess;
f = -sqrt(x0)*4*log10((0.27*roughness)/D_eff_dp+(1.26^(n_star_dp^-
1.2))/((Re_g_dp*x0^(1-0.5*n_star_dp))^(n_star_dp^-0.75)));
e=0.00015;

f_dp = x0;
 f_dp=1/(-1.8*log10((roughness/D_eff_dp/3.7)^1.11+6.9/Re_g_dp ))^2;
end
weight=0.8;
if Re_g_dp>2300&& Re_g_dp<3300

f_dp = weight*64/Re_g_dp+f_dp*(1-weight);

end


-----------------------------------------------------------------------------------------------------------

function f1 = ffric(x,gr,Re,Deff)


roughness=0.00015;

%f1 =1/x^.5-4/gr^(0.75)*log10(x^(1-gr/2)*Re)+.4/(gr^(1.2));
% #1 Dodge and Metzner (1959)

%alpha =2.63/10.5^gr;
%f1 =x-0.079/((gr^5)*(Re^alpha))
% #2 Shaver and Merill (1959)

f1 =1/x^.5-4/gr*log10(x^(1-gr/2)*Re)+.4*gr;
% #4 Thomas (1960)

%f1 =1/x^.5-4.53*log10(x^(1-gr/2)*Re)/gr-2.69*gr-0.68*(5*gr-8/gr);
```

```
% #5 Clapp(1961)

%f1 =1/x^.5-4.06*log10(x^(1-gr/2)*Re)/gr+2.78*gr-2.16;
% #6 Trinh(1969)

%f1 =x-(0.0682*gr^-0.5)/(Re^(1/gr^0.615)/6.5^(1/gr^(1+0.75*gr)));
% #8 Hanks and Ricks (1973)

%f1 =1/x^.5-3.57*log10(Re^(1/gr^0.615)/6.5^(1/(gr^(1+0.75*gr))));
% #9 Shenoy and Saini (1986)

%f1 =x-0.125*(0.0112+Re^0.3185)*gr^(gr^0.5)
% #10 Desouky and El-Emam (1990)
% Not stable for our data

%f1 =x-(gr/((3.072-0.1433*gr)*Re^(gr/(0.282-0.4211*gr)))-0.00065)/4;
% #11 El-Eman (2003)
```

Appendix D

Flowloop Measurements

Table D.1. Newtonian Fluids Flowloop Measurements

Water			1.10SG NaCl brine		
Q meas (lpm)	dPhor (mbar)	dPver (mbar)	Q meas (lpm)	dPhor (mbar)	dPver (mbar)
90.3545	186.1837	522.8387	90.8087	215.7382	593.3235
86.9806	173.6451	507.7233	86.9830	196.8798	571.7667
84.9780	168.7006	502.2786	85.0055	189.5520	562.7905
81.7778	163.1853	495.5674	82.0014	181.1279	553.1363
80.0097	147.5557	477.3412	79.9949	173.8336	544.2016
76.9993	143.1884	472.2344	76.9948	164.4322	533.7575
75.0156	139.1534	467.3471	74.9991	157.8298	526.0944
71.9949	131.4095	458.6332	71.9968	148.1524	514.7872
69.9909	126.3992	452.6802	69.9984	142.5919	508.4877
67.0002	118.8273	443.7552	66.9985	134.0365	498.7741
64.9923	114.2688	439.0419	64.9954	128.2606	493.6593
62.0009	107.2282	430.5048	62.0023	120.4395	483.1408
60.0108	102.7319	425.3635	60.0065	115.1746	477.2851
56.9931	96.3463	417.9614	56.9992	107.4186	468.2872
55.0375	93.2550	414.4661	55.0017	102.4843	462.7976
52.0081	85.3831	405.3201	52.0016	95.5581	454.7547
49.9904	82.0681	401.5165	50.0012	91.0860	449.6664
46.9906	75.8499	394.5348	47.0016	84.5281	442.3773
45.0101	72.8512	391.1079	45.0038	80.5381	437.7425
42.0029	68.1921	386.3655	42.0007	74.5094	430.9807
39.8642	63.0394	380.0864	39.9994	70.4010	426.3492
36.9904	59.6133	376.0388	37.0002	64.6341	419.8429
34.9797	56.7443	372.7301	35.0013	61.1581	415.8879
31.9498	51.7844	367.9376	31.9936	56.7908	410.7539
30.0030	49.6503	364.6989	30.0014	53.3598	407.1623
26.9216	46.6303	361.2578	27.0033	48.9876	402.9876
25.0012	43.4655	357.5606	25.0009	46.3217	399.1837
21.9686	39.9903	354.1722	22.0010	42.4879	394.9666
19.9799	38.2451	351.9719	19.9989	40.1618	392.4684
16.9924	35.6183	348.9135	16.9992	36.9589	388.9751
15.0046	33.9348	347.0423	14.9976	34.9944	386.8432
11.9956	31.6341	344.5179	11.9987	32.3930	384.0153
9.9866	30.2880	343.0485	9.9987	30.9314	382.5289
0.0000	26.7400	339.8000	0.0000	26.8700	378.6000

Table D.2. Non-Newtonian Fluids Flowloop Measurements Part A

2 g/l XCD			3 g/l XCD			4 g/l XCD		
Q meas (lpm)	dPhor (mbar)	dPver (mbar)	Q meas (lpm)	dPhor (mbar)	dPver (mbar)	Q meas (lpm)	dPhor (mbar)	dPver (mbar)
89.9959	101.6222	437.0724	89.9844	102.8142	434.3740	89.3417	113.4305	440.0911
86.9966	98.0811	431.7927	86.9978	100.1763	430.2169	88.1153	113.2791	439.9224
84.9773	95.6303	428.6299	84.9941	98.3919	426.9635	85.9988	111.3037	436.7048
81.9997	92.5025	424.4112	81.9898	95.5772	423.0287	83.9957	109.0163	433.7182
79.9188	90.9354	421.9692	79.9643	93.5792	419.8792	81.9966	107.8471	431.8744
76.9894	85.3105	414.2094	76.9958	90.7737	415.3169	80.0054	106.0855	429.1244
74.9989	83.3779	411.5939	75.0008	89.2657	412.8332	77.9850	104.1891	426.2795
72.0029	80.1006	406.6482	71.9979	86.8987	409.0036	76.0172	102.6042	424.3321
70.0002	77.7755	403.7259	70.0036	85.3305	406.6818	74.0012	100.6486	422.0072
66.9928	74.5225	399.4209	66.9949	82.9749	402.9910	72.0070	98.9567	419.6148
65.0005	72.4352	396.4840	64.9999	81.5578	400.8951	70.0097	97.5054	417.6059
62.0016	69.4732	392.2873	61.9996	79.3078	397.9985	67.9934	96.1182	415.8356
60.0009	67.1465	389.5399	60.0020	77.8559	395.8559	65.9965	94.4976	413.8985
56.9949	64.5097	385.8297	56.9960	75.6437	393.2629	63.9989	92.4065	411.5905
54.9994	62.7308	383.1542	55.0011	74.3275	391.5422	62.0002	90.5631	409.3719
52.0052	60.3918	379.4412	52.0003	72.2263	388.8418	59.9988	88.8354	407.2957
50.0004	58.9779	377.2320	49.9975	70.6373	387.2948	57.9912	87.0524	405.0838
46.9999	57.0523	374.5627	47.0020	67.8596	384.4825	56.0024	85.3645	403.1119
45.0046	55.9699	373.0165	44.9972	66.1042	382.4940	53.9671	83.5974	401.0617
41.9974	55.1113	371.2721	41.9939	64.1612	380.0227	51.9961	82.4132	399.6143
40.0562	53.1552	369.4643	40.0202	62.9338	378.7396	49.9944	80.9585	398.0918
37.0024	51.4147	367.1997	36.9983	61.1112	376.7950	48.0024	79.7603	396.6327
35.0054	50.1006	365.7502	35.0019	60.1289	375.3887	46.0069	78.5640	395.3049
31.9889	48.9532	364.0130	32.0024	58.6876	373.5922	44.0030	77.5618	393.9283
29.9958	46.9671	362.4146	30.0012	57.4268	371.6842	41.9991	76.2425	392.4964
27.0035	45.2858	360.8074	26.9949	55.7640	369.6755	40.0076	74.8663	390.2517
24.9951	44.3626	359.6639	25.0024	54.6212	368.2527	37.9969	73.4899	388.4192
22.0020	42.9903	358.1011	21.9980	53.1439	366.4987	36.0011	72.3073	386.8263
19.9916	41.9382	356.7597	20.0023	52.1718	365.2721	34.0042	71.2341	385.3234
17.0014	40.8330	355.2733	17.0011	50.8409	363.6025	32.0023	70.1566	383.8571
14.9986	40.0069	354.3587	15.0016	49.7968	362.4334	30.0010	68.9273	382.2817
11.9963	38.7838	352.8862	12.0027	48.1850	360.6283	28.0000	67.9345	380.9382
10.0042	37.9798	351.9669	9.9996	46.9698	359.2922	25.9906	66.7901	379.4133
0.0000	26.9900	341.3000	0.0000	27.2900	339.9000	23.9907	65.8355	378.2281
						21.9980	64.8899	377.0427
						19.9946	63.7803	375.7139
						17.9909	62.7245	374.3701
						15.9984	61.6118	372.9612
						13.9978	60.4875	371.7724
						12.0014	59.3328	370.4133
						0.0000	27.6500	339.2000

Table D.3. Non-Newtonian Fluids Flowloop Measurements Part B

5 g/l XCD			6 g/l XCD		
Q meas (lpm)	dPhor (mbar)	dPver (mbar)	Q meas (lpm)	dPhor (mbar)	dPver (mbar)
89.5755	127.1742	454.8619	89.3902	141.7627	468.8344
86.9882	125.5157	452.4699	87.0227	140.2397	466.8454
85.0128	123.4578	450.1369	84.9994	137.8879	463.9014
82.0079	120.6151	446.5423	82.0266	135.1951	460.3695
79.9580	118.1890	443.0659	80.0406	133.3335	457.7177
76.9938	115.9449	440.5640	76.9978	129.7810	453.9046
74.9887	114.2671	438.4986	74.9866	127.7297	451.4641
72.0096	111.4386	435.0819	71.9946	125.0251	447.8276
69.9908	109.3064	432.4433	70.0048	123.5400	445.6041
66.9876	106.3593	428.8170	66.9958	121.1457	442.5390
65.0052	104.4188	426.6319	65.0018	119.4597	440.5745
62.0047	102.3019	423.6616	62.0015	116.6399	437.9565
60.0022	100.8459	421.4809	59.9933	115.5461	435.5873
56.9987	98.8873	418.9843	56.9943	113.4722	432.6968
54.9953	97.7651	417.6581	54.9998	111.8823	430.2307
52.0202	95.9594	415.4080	51.9904	109.3265	426.6394
50.0023	94.5771	413.3586	50.0003	107.9870	424.7894
47.0019	92.4426	410.3263	47.0002	106.0240	422.1466
44.4990	90.8883	408.2616	44.9999	104.6339	420.3317
41.9998	89.0503	405.5424	41.9984	102.6034	417.5872
40.0017	87.9206	403.9314	40.0095	101.4311	416.0439
37.0044	85.9231	401.2865	37.0002	99.2846	413.2546
35.0073	84.8618	399.7919	35.0019	98.0413	411.6492
32.0047	83.1912	397.4386	32.0049	96.2918	409.3214
29.9981	82.0675	395.9929	30.0040	95.0990	407.6751
27.0051	80.3839	393.8226	26.9997	93.2007	405.3534
25.0024	79.2098	392.3823	24.9956	91.8398	403.7941
21.9980	77.4546	390.2671	22.0035	89.5567	401.2906
19.9990	76.1826	388.8485	20.0040	88.0988	399.6872
16.9878	74.1113	386.5558	16.9984	85.6822	397.0700
14.9956	72.6247	384.9560	14.9972	83.9058	395.2124
11.9961	70.1417	382.3687	12.0063	80.7274	391.8171
0.0000	27.3000	340.4000	10.0073	78.6638	389.6907